# On the Suitability of Fibre Optical Parametric Amplifiers for Use in All-Optical Agile Photonic Networks

*Nikolaos Gryspolakis*

Department of Electrical & Computer Engineering

McGill University

Montreal, Canada

June, 2009

A thesis submitted to McGill University in partial

fulfilment of the requirements of the degree of Doctorate of Philosophy

***Σέ ὅλους τοῦς ἐλευθέρως σκεπτόμενους ἀνθρώπους***
***A todos los librepensadores***
***À tous les libres penseurs***
***К всем свободным мыслителям***
***A tutti i pensatori liberi***
***To all free human thinkers***

*«La science a eu des merveilleuses applications; mais la science qui n'aurait en vue que les applications ne serait plus de la science, elle ne serait plus que de la cuisine. Il n'y a pas d'autre science que la science désintéressée. »*

*Henri Poincaré, 1911 A.D.*

*« Ἡ παιδεία, καθάπερ εὐδαίμων χώρα, πάντα τ' ἀγαθά φέρει.»*

*«Αἱ μέν ποδήρες ἐσθήτες τά σώματα, αἱ δέ ὑπέρμετροι περιουσίαι τὰς ψυχάς ἐμποδίζουσιν.»*

*-Σωκράτης 400 π.Χ.*

## Acknowledgments

Completing a Ph.D. degree, despite it not being a “doctorate of philosophy” anymore, is primarily a mental-strength challenge. Without the motivation and support I received from many people I would not have made it so far.

I am grateful to my supervisor Lawrence R.(I will never know what this R stands for) Chen for his encouragement, ample generosity in knowledge and time, his patience and understanding. I have been his student since almost the beginning of his academic career and I’ve seen him growing into an excellent supervisor and researcher. A lot of his advice on which he persistently insisted during my doctorate, I came to appreciate only at the end and proved to be of invaluable help.

The people without whom I would have not been able to even begin the pursuit of my Ph.D. are my parents, whom I would like to thank for everything they have offered me in my 31 years of life despite being on average 7813 km away during the past 8 years.

Performing a theoretical study in a one man project is a very solemn and solitary path for most of the time. Fortunately, people like Marcio Freitas and Chris Rolston made this project much easier and feasible. The former with his priceless help on the theory and insight in the world of simulations and the latter with his continued technical help on anything I could possibly need. Without these two people this research would have been much more cumbersome and laborious.

I am also grateful to my friends Karim Ali for the insight discussions and the help he offered in parts of the project, Tania Leppert, Eugene Nicolov, Jonathan Yu, Haydar Talib and Roberto Rotili for the endless electronic discussions on everything cognoscible that offered me an almost daily pleasant break from my hard work. I would also like to acknowledge all those friends and girlfriends who made Montreal a wonderful home to live in.

In particular I would like to acknowledge Zaida Marquez, my partner, for her affluent physical and psychological support and motivation. During the last arduous steps of my doctorate she kept me alive by reminding me that there is life after the Ph.D.

I would foremost like to thank Socrates who with his phrase “The unexamined life is not worth living” (ὁ δὲ ἀνεξέταστος βίος οὐ βιωτὸς ἀνθρώπῳ, Ἀπολογία (38$^{\alpha}$)) motivated me throughout my exploration of knowledge in graduate studies and is leading me now to the next phase of my life, the exploration of life, society, economy, art and the world itself. It has been

2408 years since these words were uttered in his “Apology” but they still reverberate as true and as motivating as ever.

# TABLE OF CONTENTS

# LIST OF TABLES

# LIST OF FIGURES

# ABSTRACT

The objective of this thesis is to investigate the suitability of fibre optical parametric amplifiers (FOPAs) for use in multi-channel, dynamic networks.

First, we investigate their quasi-static behaviour in such an environment. We study the behaviour of a FOPA under realistic conditions and we examine the impact on the gain spectrum of channel addition for several different operating conditions and regimes. In particular, we examine the impact of surviving channel(s) position, input power and channel spacing. We see how these parameters affect the gain tilt as well as its dynamic characteristics, namely the generation of under or over-shoots at the transition point, possible dependence of rise and fall times on any of the aforementioned parameters and how the gain excursions depend on those parameters. For these studies we assume continuous wave operation for all signals. We observe that the gain spectrum changes are a function of the position and the spacing of the channels. We also find that the gain excursion can reach several dBs (up to 5 dB) in the case of channel add/drop and are heavily dependent on the position of the surviving channels. The channels located in the middle of the transmission band are more prone to channel add/drop-induced gain changes.

Moreover, we investigate for the first time the FOPA dynamic behaviour in a packet switching scenario. This part of the study assumes that all but one channels normally vary in a packet-switched fashion. The remaining channel (probe channel) is expected to undergo gain variations due to the perturbation of the system experienced by the other channels. Furthermore, we consider several different scenarios for which the channels spacing, per channel input power (PCIP), variance of the power fluctuation and position of the probe channel will change. We find that when the FOPA operates near saturation the target gain is not achieved more than 50% of the time while the peak-to-peak gain excursions can exceed 1 dB.

Next, we introduce modulated channels to the amplifier in order to compare their effect on the Bit Error Rate (BER) performance. We consider the impact on FOPAs when employing different modulation formats, such as RZ, NRZ and RZ-DPSK. Carefully selected modulation formats can improve BER performance and reduce the effects of cross-phase modulation, four wave mixing (FWM) products generation or dispersion (non-linear and linear inter-channel interference). Especially for the case of FOPAs, because of the ultra-fast interaction times of the FWM phenomenon, cross gain modulation can be a great deterrent for using FOPAs. We use RZ-DPSK in order to suppress the WDM signal crosstalk. Only by using RZ-DPSK, we obtain an improved receiver sensitivity of 5 dB when operating at 40 Gb/s.

Finally, we investigate ways to mitigate such effects as the ones described above (gain excursions, gain tilt etc.). We demonstrate that by using a ring configuration with optical feedback for the first time in FOPAs, we can achieve all-optical gain clamping (AOGC), mitigating gain excursions and attaining gain, independent of channel input power for a large range of PCIP. For example, with the use of AOGC, we reduce the add/drop-induced gain excursions from 4 dB to 0.6 dB. Also, by the combined use of AOGC and RZ-DPSK, we mitigate most of the aforementioned hindrances described above.

# SOMMAIRE

L'objectif de cette thèse est d'explorer l'utilité des amplificateurs paramétriques à fibre optique (APFO) à l'intérieur de réseaux dynamiques à canaux multiples.

Tout d'abord, nous investiguons le comportement quasi-statique des amplificateurs dans un tel environnement. Nous étudions le comportement d'un APFO dans des conditions réalistes et nous examinons l'impact de l'addition de canaux sur le spectre d'amplification sous plusieurs conditions d'opération. En particulier, nous examinons l'impact de la position du canal survivant, de la puissance initiale et de l'espace des canaux. Nous présentons comment ces paramètres affectent l'inclinaison du spectre d'amplification ainsi que sa dynamique, incluant la présence de dépassements et de sous-dépassements au point de transition, la dépendance possible des temps de monté et de descentes sur les paramètres mentionnés précédemment et comment l'amplification varie selon ces paramètres. Pour ces études nous assumons une opération continue pour tous les signaux. Nous observons que les changements au spectre d'amplification se produisent en fonction de la position et de l'espacement des canaux. Nous remarquons aussi que la variation d'amplification peut atteindre plusieurs dB (jusqu'à 5 dB) dans le cas de l'ajout ou de la suppression de plusieurs canaux et qu'elle dépend lourdement de la position des canaux survivants. Les canaux situés au centre de la bande de transmission sont plus susceptible aux variations d'amplification due à l'ajout ou à la suppression d'autres canaux.

De plus, nous étudions pour la première fois le comportement dynamique d'un APFO dans un réseau où il y a commutation par paquets. Cette portion de l'étude assume que tous les canaux sauf un varient selon une distribution Gaussienne. Le canal restant devrait subir des variations d'amplification du aux perturbations causé par les autres canaux. Nous considérons aussi plusieurs scénarios différents pour lesquels l'espacement des canaux, leur puissance initiale,

la variance des fluctuations de puissance et la position du canal de test changent. Nous observons que lorsque l'APFO fonctionne près du point de saturation l'objectif d'amplification est atteint moins que 50% du temps et que les variations d'amplification peuvent dépasser 1 dB.

Ensuite, nous utilisons des canaux modulés avec différentes techniques (RZ, NRZ et RZ-DPSK) à fin de comparer leur impact sur le taux d'erreur des bits. Sélectionner le format de modulation optimal améliore le taux d'erreur et réduit les effets de modulation d'amplification croisée, de mélange à quatre ondes et la dispersion. À cause des temps d'interaction très rapide des effets de mélange à quatre ondes, la modulation d'amplification croisée peut être très problématique lors de l'utilisation de APFOs. Nous employons une modulation RZ-DPSK pour éliminer la diaphonie entre les canaux. En utilisant la RZ-DPSK, nous obtenons une augmentation de la sensibilité du récepteur de 5 dB en opérant à 40 Gb/s.

Finalement, nous étudions des moyens de réduire les effets mentionnés ci-dessus. Nous démontrons pour la première fois dans des APFOs qu'en utilisant une configuration en anneau avec une contre-réaction optique nous pouvons obtenir un calage d'amplification tout-optique (CATO), réduire les variations d'amplifications et réaliser une amplification constante et indépendante de la puissance initiale. Par exemple, avec l'utilisation de CATO, nous réduisons les variations d'amplification de 4 dB à 0.6 dB. De plus, en combinant le CATO et la RZ-DPSK, nous diminuons grandement la plupart des effets indésirables mentionnés précédemment.

# Chapter 1 Prologue & Motivation

## *1.1 Prologue*

The telecommunications domain has significantly progressed over the last few decades. The demand for higher bandwidth started with the explosion of the internet, but new services such as personalised high definition video applications could drive massive increases in bandwidth demand. Moreover, moving the high bandwidth lines from the backbone to the end user requires a dynamically reconfigurable optical network architecture. Such networks enable optical channels to be dynamically switched, routed, provisioned, protected and restored all within the fibre optic layer. A dynamic all-optical network provides network flexibility and eliminates the expensive, time consuming and power hungry optical-to-electronic-to-optical (O-E-O) conversion processes inherent in today's optical networking systems. Boffins suggest that demand for bandwidth over the next decade could seriously challenge the economic viability of conventional telecommunication network architectures including modern networks [1.1]. The potential for bandwidth growth, primarily driven by a higher demand for services, is immense and is estimated to be two to three orders of magnitude greater than the bandwidth provided by the present broadband networks. Simply scaling the existing technology and architectures cannot offer viable solutions. The industry and academic community need to consider new architectural approaches to building networks.

Dynamic all-optical reconfigurable networks have to be designed and investigated as increasing demand for bandwidth will make architecture solutions such as fibre to the home, economically viable. Such a network would create the potential for large bandwidth growth across the network, from backbone and metro to the end-user.

The research presented in this thesis is a part of the AAPN (Agile All-Photonic Network) project. In essence, AAPN is a research network funded by a $7 million (CAD) award by the Natural Sciences and Engineering Research Council of Canada and includes contributions from seven Canadian companies and two government laboratories. The objective of this project is to create an agile and robust network which will cumulate dynamic WDM (Wavelength Division Multiplexing) and TDM (Time Division Multiplexing). In order to create such a network, optical switches and dynamic components such as amplifiers have to be designed. The major characteristics of AAPNs are the following [1.2],[1.3]:

- rapidly reconfigurable all-optical space-switching in the core,
- agility - namely the ability to perform TDM to dynamically allocate bandwidth to traffic flows as the demand varies, and
- control and routing functionality concentrated at the edge switches that surround the photonic core.

An integral and crucial part of such a network would be the amplification of its data-carrying channels. The amplifier would have to provide uniform and constant gain under a vast range of different operating conditions that include the following: a packet based switched network with channels arriving at different time instances having travelled different distances, channels being dropped or added constantly and channels travelling at different wavelengths occupying as big of a part as possible of the usable optical bandwidth.

## *1.2 Amplification in Optical Networks*

Optical amplifiers along with low-loss Single Mode Fibre (SMF) are the two principle inventions that have enabled long-haul optical communications and with them the rapid development of applications making use of them. In this section, we will describe the primary fibre amplifier technologies used today, along with their brief history and shortcomings. We will succinctly compare the characteristics, advantages and disadvantages of the main competitors in the fibre optical amplifier field in order to better understand the need to characterize Fibre Optical Parametric Amplifiers (FOPAs) if they are to be considered as an alternative optical amplifier technology.

### 1.2.1 Erbium Doped Fibre Amplifiers

Erbium Doped Fibre Amplifiers (EDFAs) are commonly used in modern fibre optic communication systems. EDFAs were invented simultaneously by a group at the University of Southampton [1.4] and at AT&T Bell Laboratories [1.5]. EDFAs gained interest due to their capability of amplifying light in the wavelength range of 1550 nm where SMF exhibits its minimum loss. Amongst its other advantages, EDFAs offer polarization insensitive gain, high efficiency, high gain, relatively low NF, multi-channel amplification, low crosstalk and the possibility to operate in saturated mode.

In addition, the topology of such an amplifier is fairly simple and merely consists of a pump source and a piece of silica fibre whose core is doped with ionized atoms of the rare earth element Erbium ($Er^{+3}$) and some wavelength selective components. This fibre is pumped using a laser, either at a wavelength of 980 nm or 1480 nm. The photons from the pump excite $Er^{+3}$ atoms which in turn amplify signals of around 1550 nm by stimulated emission. In principle, doped-fibre amplifiers have been theoretically studied as early as the 1960s. However, only in the 1990s did their use become practical, after the techniques for fabrication and characterization of low-loss doped fibres were perfected and after the development of 980 nm and 1480 nm high-power semiconductor lasers.

It has been shown that EDFAs demonstrate a saturation and recovery time in the order of hundreds of μs or even several ms [1.6]. In this way, EDFAs are immune to patterning and crosstalk effects at high bit-rates. The common gain spectrum for EDFAs is the C-band (1530 nm-1570 nm). However, amplification has been demonstrated both for the L-band (1570 nm-1610 nm) [1.7] and the S-band (1480 nm-1510 nm) [8]. The bandwidth of the EDFA is particularly useful in WDM systems for its ability to amplify several channels simultaneously, although the non-uniform gain spectrum has to be considered. Practically, the gain provided by EDFAs can reach 54 dB with a Noise Figure (NF) of 3.1 dB [1.9]. Flat gain above 15 dB with a maximum gain variation of 2.6 dB over a bandwidth of 105 nm has also been presented [1.10].

The dynamic and static properties of EDFAs have been extensively studied during the last two decades. One potential hindrance that has been investigated are the gain excursions observed in the case of channel add/drop. For example, when one, four or seven out of eight channels are dropped, the surviving channels exhibit large power excursions that can last for tens of μs [1.11]. As in-line amplifiers are used in cascade in order to reduce the number of costly repeaters, such excursions become more accentuated as they propagate through more amplifiers. In addition, issues such as gain tilt and crosstalk in dynamic WDM systems have been widely studied and analysed [1.12],[1.13]. In Chapter 5, we will specifically present techniques that have been used in order to mitigate such impediments.

### 1.2.2 Fibre Raman Amplifiers

The dramatic growth of the internet invited unprecedented rapid deployment of WDM transmission systems based on EDFAs. The insatiable demand for high-capacity data transport dragged many newly born inventions out of research labs into real fields, most of which matured in the course of field applications. As a result, WDM transmission ended up using up the entire gain bandwidth of EDFAs, e.g., C- and L-bands already at the end of the 1990s. Even though the entire bandwidth of EDFAs is fully utilized and very high spectral efficiency was obtained through soliton technologies and more spectrally efficient modulation formats, the EDFA-based transmission technology was not enough to satisfy the future needs of optical communications. The use of Fibre Raman Amplifiers (FRAs) offered expanded transmission capacity for optical telecommunications networks over longer transmission lengths, using high bit rates with increased spectral efficiency and gain bandwidth [1.14],[1.15].

Even though the Raman phenomenon has been known since 1932 and people have experimented with Raman amplification since the beginning of 1970s, it was not until the early 1990s that this technology attracted some attention from the market. As explained in section 1.2.1, in optical amplifiers based on Erbium or other rare earth-doped fibre, the amplification band is determined by the energy levels of the ions. On the other hand, in Raman amplifiers the gain wavelength is determined by the wavelength of the pump source and the amplification medium [1.16]. This makes it possible to amplify any desired wavelength range simply by selecting the appropriate pump wavelength.

The principle of Raman amplification in optical fibres was demonstrated experimentally by Stolen *et al.* [1.17]. Their measurement showed that the Stokes shift of silica fibre is approximately 13.2 THz. Later, Edagawa *et al.* demonstrated WDM transmission using Raman amplifiers pumped by laser diodes [1.18]. At the time, however, obtaining sufficient gain required several hundred milliwatts of pump power which could only be delivered by solid-state lasers. Thus, in telecommunications applications, priority was given to EDFAs which could operate perfectly well on a few tens of milliwatts of pump power. Highly efficient EDFAs pumped by laser diodes came into wide use, while FRAs were left on the sidelines. Research on FRAs continued, however, and two broad advantages were identified. The first was that FRAs can provide distributed amplification so that noise levels for the system as a whole can be reduced [1.14]. The second advantage is that by using multiple pump wavelengths (so-called rainbow pumps) the gain bandwidth can greatly exceed that of EDFAs [1.19]. Also, by properly distributing the power amongst the pump wavelengths, a wide and flat composite gain spectrum can be achieved for FRAs [1.20].

Even though FRAs were demonstrated in experiments using large-scale solid-state lasers before EDFAs, they were not actually deployed in real field systems. FRAs were not deployed until recently, when high-power diode pump sources became commercially available. Pumping in FRAs, like in EDFAs, can also be counter-propagating to the WDM channels since the gain in this amplifier is bi-directional. In practise, FRAs are commonly pumped with a counter-propagating scheme in order to reduce the relative intensity noise transfer from the pump to the signal channels. In terms of pump power, the Raman amplifier requires one or two orders of magnitude more pump power than an ordinary EDFA. In addition, Raman amplifiers demonstrate a polarization dependence, although this can greatly be reduced when using a counter propagating pumping scheme. Usually, pairs of pump laser diodes are depolarized in a polarization beam combiner. Finally, FRAs can achieve gain at an arbitrary wavelength. Particular attention must be given to the design of the FRAs because of the non-linear interactions between the pumps and the signals [1.31]. Similar to their more common counterparts, FRAs are also sensitive to power transients and gain tilts when operating in dynamic environments [1.21],[1.22].

### 1.2.3 Fibre Optical Parametric Amplifiers

Although using the highly-efficient Four Wave Mixing (FWM) process to achieve amplification has been suggested since the 1980s, only in the middle of the previous decade did the first extensive investigations of FOPAs start attracting some attention. In Chapter 2, we will give more details on how the FWM phenomenon is used to build a FOPA and we will present their properties and physical description. FOPAs have attracted considerable interest primarily owing to their great range of applications such as all-optical signal processing [1.23], wavelength conversion [1.24], pulsed sources [1.25], de-multiplexers [1.26] and, of course, amplification [1.27],[1.28]. While the ultrafast gain response that FOPAs exhibit (less than 8 fs) enables fast optical processing, it can also be a drawback leading to crosstalk amongst channels present in the amplifier. Moreover, in FOPAs, gain is exponentially proportional to the applied pump power and can be achieved in any arbitrary bandwidth (depending on the wavelength of the pump and the zero-dispersion wavelength of the amplification medium), a property that can enable the use of new bands in optical communication systems.

Some of the recognized shortcomings of FOPAs include the high pump-power requirement and their polarization sensitivity. An additional concern that often arises is their susceptibility to the Stimulated Brillouin Scattering (SBS) effect, which limits the amount of optical pump power that can be injected into a fibre. As opposed to FRAs, FOPAs can only achieve gain in one direction, thus making them less sensitive to saturation effects arising from noise being amplified in both directions. The typical values for the characteristics of EDFAs, FRAs and the FOPAs are presented in Table 1.1.

**Table 1.1** Comparison of EDFA, FRA and FOPA characteristics

| Type | G (dB) | BW (nm) | Centre Wavelength | Noise Figure (dB) | Pump Power (mW) | Response Time | Cross Talk | Pumping Directions | Wavelength Conversion |
|---|---|---|---|---|---|---|---|---|---|
| EDFA | 35-50 | ~ 40 | Fixed | 4-5 | 10-100 | ms | No | Bi-directional | No |
| Raman | >40 | ~ 90 | λ-pump dependent | 3-5 | >300 | fs | No | Bi-directional | No |
| FOPA | >35 | >50 | λ-pump dependent | 3.7-4.2 | >1000 | fs | Yes | Uni-directional | Yes |

## *1.3 Research Motivation*

While EDFAs have served optical networks well for the past 20 years, their limitations such as fixed operating band, high noise etc., has motivated the photonics community to investigate other possible amplification candidates. EDFAs have been exhaustively studied and their dynamic as well as steady-state properties have well been established. Likewise, FRAs, whether in their distributed or discrete form, have been also well studied and have already been deployed in the field.

Recently, there has been increased interest in FOPAs [1.30-1.35]. This has been prompted by their relatively straight-forward implementation as well as developments in the required component technologies such as highly nonlinear fibre (HNLF) and high-power pump sources. With suitable pumping, FOPAs can operate at any wavelength to provide gains as high as 60 dB [1.35], [1.36], with bandwidths spanning the entire C-band, L-band and S-band transmission window [1.37] and beyond [1.38] using relatively short lengths of fibre [1.39]. Additional appealing features include their low NF [1.41-1.44] (as low as 3.7 dB) and the fact that they can become polarization-independent for single or 2-pump configurations [1.44], [1.45].

Multi-channel amplification using FOPAs has been considered during the past few years. These studies have largely focused on optimizing amplifier parameters, such as fibre dispersion, using multiple pumps, etc., in order to obtain a flattened gain spectrum for a specific operating condition (e.g., a fixed number of wavelengths or channels at a specific input power) [1.46], [1.47]. In addition, other studies have looked into the crosstalk between WDM channels resulting from Cross-Gain Modulation (XGM) and FWM, again under constant operating conditions and have also investigated ways to mitigate such effects [1.48],[1.49].

However, modern multi-channel networks do not function under fixed operating conditions. It becomes apparent that if input parameters of such a system, such as channel power or number of channels change, the performance of the amplifier may be severely altered. Therefore, any conclusions that have been drawn by the research on multi-channel FOPAs cannot be entirely applied to reconfigurable networks. Their dynamic and packet-switched nature means that in order for FOPAs to be considered as worthy candidates for agile, multi-wavelength photonic networks, they have to be investigated and tested under varying operating conditions.

In contemporary agile networks, the number of channels passing through the amplifier will vary in response to bandwidth demand or as a result of network reconfiguration, or component failures that can cause one or more channels to be droped. Furthermore, even when the number of channels remains the same, their power can significantly change on a packet level basis but also as a result of different optical distances that each channel sees within a complex optical network. Consequently, the Total Input Power (TIP) to the amplifier will vary as a function of time. Since it is well established that the amplifier gain is a function of TIP [1.50], as the number or the power of input channels varies, there will be changes in the gain spectrum. Thus, even if an amplifier has been designed to have a flat gain spectrum, this is only the case so as long as the operating conditions remain constant. Such variations can result to serious gain tilt which, over several amplifiers, will significantly deteriorate the amplifier's performance. In EDFAs, and to a lesser degree in FRAs, the change in the gain spectrum is uniform over the frequency spectrum, or at least predictable [1.51], [1.52]. However, there have been no studies on the steady-state gain characteristics of FOPAs in order to investigate their static gain performance. Their behaviour, namely changes in the gain spectrum as a function of the TIP or as a result of channel add/drop, has to be examined and, if possible, explained.

Yet again, it is important to study the use of FOPAs in actively routed networks carrying bursty data. In such applications, low output power transients are a critical requirement. These challenges grow increasingly strict as the network grows in complexity and reach, particularly in a large agile network where dynamic reconfiguration aggravates the difficulties and imposes stringent demands on all components. One of the most important of these challenges is commonly referred to as transient cross-saturation or gain dynamics. These are the channel gain excursions observed in time. Some research has been carried out on the bit level dynamics of FOPAs where it was shown that such transients can significantly degrade the performance of a network employing FOPAs [1.49]. However, the transient effects on a packet level, despite their important role, have never been studied.

Amplifiers are usually operating near saturation in order to optimize efficiency and noise performance, while the total output power of a saturated optical amplifier is very nearly constant, independent of the number of channels. Hence, the gain experienced by each channel will depend on the number of channels present. This will induce time-varying perturbations via transient cross-saturation in the amplifier on other wavelengths. These perturbations can build up along the amplifier chain. The transient gain changes that occur at the time of channel dropping present a particular challenge in amplifier cascades and have been extensively studied in the case of EDFAs [1.53], [1.54] and in FRAs [1.55]. Their importance on system performance degradation has been established and several ways have been proposed to mitigate these effects [1.56], [1.57]. There have been no such studies on FOPAs.

Cross-saturation in the network's amplifiers can induce power transients in the surviving channels. The increased gain when channels are dropped can give rise to surviving channel errors since the power of the surviving channels may surpass the thresholds for other nonlinear effects such as Brillouin scattering. Rapidly changing gain, due to channel add/drop can lead to errors as the receiver's ability to adapt to changing power levels is exceeded. It is apparent that FOPAs will not be used in multi-wavelength optical networks unless information in one channel is not degraded by any changes in other channels. Such phenomena have to be studied and if possible mitigated using techniques that have been successfully employed in other amplifier technologies.

## *1.4 Thesis Objectives, Contributions and Organization*

As shown from the literature review, only a few studies exist for FOPAs in the context of a WDM system. Moreover, these studies assume constant operating conditions and do not examine what happens in a dynamic environment. The general objectives of this thesis are the theoretical study and the characterization of a FOPAs' dynamics, gain tilt, gain variation statistics and the effect of several modulation formats used in FOPAs. Subsequently, the final objective is the control and/or mitigate the impediments generated by the aforementioned phenomena.

The remainder of this thesis is organized as follows. In Chapter 2 we review the status of research on FOPAs and their applications. We start by showing the first investigations on FOPAs and how some of their fundamental drawbacks were solved. We continue by presenting the most recent attempts to use FOPAs in a modern WDM network and the challenges this technology is facing. Furthermore, we illustrate their basic operating characteristics through demonstration of results acquired by our own simulation system.

Our subsequent investigation assumes realistic conditions for WDM systems under which channel power sways and add/drops are a frequent phenomenon. For the first time in Chapter 3, we study the behaviour of a FOPA under such conditions. Moreover, we examine the impact on the gain spectrum of channel addition for several different operating conditions and regimes. In particular, we examine the impact of surviving channel(s) position, input power and channel spacing. We see how these parameters affect the gain tilt as well as its dynamic characteristics, namely the generation of under or over-shoots at the transition point, possible dependence of rise and fall times on any of the aforementioned parameters and how the gain excursions depend on those parameters.

Moreover, in Chapter 3 we investigate for the first time the FOPA dynamic behaviour in a packet-switching scenario. This part of the study assumes that all but one channel normally vary in a packet switched fashion. The remaining channel (probe channel) is expected to undergo gain variations due to the perturbation of the system experienced by the other channels. Furthermore, we consider several different scenarios for which the channels spacing, per channel input power (PCIP), variance of the power fluctuation and position of the probe channel will change.

In Chapter 4, we introduce modulated channels to the amplifier in order to compare their effect on the Bit-Error Rate (BER) performance of our system. We consider the impact on FOPAs when employing different modulation formats, such as Return-to-zero (RZ), Non-

Return-to-zero (NRZ) and Return-to-zero Differential Phase Shift Keying (RZ-DPSK). Carefully selected modulation formats can improve the system's performance and reduce the effects of cross-phase modulation, FWM products generation or dispersion (non-linear and linear inter-channel interference). Especially for the case of FOPAs, because of the ultra-fast interaction times of the FWM phenomenon, XGM can be a great deterrent for using FOPAs. We use RZ-DPSK in order to suppress the WDM signal crosstalk.

In Chapter 5 we investigate ways to mitigate such effects as the ones described above (gain excursions, gain tilt etc.). Using an optical feedback in a ring configuration, for the first time in FOPAs we achieve All-Optical Gain Clamping (AOGC) and show that it is effective for alleviating gain excursions and attaining and amplifier gain that is independent of channel input power for a large range of PCIP.

Finally, in Chapter 6 we summarize the contributions of this thesis and conclude.

The main contributions of this thesis have been reported in the following publications:

- N. Gryspolakis and L. R. Chen, "On the suitability of fibre optical parametric amplifiers for agile photonic networks", OSA Topical Meetings on Information Photonics, Charlotte, North Carolina, USA, (2005).
- N. Gryspolakis and L. R. Chen, "Statistical analysis of multi-channel fibre optical parametric amplifiers in agile photonic networks", IEEE Laser and Electro-Optics Society Annual Meeting, Montréal, Québec, Canada, (2006).
- N. Gryspolakis and L. R. Chen "Response of fibre optic parametric amplifiers to channel add/drop in agile all-photonic networks", Optics Communications, vol. 278, no. 1, pp. 168-174, (2007).
- N. Gryspolakis and L. R. Chen, "Using Gain-Clamping to Mitigate Gain Transients in Fibre Optical Parametric Amplifiers", Conference on Lasers and Electro Optics, Baltimore, USA, (2009).
- N. Gryspolakis and L. R. Chen, "All-Optical Gain-Clamping in Fibre Optical Parametric Amplifiers", Opto-Electronics and Communications Conference, Hong Kong, China, (2009).

## References

[1.1] D. B. Payne and R. P. Davey, “The future of fibre access systems”, BT Technology Journal, vol.20, no.4, (2002).

[1.2] G. v. Bochmann, T. Hall, O. Yang, M. J. Coates, L. Mason and R. Vickers, “The Agile All-Photonic Network: an architectural outline”, Queen's University 22nd Biennial Symposium on Communications, paper Boch04b, pp. 217-219, Kingston, Canada, May (2004).

[1.3] L. Mason, A. Vinokurov, N. Zhao and D. Plant, “Topological design and dimensioning of Agile All Photonic Networks”, Computer Networks, vol. 50, pp. 268-287, (2006).

[1.4] R. J. Mears, L. Reekie, I. M. Jauncey and D. N. Payne: “Low-noise Erbium-doped fibre amplifier at 1.54pm”, Electronics Letters, vol. 23, pp. 1026-1028, (1987).

[1.5] E. Desurvire, J. Simpson and P.C. Becker, “High-gain erbium-doped traveling-wave fiber amplifier”, Optics Letters, vol. 12, no. 11, pp. 888-890, (1987).

[1.6] E. Desurvire, “Analysis of transient gain saturation and recovery in Erbium-doped fiber amplifiers”, Photonics Technology Letters, vol. 1, no. 8, pp. 196-199, (1989).

[1.7] F. A. Flood, “L-band Erbium-doped fiber amplifiers”, Optical Fiber Communication Conference, paper WG1-1, Baltimore, USA, March 6 - 10 (2000).

[1.8] J. Kani and M. Jinno, “Wideband and flat-gain optical amplification from 1460-1510 nm by serial combination of thulium-doped fluoride fibre amplifier and fibre Raman amplifier”, Electronics Letters, vol. 35, no. 12, pp. 1004-1006, (1999).

[1.9] S. Aozasa, H. Masuda, H. Ono, T. Sakamoto, T. Kanamori, Y. Ohishi and M. Shimizu, “1480-1510 nm-band Tm doped fiber amplifier (TDFA) with high power conversion efficiency of 42%”, Optical Fiber Communication Conference, paper PD1, San Francisco, USA, February 18 - 23 (2001).

[1.10] Y. B. Lu, P. L. Chu, A. Alphones and P. Shum, “A 105 nm ultrawide-band gain-flattened amplifier combining C-and L-band dual-core EDFAs in a parallel configuration”, Photonics Technology Letters, vol. 16, no. 7, pp. 1640-1642, (2004).

[1.11] A. K. Srivastava, Y. Sun, J. L. Zyskind and J. W. Zulhoff, “EDFA transient response to channel loss in WDM transmission system”, Photonics Technology Letters, vol. 9, no. 3, pp. 386-388, (1997).

[1.12] E. Desurvire, *Erbium-Doped Fiber Amplifiers*. New York: Wiley, (1994).

[1.13] P. C. Becker, N. A. Olsson and J. R. Simpson, *Erbium-Doped Fiber Amplifiers*. New York: Academic, (1999).

[1.14] M. Nissov, C. R. Davidson, K. Rottwitt, R. Menges, P. C. Corbett, D. Innis and N. S. Bergano, “100 Gb/s (10 × 10 Gb/s) WDM transmission over 7200 km using distributed Raman amplification”, European Conference on Optical Communication , Post deadline paper 448, Edinburgh, Scotland, September 22 - 25 (1997).

[1.15] H. Suzuki, J. Kani, H. Masuda, N. Takachio, K. Iwatsuki, Y. Tada and M. Sumida, “25 GHz-spaced, 1 Tb/s (100 ×10 Gb/s) super dense-WDM transmission in the C-band over a dispersion-shifted fiber cable employing distributed Raman amplification”, European Conference on Optical Communication , Post deadline paper PD2-4, Nice, France, September 26 - 30 (1999).

[1.16] G. P. Agrawal, *Nonlinear fiber optics*, 2nd ed., Academic Press, pp. 316-369, (1995).

[1.17] R. H. Stolen and E. P. Ippen, “Raman gain in glass optical waveguides”, Applied Physics Letters, vol. 22, pp. 276-278, (1973).

[1.18] N. Edagawa, S. Ryu, K. Mochizuki and H. Wakabayashi, “Characteristics of Optical Raman Amplification”, Technical Report of IEICE, paper OQE88-33, (1988).

[1.19] Y. Emori, Y. Akasaka and S. Namiki, “Less than 4.7 dB noise figure broadband in-line EDFA with a Raman amplified -1300 ps/nm DCF pumped by multi-channel WDM laser diodes”, Optical Amplifiers and their Applications, paper AB3, Vail, USA, July 26 - 29 (1998).

[1.20] Y. Emori and S. Namiki, “100 nm bandwidth flat gain Raman amplifiers pumped and gain-equalized by 12-wavelength-channel WDM high power laser diodes”, Optical Fiber Communication Conference, paper PD19, San Diego, USA, February 21-26 (1999).

[1.21] A. Berntson, S. Popov, E. Vanin, G. Jacobsen and J. Karlsson, “Polarisation dependence and gain tilt of Raman amplifiers for WDM systems”, Optical Fibre Communication, vol.1, pp. MI2-1 , Anaheim, USA, March 17 - 22 (2001).

[1.22] Y. Sugaya, S. Muro, Y. Sato and E. Ishikawa, “Suppression method of transient power response of Raman amplifier caused by channel add/drop”, European Conference on Optical Communication , Paper 5.2.3., Copenhagen, Denmark, September 8-12 (2002).

[1.23] J. Li, J. Hansryd, P. O. Hedekvist, P. A. Andrekson and S. N. Knudsen, “300 Gb/s eye-diagram measurement by opical sampling using fiber-based parametric amplification”, Photonics Technology Letters, vol. 13, no. 9, pp. 987-989, (2001).

[1.24] K. Inoue, “Arrangement of fiber pieces for a wide wavelength conversion range by fiber four-wave mixing”, Optics Letters, vol. 19, no. 161, pp. 1189-1191, (1994).

[1.25] J. Hansryd and P. A. Andrekson, "Wavelength tunable 40 GHz pulse source based on fibre optical parametric amplifier", Electronics Letters, vol. 37, pp. 584-585, (2001).

[1.26] J. Hansryd and P. A. Andrekson, "O-TDM demultiplexer with 40 dB gain based on a fiber optical parametric amplifier", Photonics Technology Letters, vol. 13, pp. 732-734, (2001).

[1.27] K. K. Y. Wong, K. Shimizu, K. Uesaka, G. Kalogerakis, M. E. Marhic and L. G. Kazovsky, "Continuous-wave fiber optical parametric amplifier with 60-dB gain using novel two-segment design", Photonics Technology Letters, vol. 15, no. 12, pp. 1707-1709, (2003).

[1.28] M. E. Marhic, F. S. Yang, M-C. Ho and L. G. Kazovsky, "High-Nonlinearity Fiber Optical Parametric Amplifier with Periodic Dispersion Compensation", Journal of Lightwave Technology, vol. 17, no. 2, pp. 210-215, (1999).

[1.29] M. C. Ho, F. S. Yang, M. E. Marhic and L. G. Kazovsky, "Optical parametric amplification in a high-nonlinearity fiber", Conference on Lasers and Electro-Optics, paper CFA6, pp. 496-497, San Francisco, CA, May 3-8 (1998).

[1.30] J. Hansryd, P. A. Andrekson, M. Westlund, J. Li and P. O. Hedekvist, "Fiber-based optical parametric amplifiers and their applications", IEEE Journal of Selected Topics in Quantum Electronics, vol. 8, pp. 506-520, (2002).

[1.31] M. N. Islam and O. Boyraz, "Fiber parametric amplifiers for wavelength band conversion", IEEE Journal of Selected Topics in Quantum Electronics, vol. 8, pp. 527-537, (2002).

[1.32] C. J. McKinstrie, S. Radic and A. R. Chraplyvy, "Parametric amplifiers driven by two pump waves", IEEE Journal of Selected Topics in Quantum Electronics, vol. 8, pp.538-547, (2002).

[1.33] S. Radic, C. J. McKinstrie, A. R. Chraplyvy, G. Raybon and J. C. Centanni, C. G. Jorgensen, K. Brar and C. Headley, "Continuous-wave parametric gain synthesis using nondegenerate pump four-wave mixing", Photonics Technology Letters, vol. 14, pp.1406-1408, (2002).

[1.34] S. Radic and C. J. McKinstrie, "Two-pump fiber parametric amplifiers", Optical Fiber Technologies, vol. 9, pp.7-23, (2003).

[1.35] K. Y. Wong, K. Shimizu, K. Uesaka, G. Kalogerakis, M. Marhic and L. G. Kazovsky, "Continuous-wave fiber optical parametric amplifier with 60-dB gain using a novel two-segment design", Photonics Technology Letters, vol. 15, pp. 1707-1709, (2003).

[1.36] K. Shimizu, K. Wong, G. Kalogerakis, K. Uesaka, M. Marhic and L. Kazovsky, "High repetition-rate pulsed-pump fiber OPA for 10 Gb/s NPZ modulated signals", Optical Fiber Communication Conference, vol. 2, pp. 566-567, Atlanta, USA, March 23-28 (2003).

[1.37] M. C. Ho, M. E. Marhic, Y. Akasaka, F. S. Yang and L. G. Kazovsky, "Fiber optical parametric amplifier with 120nm bandwidth", Nonlinear Guided Waves and their Applications, paper WB6, Dijon, France, September 1 - 3 (1999).

[1.38] M. C. Ho, K. Uesaka, M. E. Marhic, Y. Akasaka and L. G. Kazovsky , "200-nm-Bandwidth Fiber Optical Amplifier Combining Parametric and Raman Gain", Journal of Lightwave Technology, vol. 19, no. 7, pp. 977-981, (2001).

[1.39] S. Radic, C. J. McKinstrie, R. M. Jopson, J. C. Centanni, Q. Lin and G. P. Agrawal, "Record performance of parametric amplifier constructed with highly nonlinear fiber", Electronics Letters, vol. 39, pp. 838-839, (2003).

[1.40] K. K. Y. Wong, K. Shimizu, M. E. Marhic, K. Uesaka, G. Kalogerakis and L. G. Kazovsky, "Continuous-wave fiber optical parametric wavelength converter with +40 -dB conversion efficiency and a 3.8-dB noise figure", Optics Letters, vol. 28, pp. 692, (2003).

[1.41] J. L. Blows and S. E. French, "Low-noise-figure optical parametric amplifier with a continuous-wave frequency modulated pump", Optics Letters, vol. 27, pp. 491, (2002).

[1.42] K. Inoue and T. Mukai, "Experimental study on noise characteristics of a gain-saturated parametric amplifier", Journal of Lightwave Technology, vol. 20, pp. 969, (2002).

[1.43] P. L. Voss, R. Y. Tang and P. Kumar, "Experimental measurement of the photon statistics and noise figure of a parametric fiber amplifier", Optics Letters, vol. 28, pp. 549, (2003).

[1.44] K. K. -Y. Wong, M. E. Marhic, K. Uesaka and L. G. Kazovsky, "Polarization-independent fiber optical parametric amplifier", Opto-Electronics and Communications Conference, pp. 609-610, Sydney, Australia, July 1 - 5 (2001).

[1.45] K. K. -Y. Wong, M. E. Marhic, K. Uesaka and L. G. Kazovsky, "Polarization-independent Two-Pump Fiber Optical Parametric Amplifier", Photonics Technology Letters, vol. 14, no. 7, (2002) .

[1.46] L. Provino, H. Maillotte, E. Lantz, T. Sylvestre and J. M. Dudley, "Broadband and nearly flat parametric gain in single-mode fibers", Conference of Lasers and Electro-Optics Europe, paper CTuI 3, Nice, France, September 15 (2000).

[1.47] J. M. Chavez Boggio, J. D. Marconi and H. L. Fragnito, "Double-pumped fiber optical parametric amplifier with flat gain over 47-nm bandwidth using a conventional dispersion-shifted fiber", Photonics Technology Letters, vol. 17, no. 9, pp. 1842 - 184, (2005).

[1.48] K. Krastev and J. Rothman, "Crosstalk in fiber parametric amplifier", European Conference on Optical Communication , paper We.L.3, Amsterdam, Netherlands, September 30 - October 4 (2001).

[1.49] F. A. Callegari, J. M. Chavez Boggio and H. L. Fragnito, "Crosstalk mitigation in fiber optic parametric amplifier", IEEE Laser and Electro-Optics Society Annual Meeting, paper WB3, Glasgow, Scotland, November 10 - 14 (2002).

[1.50] N. Gryspolakis, L. R. Chen and T. Zambelis, "Performance of two-stage discrete fiber Raman amplifiers with and without all-optical gain clamping", Applied Optics, vol. 44 no. 1, pp. 83, (2005).

[1.51] J. C. Dung, H. Y. Cheng and S. Chi, "The gain stability of Raman amplifier in WDM system", Conference of Lasers and Electro-Optics/Pacific Rim, paper W4A-13-5, Taipei, Taiwan, July 22 - 26 (2003) .

[1.52] K. Motoshima, N. Suzuki and K. Shimizu, "A channel-number insensitive Erbium-Doped fiber amplifier with automatic gain and power regulation function", Journal of Lightwave Technology, vol. 19, no. 11, (2001).

[1.53] A. K. Srivastava, Y. Sun, J. L. Zyskind and J. W. Sulhoff, "EDFA transient response to channel loss in WDM transmission system", Photonics Technology Letters, vol. 9, no. 3, pp. 386-388, (1997).

[1.54] M. Karasek and F. W. Willems, "Channel addition/removal response in cascades of strongly inverted erbium-doped fiber amplifiers", Journal of Lightwave Technology, vol. 16, no. 12, pp. 2311 - 2317, (1998).

[1.55] J. Gest and L. R. Chen, "Performance analysis of all-optical gain-clamped discrete fiber Raman amplifiers", IEEE Laser and Electro-Optics Society Annual Meeting, paper ThV3, Rio Grande, Puerto Rico, November 8 - 9 (2004).

[1.56] J. Gest and L. R. Chen, "Comparison of Two All-Optical Gain-Clamping Techniques for Discrete Fiber Raman Amplifiers", 22nd Biennial Symposium on Communications, paper 33, Kingston, Ontario, May 29 - June 1 (2004).

[1.57] A. Bianciotto, V. Ferrero and R. Gaudino, "EDFA gain transients: experimental demonstration of a low cost electronic control", Photonics Technology Letters, vol. 15, no. 10, pp. 1351-1353, (2003).

# Chapter 2 Fibre Optical Parametric Amplifiers

As discussed in Chapter 1, fibre parametric amplification is based on highly efficient FWM in optical fibres [2.1]. In order to achieve high FWM efficiency, HNLF is commonly used when designing FOPAs [2.2]. The efficiency of the mixing process is enhanced by the dispersion profile of the HNLF. Specifically, the amount of dispersion is required to be very low compared to traditional transmission fibres. In addition, it is required that the amplifier operates close to the zero-dispersion wavelength as we will explain later in this chapter.

In section 2.1 of this chapter, we will describe the fundamentals of FWM and how this phenomenon is used in order to achieve parametric amplification. Subsequently, in section 2.2, we will describe the most important characteristics of parametric amplification and illustrate how FOPAs are implemented. In addition, we will discuss the current status of FOPAs, their advantages and their drawbacks. In this context, we will review the key results that have been obtained during the last few years, towards the implementation of a practical FOPA that can be employed in modern telecommunication networks.

Finally, in section 2.3, we will present in detail, the basic operating characteristics of FOPAs and we will specify how their behaviour depends on several important parameters such as the pump power, the dispersion etc., in order to better understand their operating principles. This will help the reader follow through the results presented in the subsequent chapters.

## *2.1 Four-Wave Mixing*

To understand the FWM process, we begin by considering the general case of three electromagnetic fields interacting with each other to produce a fourth field. Physically, we can comprehend this process by considering the individual interactions of the fields within a dielectric medium. An oscillating polarization is caused by the first input field ($\omega_1$) in the dielectric medium, which in turn re-radiates. However, this time it is phase shifted by an amount which is determined by the damping of the individual dipoles. So far, what we have explained is simple Rayleigh scattering described by linear optics.

If we are to apply a second field ($\omega_2$), the same process will repeat. Thus, the polarization of the dielectric will be driven, and the interference of the two waves will generate harmonics in the polarization at the sum ($\omega_1 + \omega_2$) and difference ($\omega_1 - \omega_2$) frequencies. Subsequently, the application of a third field will also drive the polarization, and this will beat with both the other input fields as well as the sum and difference frequencies. This beating with the sum and difference frequencies is what gives rise to the fourth field in FWM. Since each of the beat frequencies produced can also act as new source field, an enormous number of interactions and fields may be produced from this basic process.

Hence, the FWM process is a non-linear coupling between four interacting optical fields and can occur in any non-linear medium. When two optical fields with different frequencies ($\omega_1$ and $\omega_2$) co-propagate in an optical fibre they will continuously beat with each other. The beating results in an intensity modulation of the refractive index via the nonlinear Kerr effect with the frequency $\omega_2 - \omega_1$. The intensity modulated refractive index will in turn affect a third frequency $\omega_3$ through Phase Modulation (PM), resulting in the creation of frequencies at $\omega_3 \pm (\omega_2 - \omega_1)$. However, the frequency $\omega_3$ will also beat with $\omega_1$, repeating the process described above. Thus interaction with $\omega_2$ will give rise to new frequencies at $\omega_2 \pm (\omega_3 - \omega_1)$. In a system with three frequencies, nine new frequencies will be generated at frequencies $\omega_{abc} = \omega_a + \omega_b - \omega_c$ as depicted in Fig. 2.1. The frequencies annotated under the arrows denote the components that contribute power to that frequency.

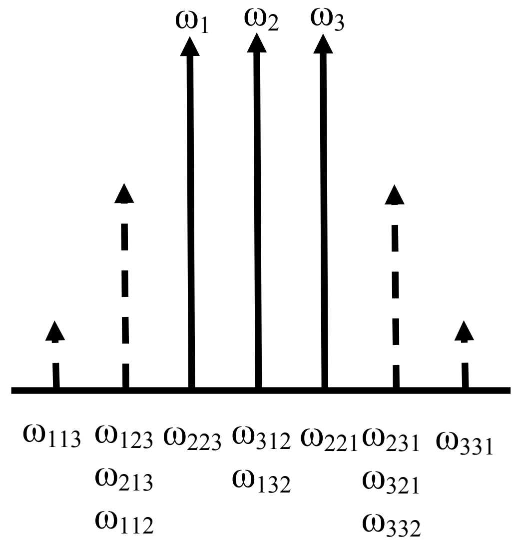


**Fig. 2.1** FWM products, generated at frequencies $\omega_{abc} = \omega_a + \omega_b - \omega_c$.

When any of the $\omega_1$, $\omega_2$ and $\omega_3$ waves are identical, the term "degenerate four wave mixing" is used. In the next section we will explain how this phenomenon can be used in optical communications in order to amplify information carrying signals and we will present the main developments in parametric amplification during the past few years.

## *2.2 Parametric Amplification*

For parametric amplification, we consider the case of degenerate FWM. The overlapping waves (e.g., $\omega_2$ and $\omega_3$) are referred to as the "pump" and its corresponding frequency "$\omega_p$", while $\omega_1$ is denoted as the signal and its corresponding frequency "$\omega_s$". As a result of the FWM process between the signal and the pump, one photon of the pump will be transferred to the signal and one photon to the frequency $\omega_i = 2\omega_p - \omega_s$ creating a new wave named the "idler" as seen in Fig. 2.2. The transfer of photons from the pump to the signal is what constitutes amplification. The idler is an exact copy of the signal but of conjugate phase.

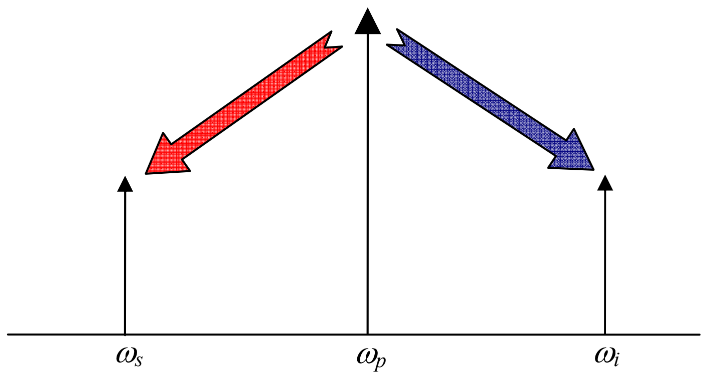


**Fig. 2.2** Degenerate FWM, where a pump and a signal interact to give rise to an idler and amplify the existing signal.

Inserting the wave field functions of $\omega_1$, $\omega_2$ and $\omega_3$ in the nonlinear Schrödinger equation we obtain the coupled differential equations that govern the interactions between the signal, the generated idler and the pump that are presented below [2.3]:

$$\frac{dA_p}{dz} = i\gamma\left[\left(\left|A_p\right|^2 + 2\left(\left|A_s\right|^2 + \left|A_i\right|^2\right)\right)A_p + 2A_s A_i A_p^* \cdot \exp\left(i\Delta\beta z\right)\right] \quad \text{Eq. (2.1a)}$$

$$\frac{dA_s}{dz} = i\gamma\left[\left(\left|A_s\right|^2 + 2\left(\left|A_i\right|^2 + \left|A_p\right|^2\right)\right)A_s + A_p^2 A_i^* \cdot \exp\left(-i\Delta\beta z\right)\right] \quad \text{Eq. (2.1b)}$$

$$\frac{dA_i}{dz} = i\gamma\left[\left(\left|A_i\right|^2 + 2\left(\left|A_s\right|^2 + \left|A_p\right|^2\right)\right)A_i + A_p^2 A_s^* \cdot \exp\left(-i\Delta\beta z\right)\right] \quad \text{Eq. (2.1c)}$$

where $A_p$, $A_s$ and $A_i$ are the amplitudes of the three optical fields, and $\gamma$ is the nonlinear coefficient which is related to the non-linear refractive index $n_2$ through:

$$\gamma = \frac{2\pi n_2}{\lambda A_{eff}} \quad \text{Eq. (2.2)}$$

where $A_{eff}$ is the effective area of the light mode inside the fibre. The value of the nonlinear coefficient $\gamma$ is in the order of 2 (W km)$^{-1}$ for a single mode fibre, while it can reach 10 to 22 (W km)$^{-1}$ for an HNLF. For this reason, HNLFs are used for parametric amplification as the efficiency of the process can increase almost ten-fold compared to SMF. The linear phase mismatch $\Delta\beta$ which determines the efficiency of the process is given by

$$\Delta\beta = -\frac{2\cdot\pi\cdot c}{(\lambda_0)^2}\cdot\frac{dD}{d\lambda}\cdot(\lambda_p-\lambda_0)\cdot(\lambda_p-\lambda_s)^2 \qquad \text{Eq. (2.3)}$$

where $\lambda_p$ is the pump wavelength, $\lambda_s$ the signal wavelength, $\lambda_0$ the zero-dispersion wavelength and $\frac{dD}{d\lambda}$ is the slope of the dispersion at the zero-dispersion wavelength. As described by Stolen *et al.* in [2.4],

$$\frac{d\theta}{dz} \approx \Delta\beta + \gamma(2P_p - P_s - P_i) \qquad \text{Eq. (2.4)}$$

where $\theta$ is the relative phase difference between the signals involved in the FWM process. This represents the linear ($\Delta\beta$) and nonlinear [$\gamma$ ($2P_p - P_s - P_i$)] phase mismatch components. In section 2.3, we will analytically describe how the linear and nonlinear phase mismatch affect the gain characteristics of the amplifier.

### 2.2.1 FOPA Topology

One of the key advantages of FOPAs is their simple topology. The signal we want to amplify is coupled into a length of HNLF along with a strong optical wave acting as the pump. Practically, the pump is broadened by means of PM, in order to suppress the effects of SBS [2.5], [2.6]. If $\lambda_p$ and $\lambda_s$ are carefully selected (relative to $\lambda_0$) then the process we described in the preceding section will take place within the fibre as illustrate in Fig. 2.3, thus amplifying the signal and generating an idler at $\omega_i$.

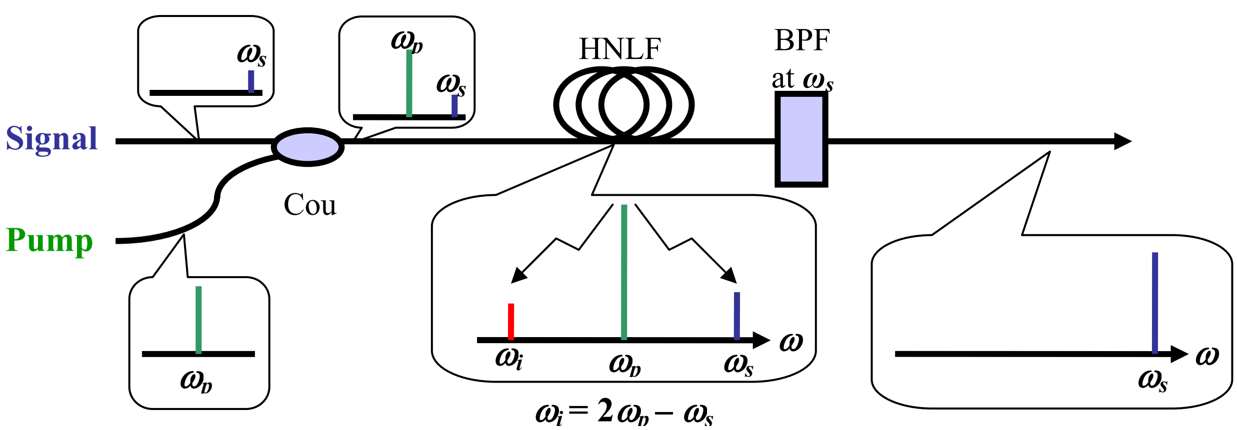


**Fig. 2.3** Configuration of FOPA. BPF: Bandpass filter.

Commonly, a bandpass filter (BPF) at the end of the amplifier is used to isolate the amplified signal and remove the pump, and the idler generated during the amplification process. Nevertheless, the idler can have several useful applications. Apart from the obvious signal wavelength conversion, as the generated idler is an exact frequency-shifted and phase-conjugated image of the signal, by detecting the idler one can monitor the signals without disrupting the flow of information within an optical transmission link. Furthermore, transmission of the idler, rather than the signal, makes possible frequency-dependent routing. Finally, because the idler is a phase-conjugate image of the signal, transmission of the idler makes possible the reduction of impairments caused by phenomena such as pulse distortion, pulse arrival-time and phase jitter, and inter-pulse FWM [2.7].

### 2.2.2 Stimulated Brillouin Scattering

SBS is a nonlinear process occurring in any nonlinear medium. When intense light is travelling through such a medium, the changes in the electric field of the light itself generate acoustic vibrations in the medium via electrostriction. The light is subject to SBS from these vibrations, usually in opposite direction to the incoming beam. In practical terms, SBS can reflect big part of the pump power if it exceeds a specific threshold. This threshold can be relatively low and can thus deplete the especially high power pump used in FOPAs. Even if numerous techniques exist to reduce or suppress SBS, the most common approach is to phase modulate the pump. In this way, the pump spectrum is widened to more than the Brillouin gain bandwidth, which is around 50 GHz [2.8], thus increasing the Brillouin threshold for the pump power.

### 2.2.3 Noise Performance of FOPAs

Parametric amplification has another unique feature that allows us to achieve very low noise amplification. In particular, FOPAs can be operated in a phase-sensitive mode providing a NF even below the quantum limit (which is a NF of 3 dB [2.9]). This limit is a direct consequence from the uncertainty principle in terms of quantum theory. Therefore, because of it, all kinds of phase-insensitive amplifiers such as semiconductor optical amplifiers and Raman amplifiers cannot achieve a NF below the quantum limit when they provide high gain. Thus, by using phase-sensitive parametric amplifiers, we can significantly improve the signal-to-noise ratio (SNR) of an optical telecommunication system [2.10]. During the phase-sensitive operation of a FOPA, only the in-phase component of the signal is being amplified, while at the same time the quadrature-phase component is being attenuated. This way the uncertainty principle is not violated, while at the same time no excess noise is added to the signal [2.8]. Levandovsky *et al.* achieved a NF of 0.4 dB using a phase-sensitive parametric amplifier for a provided gain of 1.7 dB [2.11]. Also, Bencheikh *et al.* [2.12] experimentally demonstrated that a phase-sensitive optical parametric amplifier used to amplify the incoming optical signal on a lossy photodiode can improve the NF of detection. At high parametric gain, the NF approaches to 0 dB, which corresponds to a detection quantum efficiency that approaches 100%.

### 2.2.4 Gain Bandwidth and Spectrum

A typical gain spectrum for a single pump FOPA is shown in Fig. 2.1 [2.13]. The parameters upon which depends the shape of the gain spectrum will be discussed in detail in section 2.3.

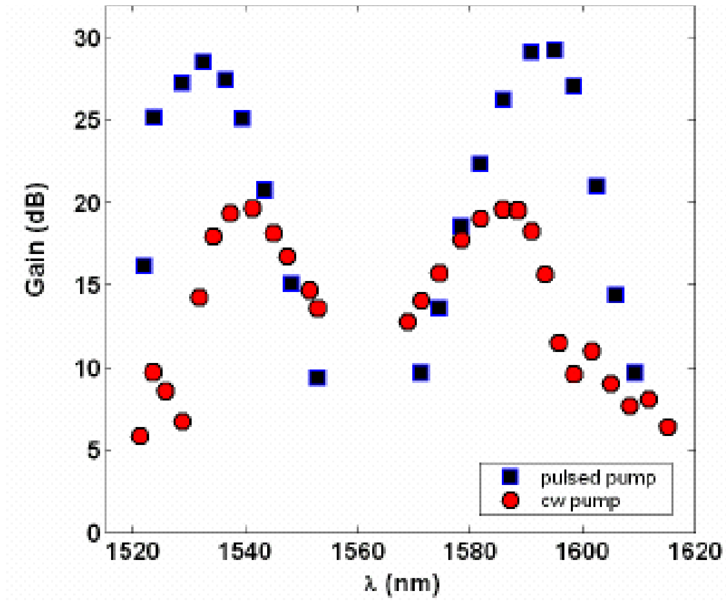


**Fig. 2.4** Experimental single pump FOPA gain spectra for a CW pump and a pulsed pump [2.13].

However Nazemosadat *et al*. have shown [2.14] that the gain spectrum for a single-pumped FOPA can be considerably controlled, achieving a notably flat gain by optimising higher order dispersion ($\beta_2$ and $\beta_4$) and the length of the amplifier as shown in Fig. 2.5.

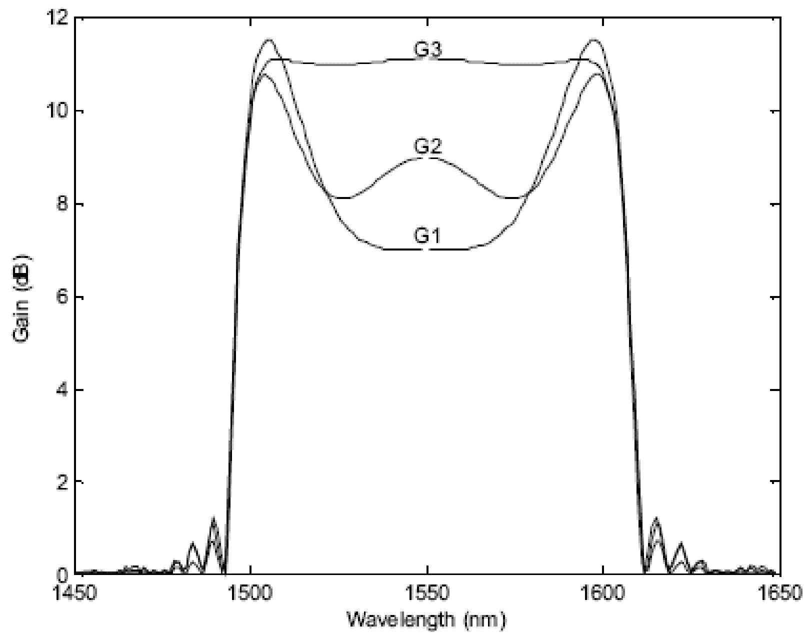


**Fig. 2.5** Gain spectra of single pump FOPA for three different combinations of three optimized parameters $\beta_2$, $\beta_4$ and the fibre length [2.14].

As mentioned before, FOPAs can have a significantly wide amplification spectrum, easily exceeding the EDFA gain bandwidth. This characteristic makes it possible to amplify signals in wavelengths not feasible today. Using a pulsed pump Ho *et al.* demonstrated a gain bandwidth of 200 nm with a peak gain of 25 dB [2.15] while Radic *et al*. demonstrated a FOPA with a flat gain of 40 dB over a bandwidth of 34 nm [2.16]. Using a pulsed source as a pump leads to a time-varying gain and thus makes it impractical for in-the-field use. However, it should be noted that as long as the amplified signals generate an idler each, only half of the bandwidth is available to be used as gain bandwidth. Full bandwidth utilization can be achieved by using an interleaver filter in order to separate the odd and even signals, amplify them in two different branches, subsequently filter their corresponding idlers and then recombining them together.

Directly following from Eq. (2.3), if we place the pump at $\lambda_0$, we should theoretically obtain infinite gain bandwidth. However, the bandwidth of the gain is limited due to the existence of higher order dispersion, Raman gain and polarization mode dispersion. More importantly, as $\lambda_0$ is not exactly constant along the fibre, in practical applications the gain bandwidth becomes limited and non-flat. This $\lambda_0$ variation is due to the manufacturing procedure that makes it almost impossible to produce a fibre with constant refractive index profile and core radius. As such $\lambda_0$ variations can also be the result of temperature change and fibre strain, a FOPA can also be used as a highly-sensitive sensor [2.17].

### 2.2.5 Two-Pump Configuration

Another way of achieving a wide, flat gain is by using a two-pump configuration [2.18], [2.19]. In this case, the two pumps have to be placed symmetrically with respect to $\lambda_0$ and must have the same power. Finally, the two pumps also have to be in opposite phase from each other.

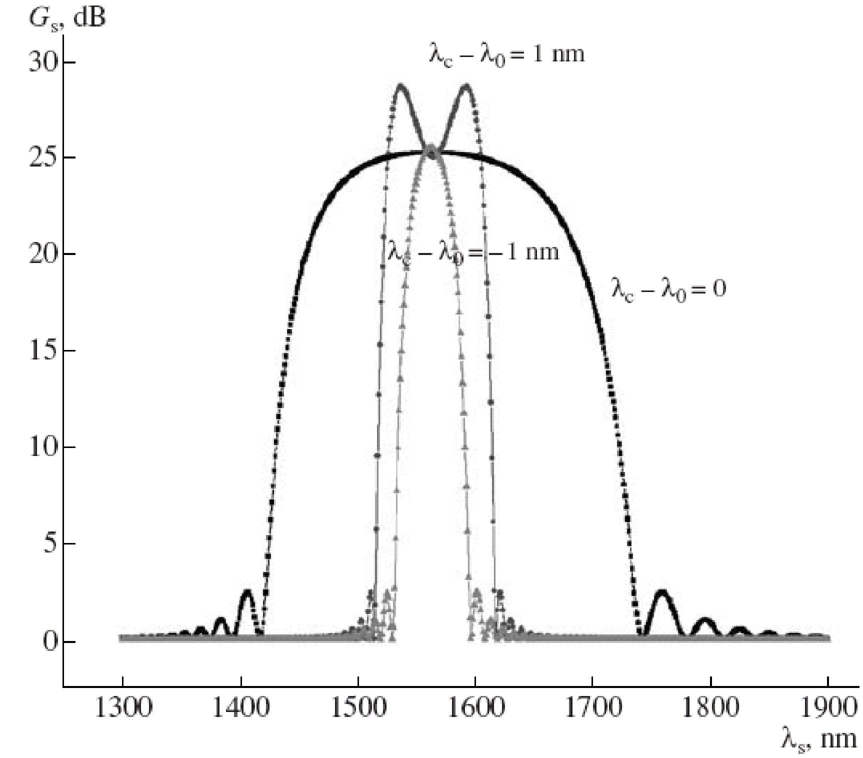


**Fig. 2.6** Influence of the centre wavelength of two pump deviations from the fibre zero-dispersion wavelength on the signal gain [2.20]

Both the bandwidth and the width of the gain spectrum however, heavily depend on the positioning of the two pumps relatively to $\lambda_0$, as Chen *et al.* have shown [2.20]. When $\lambda_c$ - $\lambda_0$ (where $\lambda_c$ is the middle of the distance between the two pumps) is positive, the gain spectrum is similar to that of a single pump positioned at $\lambda_c$. However, when this becomes negative, the gain spectrum resembles a single lobe symmetric along $\lambda_c$. Finally, when $\lambda_c$ - $\lambda_0$ is zero, the gain spectrum becomes a much wider lobe with a fairly flat middle section (see Fig. 2.6).

Yang *et al.* [2.21] first demonstrated a two-pump operated FOPA using two pulsed pumps with a peak gain of 2.3 W each on a 200 m Dispersion-Shifter Fibre (DSF), while Chavez Boggio *et al.* [2.22] presented a similar configuration using CW lasers of 130 mW each and a fibre of 25 km. In this case, the gain achieved was 26 dB over a bandwidth of 30 nm. Finally, Gao *et al.* [2.23] using a multivariate stochastic optimization algorithm, designed a broadband

FOPA with two section HNLFs was designed, theoretically providing a uniform gain of 20.3 dB with 0.2 dB uniformity over an incredible 346 nm bandwidth.

### 2.2.6 WDM Amplification

An optical fibre amplifier is most commonly designed to operate within a WDM telecommunication system. Therefore, if an amplifier technology is to be considered for employment in such an environment, offering efficient multi-channel amplification is imperative. As previously mentioned, EDFAs are used to amplify WDM channels, albeit within a limited bandwidth. A typical operating bandwidth for an EDFA is 30-40 nm. As we saw previously, FOPAs can vastly exceed such a limitation and are only restricted by the availability of laser pumps and the dispersion of the fibre used as the amplifying medium.

Considerable amount of work has been done during the last few years to assess the suitability of FOPAs in multi-channel amplification. Multi-channel operation for FOPAs has been demonstrated for up to 64 channels [2.24-2.26]. However, it has been demonstrated that FWM, Cross-Gain Modulation (XGM) and crosstalk are the three main limiting factors in multi-channel operation for FOPAs. These phenomena result in serious performance degradation [2.26]. XGM will be further explained in Chapter 4.

Early on, Krastev *et al.* with their study on crosstalk in FOPAs [2.27], made it evident that intra-channel crosstalk was a severe hindrance that would have to be tackled with. Clearly, as the number of WDM channel present in the amplifier increases, so does the crosstalk [2.24]. Several methods for crosstalk reduction have been investigated. It has been shown by Forghieri *et al.*, that suitable unequal channel separations can be found, for which no FWM product term is superimposed on any of the transmitted channels [2.28]. Nevertheless, the use of such a technique would make the system employing it incompatible with the standard ITU WDM channel placement. Mussot *et al.*[2.29] showed that crosstalk can be reduced by properly tuning the WDM signal allocation with respect to the pump wavelength. Moreover, they showed that crosstalk is also reduced when the signals are located on the Stokes side of the pump frequency because of the absence of phase-matching. In addition, Blows [2.30] showed that for a particular design starting point, crosstalk is minimized by increasing the pump power and decreasing fibre nonlinearity and length.

Kuo *et al.* [2.31] showed that a substantial crosstalk suppression can be achieve by using RZ-DPSK modulation format. RZ-DPSK's amplitude is pattern independent and along with its subunity duty cycle, they are effective in significantly reducing the XGM and FWM effects. These results were independently demonstrated and thus confirmed, as part of this thesis and are analytically presented in Chapter 4.

## *2.3 Single Channel Characteristics of FOPAs*

In order to understand the behaviour of parametric amplification, in this section we will investigate the gain characteristics of FOPAs as a function of fibre length, signal input power, pump power, dispersion slope. When studying the dependence of parametric amplification on the dispersion slope, we will look deeper at the relationship between the dispersion and pump positioning in the anomalous and normal regime. Finally, in order to understand the FWM interaction in time, we will present the power evolution of the pump and the signal along the fibre length. All the simulations were performed by solving Eq. (2.1a), (2.1b) and (2.1c). Unless otherwise stated, the parameters used in the simulations are given in Table 2.1 and all waves are assumed to be continuous waves (CW). The spectra provided are plotted by tuning the signal wavelength in steps of 2 nm.

**Table 2.1.** FOPA parameters used in simulations

| **Fibre Length** $L$ **(km)** | **Non-Linearity Parameter** $n_2$ **(m$^2$/W)** | **Effective Area** $A_{eff}$ **(μm$^2$)** | **Zero Dispersion Wavelength** $\lambda_0$ **(nm)** | **Dispersion Slope** $S$ **(ps/nm$^2$/km)** | **Pump Power** $P_p$ **(W)** | **Pump Wavelength** $\lambda_p$ **(nm)** |
|---|---|---|---|---|---|---|
| *0.5* | $2.6\times10^{-20}$ | 9.5 | 1559 | 0.03 | 1.4 | 1560.7 |

### 2.3.1 Gain as a Function of Amplifier Length

Fibre lengths of 100 m, 250 m, 500 m and 1000 m are simulated in this study. For each fibre length, we vary $\lambda_s$ and plot its gain as a function of wavelength. The signal input power used in this case is -30 dBm.

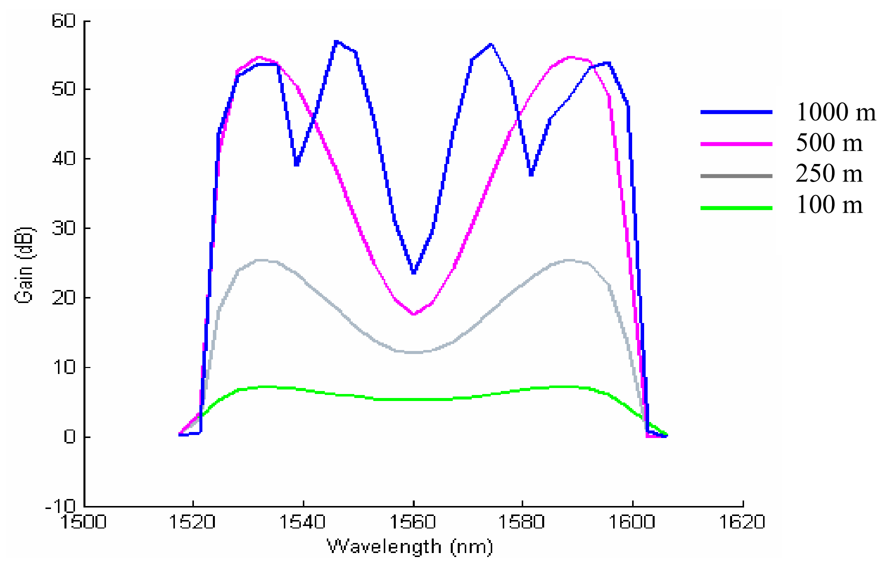


**Fig. 2.7** Gain as a function of wavelength for an amplifier length of 100 m, 250 m, 500 m and 1000 m.

Fig. 2.7 shows that the FOPA gain increases with the length of the fibre. For the given pump and input signal power, the maximum gain is reached for an HNLF length of 500 m. Thus, we can deduce that 500 m is the optimum length for such an amplifier with regard to the gain. The reason for this upper limit of provided gain is the periodic exchange of energy between the pump and the signal. In other words, a reverse of roles is taking place as the signal almost completely depletes the pump, the signal itself starts acting as a pump, transferring energy back to the initial pump. This process happens in a periodic fashion along the fibre while the maximum transfer of energy happens at a specific fibre length for every wavelength. For some wavelengths this conversion of pump energy into signal energy happens with greater efficiency. As a consequence, when the fibre exceeds the aforementioned length the signal, when placed at these wavelengths, starts acting as a pump and thus losing gain. This is how the gain dips observed for the 1000 m configuration, are explained in Fig. 2.7.

### 2.3.2 Gain as a Function of Input Signal Power

We now examine the effect of the input signal power variation, on the gain spectrum. The signal power is varied between -40 dBm and -10 dBm in steps of 10 dB and the results are illustrated in Fig. 2.8.

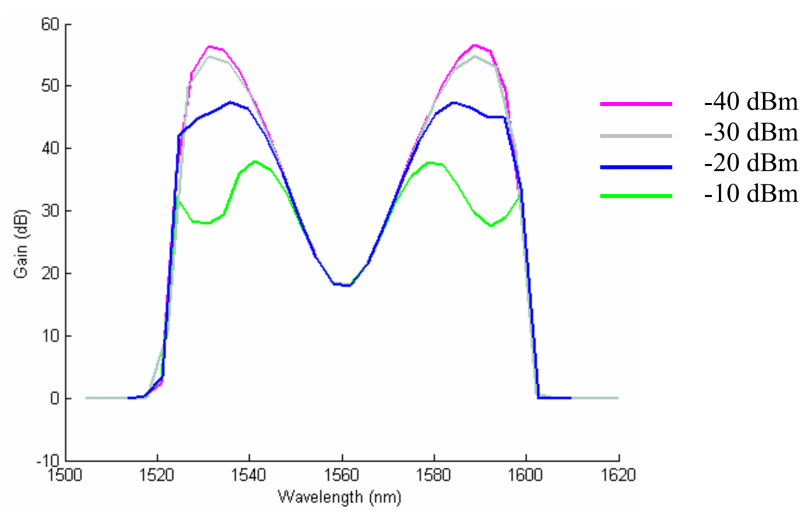


**Fig. 2.8** Gain as a function of wavelength for signal input powers of -40 dBm, -30 dBm, -20 dBm and -10 dBm.

As the input signal power decreases from -10 dBm to -40 dBm, the provided gain increases. Moreover, the separation between the peaks of the gain spectrum increases as the input signal power decreases. When operating in the small signal regime, the provided gain peaks at around 56-57 dB and does not increase further when the signal power is reduced even more. Therefore, this is the maximum gain a 500 m amplifier can provide with a pump of 1.4 W. The reason for the dips observed for a signal power of -10 dBm are similar to the ones discussed above. For a higher PCIP, the point at which the maximum amount of energy has been transferred to the signal for these specific wavelengths, is reached earlier; thereafter, the signal starts losing gain as its energy starts being transferred back to the pump.

### 2.3.3 Gain as a Function of Pump Power

Subsequently, we vary the pump power and we examine its effect on the gain bandwidth and the peak of the gain spectrum. The pump powers used are 0.6 W, 1 W, 1.4 W and 1.8 W.

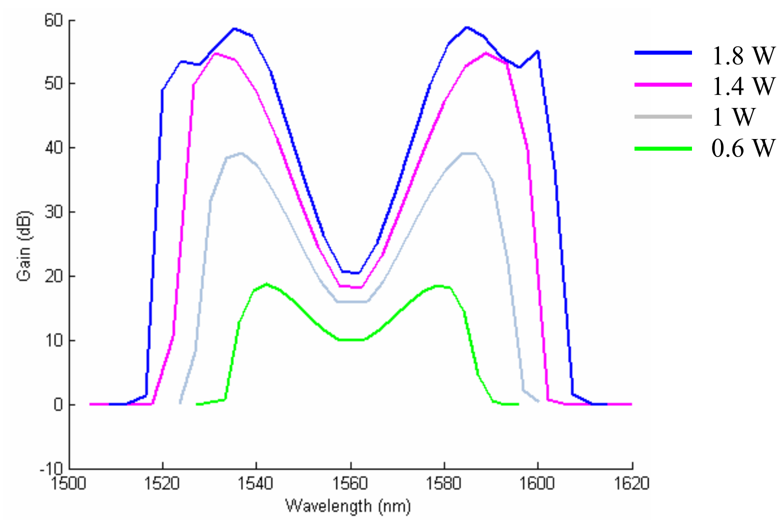


**Fig. 2.9** Gain as a function of wavelength for pump powers of 0.6 W, 1 W, 1.4 W and 1.8 W.

The input signal power used is -30 dBm and as we see in Fig. 2.9, increasing the pump power does not result in an indefinite increase in gain for a fixed amplifier length. However, we observe an increase of the gain around the pump wavelength as well as an increase of the gain bandwidth as predicted [2.32]. More specifically, from Eqs. (2.3) and (2.4), it follows that for a fixed $\lambda_p$, the gain spectrum will be formed in two lobes on each side of $\lambda_p$, with each lobe having its peak gain for a phase mismatch

$$\Delta\beta + \gamma\,(2P_p - P_s - P_i) = 0 \Rightarrow \gamma\,(2P_p - P_s - P_i) = -\Delta\beta \propto (\lambda_p - \lambda_0)(\lambda_p - \lambda_s) \quad \text{(Eq. 2.5).}$$

Hence, the separation between the two peaks (and thus the gain bandwidth) will increase with $P_p$ for a fixed $\lambda_p$.

### 2.3.4 Gain for Constant $P_p{\cdot}L$ Product

For the special case of no pump depletion the analytical expression described in [2.32] tells us that the two peak gains are $\gamma{\cdot}P_p{\cdot}L$. To illustrate this, in Fig. 2.10 we plot the gain spectrum for four different combinations that give us a constant pump power - amplifier length product (as long as $\gamma$ is kept constant): $0.7\times1000$ W·m, $1.4\times500$ W·m and $2.8\times250$ W·m.

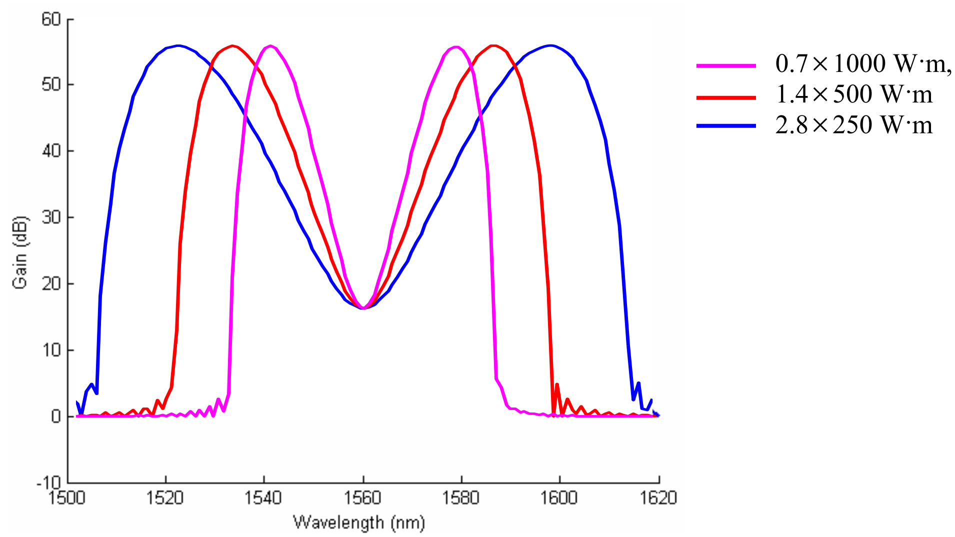


**Fig. 2.10** Gain as a function of wavelength for $\gamma{\cdot}P_p$ products of $0.7\times1000$ W·m, $1.4\times500$ W·m and $2.8\times250$ W·m.

Ostensibly, by keeping the product $\gamma{\cdot}P_p{\cdot}L$ constant, we get equal maximum gain, albeit with an increased bandwidth as predicted by Eq. (2.5).

### 2.3.5 Gain as a Function of Dispersion Slope

Next, we examine the effect of the dispersion slope $S = \dfrac{dD}{d\lambda}$ on the gain spectrum. The values we use for $S$ are 0 ps/(nm$^2$·km), 0.01 ps/(nm$^2$·km), 0.03 ps/(nm$^2$·km), 0.05 ps/(nm$^2$·km) and 0.07 ps/(nm$^2$·km). The input signal power is -30 dBm.

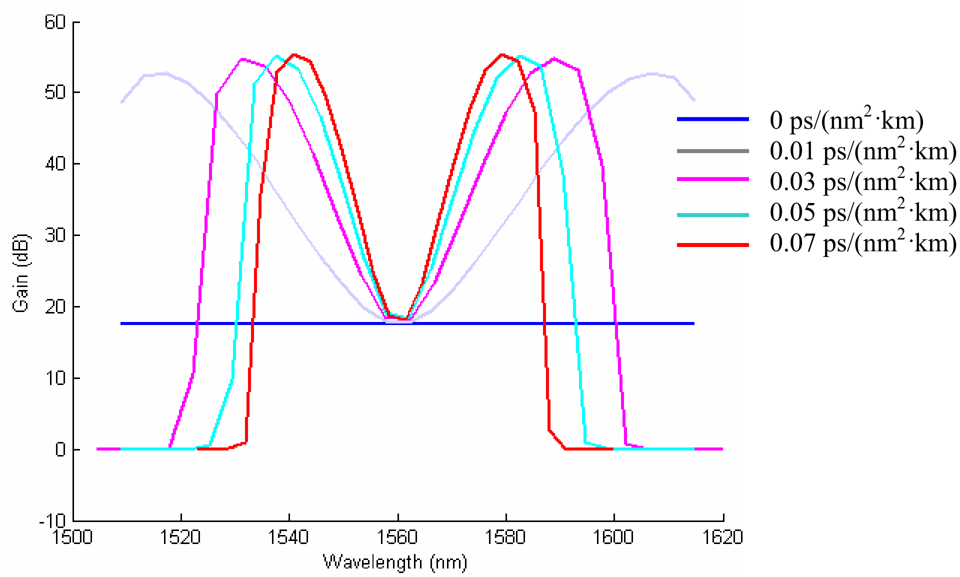


**Fig. 2.11** Gain as a function of wavelength for a dispersion slope value of 0 ps/(nm$^2$·km), 0.01 ps/(nm$^2$·km), 0.03 ps/(nm$^2$·km), 0.05 ps/(nm$^2$·km) and 0.07 ps/(nm$^2$·km).

As the dispersion slope decreases, the gain spectrum becomes wider. However, while the peak gain slightly decreases, the minimum around $\lambda_p$ remains constant. When $S$ becomes zero the gain turns out to be independent of the signal wavelength, as expected. Note that in the above simulations, $S > 0$. On the other hand, if we further decrease the dispersion slope and make it negative, then the gain spectrum shape is completely altered. Fig. 2.12 below shows this dramatic change.

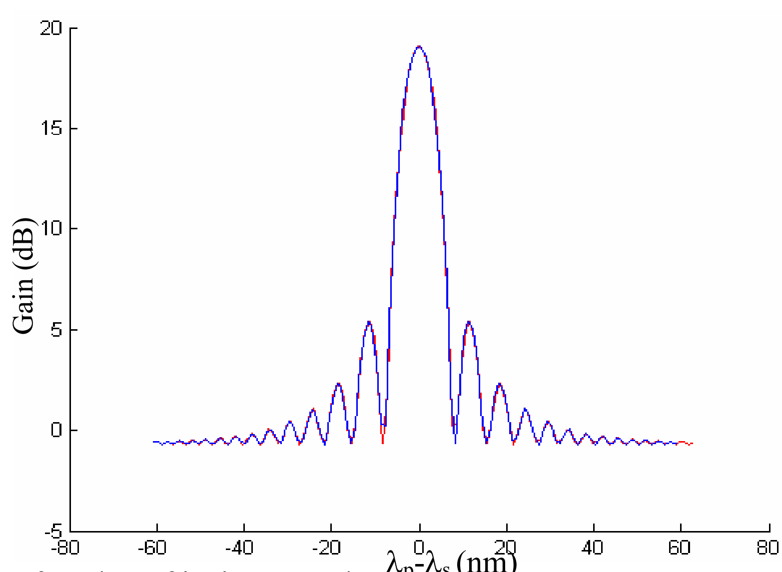


**Fig. 2.12** Gain as a function of $\lambda_p$-$\lambda_s$ separation.

When the pump is positioned in the anomalous dispersion regime and $S$ is positive, then from Eq. (2.5) we can see that the gain bandwidth increases as $S$ approaches zero. This happens because $\Delta\beta$ is very small over a greater wavelength range and thus parametric amplification is efficient over a greater bandwidth. For $S = 0$, the phase mismatch $\Delta\beta$ becomes zero for every wavelength and thus the gain is constant and equal for all wavelengths. When $S$ becomes negative, then the gain spectrum changes shape and becomes much narrower. The opposite is true for when the pump is placed in the normal dispersion regime.

More specifically, in Fig. 2.13a we see the variation of $\Delta\beta$ as a function of $\lambda_p$-$\lambda_s$ when $\lambda_p$ = 1557.3 nm. The red line is for $\frac{dD}{d\lambda}$ = 0.03 ps/(nm$^2$·km) and the blue line is for $\frac{dD}{d\lambda}$ = -0.03 ps/(nm$^2$·km). In Fig. 2.13b we see the variation of $\Delta\beta$ as a function of $\lambda_p$-$\lambda_s$ separation when $\lambda_p$ = 1560.7 nm. This time, the red line is for $\frac{dD}{d\lambda}$ = -0.03 ps/(nm$^2$·km) and the blue is for $\frac{dD}{d\lambda}$ = 0.03 ps/(nm$^2$·km).

a)

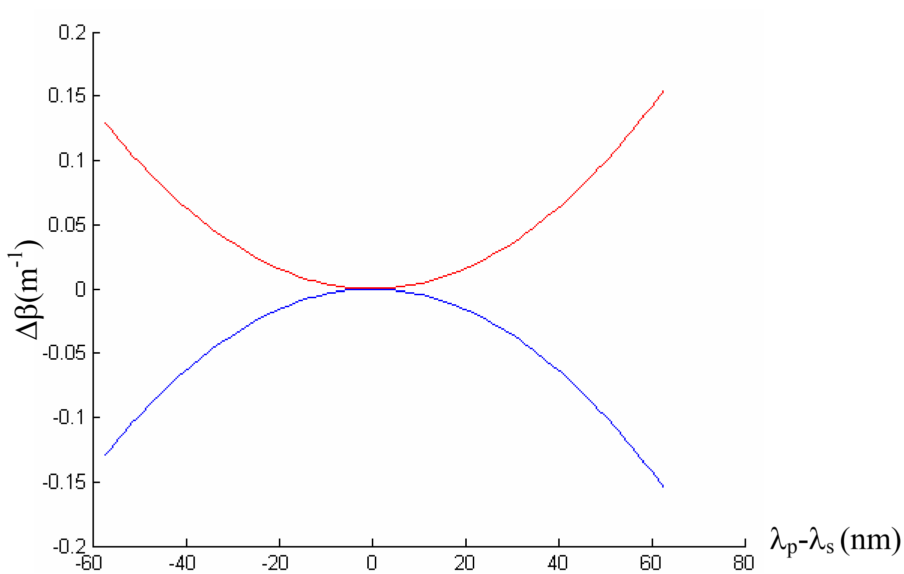

b)

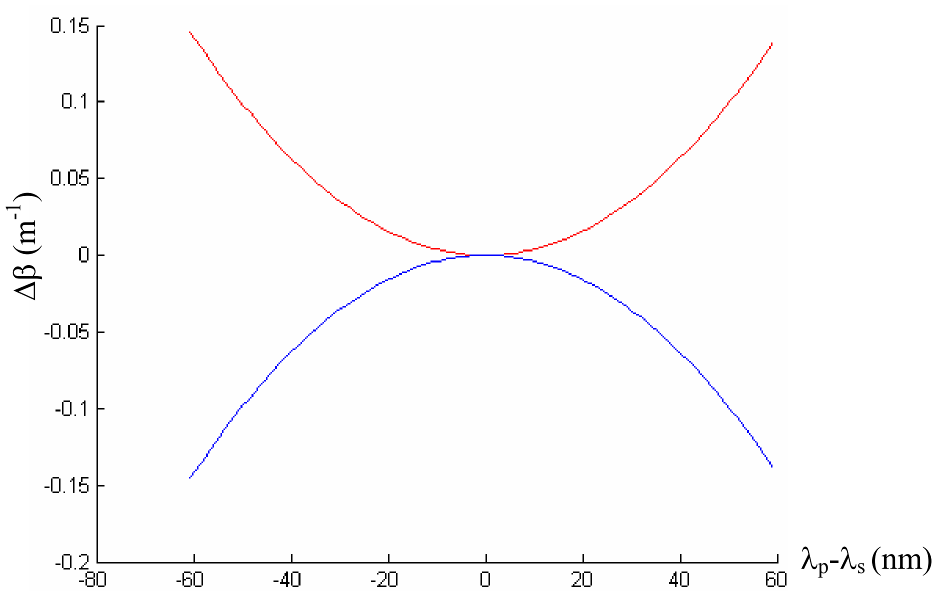


**Fig. 2.13** $\Delta\beta$ as a function of $\lambda_p$-$\lambda_s$ separation when a) $\lambda_p$ = 1557.3 nm and, for $\frac{dD}{d\lambda}$ = 0.03 and -0.03 ps/(nm$^2$·km) (red and blue accordingly) and b) $\lambda_p$ = 1560.7 nm for $\frac{dD}{d\lambda}$ = 0.03 and -0.03 ps/(nm$^2$·km) (blue and red accordingly).

Assuming $\frac{dD}{d\lambda} > 0$, if $\lambda_p$ is positioned in the normal dispersion regime ($\lambda_p < \lambda_0$), the accumulated phase mismatch ($\Delta\beta$) will increase with increasing signal wavelength $\lambda_s$, thereby decreasing the efficiency of parametric amplification. By positioning the pump wavelength in the anomalous dispersion regime, $\Delta\beta$ becomes negative. Then it is possible to compensate for the non-linear phase mismatch $\gamma(2P_p - P_s - P_i)$ by the linear phase mismatch $\Delta\beta$ as seen in Eq. 2.5. Fig. 2.14 summarises the gain spectrum, the dispersion slope and the dispersion, helping us visualise the relationships discussed above..

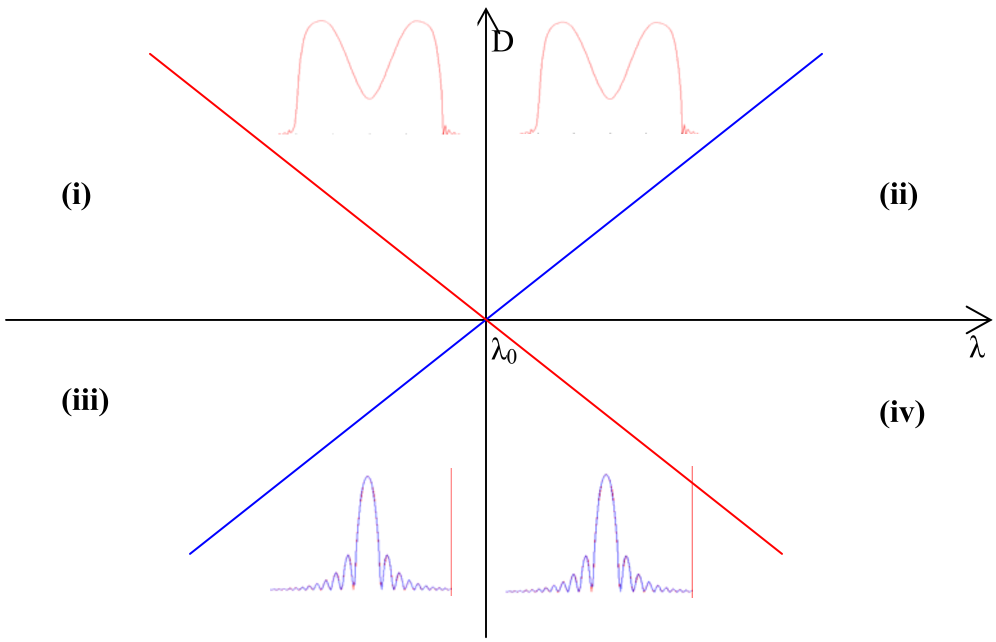


**Fig. 2.14** Visualization of the dependence of the gain spectrum shape on the dispersion slope sign and the position of $\lambda_p$ relative to zero-dispersion wavelength. The insets show the corresponding gain spectrum.

There are four areas of interest. In area (i) and (ii), $D$ is positive while $S$ is negative in (i) and positive in (ii). On the other hand, in areas (iii) and (iv), $D$ is negative and $S$ is positive in (iii) and negative in (iv). Therefore, in (i) and (ii), for $\lambda_p = \lambda_0 \pm \Delta\lambda$, the same gain spectrum is obtained. Regardless of where $\lambda_p$ is placed, when $D$ is positive, blue wavelengths will travel faster and thus the transfer of energy from $\lambda_p$ to $\lambda_s$ will have similar characteristics. Similarly, when $D < 0$, red wavelengths will travel faster and the gain characteristics of areas (iii) and (iv) will again be similar. The shape of the gain spectrum of a FOPA depends on the sign of $D$ at the wavelength where $\lambda_p$ is placed.

To further strengthen our argument, in Fig. 2.15 we demonstrate the power evolution of the idler and the signal throughout the fibre for a) $\lambda_p$ = 1558 nm, $\lambda_s$ =1554 nm and b) $\lambda_p$ = 1560 nm, $\lambda_s$ =1564 nm, for $S = \pm$ 0.03 ps/(nm$^2$·km). In other words, in each case, the pump and the signal are placed anti-diametrically about the zero-dispersion wavelength.

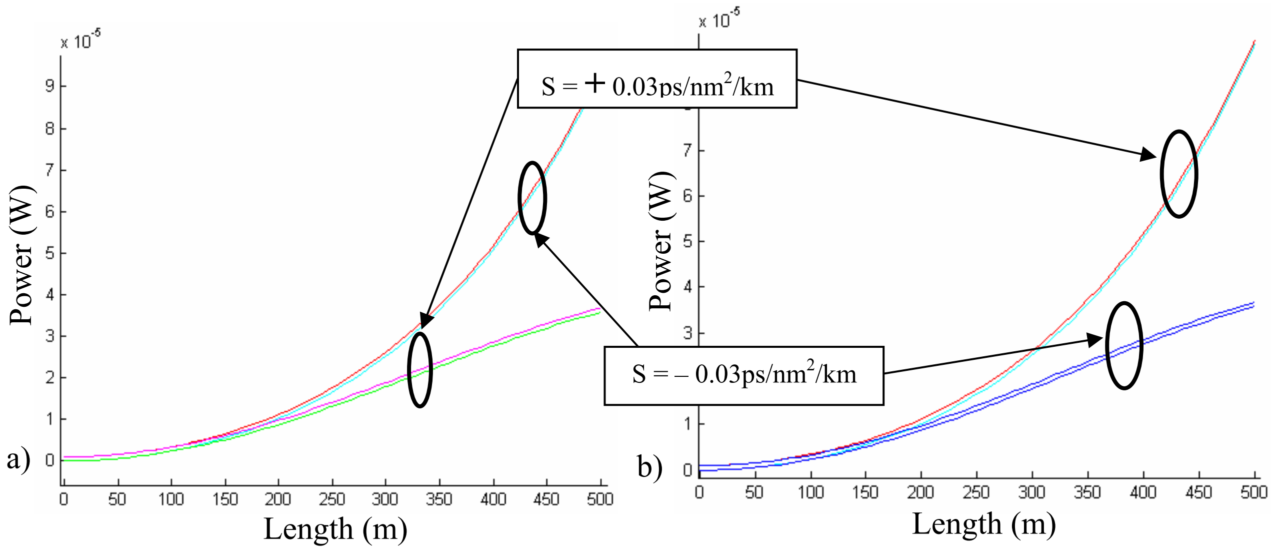


**Fig. 2.15** Power evolution of the idler (bottom line of each pair) and the signal (top line of each pair) throughout the fibre for a) $\lambda_p$ = 1558 nm, $\lambda_s$ =1554 nm and b) $\lambda_p$ = 1560 nm, $\lambda_s$ =1564 nm, for $S = \pm$ 0.03 ps/(nm$^2$·km).

As we see, the graphs are identical which shows why the gain is also identical in both cases. Put differently, as long as the pump experiences the same amount of dispersion and the signal is placed at the same distance from the pump, the power evolution, and thus the gain characteristics of the amplifier, will be identical.

### 2.3.6 Power Evolution in the Fibre

Finally, in order to demonstrate the transfer of energy from the pump to the signal and idler, in Fig. 2.16, we present the power evolution for a 2 km long amplifier with $\lambda_s$ = 1534 nm. In this case, we assume that the fibre attenuation is equal to zero.

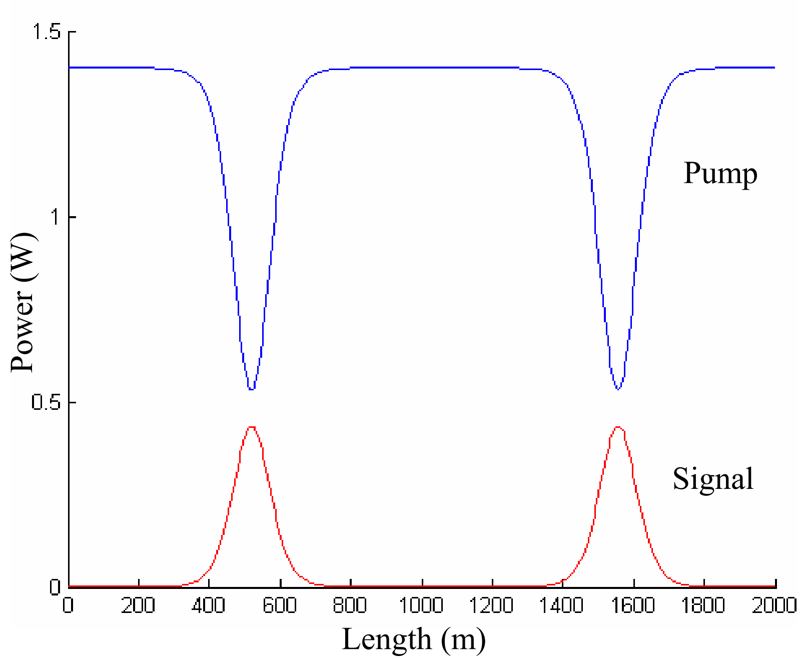


**Fig. 2.16** Power evolution of pump (blue) and signal (red) in 2 km of HNLF for λs = 1534 nm. As we see, the exchange of energy between the signal and the pump is periodic, as expected. The maximum power for the signal is achieved 518 m in the fibre and then again at 1556 m.

## *2.4 Summary*

In this chapter, we have summarized several key achievements in the field of FOPAs during the last few years. We presented the advantages that can be garnered by using FOPAs in optical telecommunication networks, but we also presented their drawbacks. Many investigations have focused on determining the characteristics of FOPAs. Several methods have been proposed to alleviate many of these shortcomings bringing us closer to a practical FOPA design. However, many of them have not been adequately investigated.

In particular, while multi-channel configurations have been demonstrated and their setbacks well documented (several of which have been solved), these studies focused on networks operating under fixed conditions, i.e., the networks are not assumed to be packet-switched and thus, the number of channels and the PCIP are considered to be constant.

In addition, in this chapter, we tried to give a complete picture about the characteristics of FOPAs and the theory behind parametric amplification. We presented their behaviour and the dependence of their performance on several parameters such as the pump power, input signal power, fibre dispersion, etc. Having acquired a concrete idea about how FOPAs work and what their current status is, we now proceed, with the investigation on the suitability of FOPAs within the context than of an agile, reconfigurable network.

It should be noted that the above results presented in the present chapter were subsequently also verified with published results as well as with the Optisystem™ simulation package that is used in the rest of this thesis in order to perform the theoretical study of FOPAs. The simulation package is described in greater detail in Chapter 3 of this thesis.

**References**

[2.1] G.P Agrawal, *Nonlinear fiber optics*, second edition, Academic Press, San Diego, USA, (1995).

[2.2] M. Onishi, T. Okuno, T. Kashiwada, S. Ishikawa, N. Akasaka and M. Nishimura, "Highly nonlinear dispersion-shifted fibers and their application to broadband wavelength converter", Optical Fiber Technology, vol. 4, no. 2, pp. 204-214, (1988).

[2.3] J. Hansryd, P. A. Anderkson, M. Westlund, J. Li and P. O. Hedekvist, "Fibre-based optical parametric amplifiers and their applications", IEEE Journal of Selected Topics in Quantum Electronics, vol. 8, no. 3, (2002).

[2.4] R.H. Stolen and J. Bjorkholm, "Parametric amplification and frequency conversion in optical fibres", IEEE Journal of Selected Topics in Quantum Electronics, vol. 18, pp. 1062-1072, (1982).

[2.5] S. K. Korotky, P. B. Hansen, L. Eskildsen and J. J. Veselka, "Efficient phase modulation scheme for suppressing stimulated Brillouin scattering", Conference of Integrated Optics and Optical Fiber Communication, paper WD2-1, Hong Kong, China, June 26 - 30 (1995).

[2.6] S. Radic, R. M. Jopson, A. Gnauck, C. J. McKinstrie, J. C. Centanni and A. R. Chraplyvy, "Stimulated-Brillouin-scattering suppression using single modulator in two-pump parametric architectures", Optical Fibre Communications, paper OWN5, Anaheim, USA, March 6 (2005).

[2.7] C. McKinstrie, M. Yu, M. G. Raymer and S. Radic, "Quantum noise properties of parametric processes", Optics Express, vol. 13, pp. 4986-5012, (2005).

[2.8] M. E. Marhic, G. Kalogerakis and L. G. Kazovsky, "Current status of fiber optical parametric amplifier", Society of Photographic Instrumentation Engineers, vol. 6014, pp. 5-10, (2005).

[2.9] C. M. Caves, "Quantum limits on noise in linear amplifiers", Physical Review D, vol. 26, pp. 1817–1839, (1981).

[2.10] A. Mecozzi and P. Tombesi, "Parametric amplification and signal-to-noise ratio in optical transmission lines", Optics Communications, vol. 75, pp. 256–262, (1990).

[2.11] D. Levandovsky, M. Vasilyev and P. Kumar, "Near-noiseless amplification of light by a phase-sensitive fibre amplifier", Indian Academy of Sciences Journal of Physics, vol. 56, no.2, (2001).

[2.12] K. Bencheikh, O. Lopez, I. Abram and J. A. Levenson, "Improvement of photodetection quantum efficiency by noiseless optical preamplification", Applied Physics Letters, vol. 66, pp. 399, (1995).

[2.13] G. Kalogerakis, K. Shimizu, M. E. Marhic, K. K.-Y. Wong, K. Uesaka and L. G. Kazovsky, "High-repetition-rate pulsed-pump fiber OPA for amplification of communication signals", Journal of Lightwave Technology, vol. 24, no. 8, pp. 3021, (2006).

[2.14] E. S. Nazemosadat, P. P. Shum and X. Xiaosheng, "Controlling higher order dispersion in a single pump optical parametric amplifier", Opto-Electronics and Communications Conference, paper 4610336, Sydney, Australia, July 7 - 10 (2008).

[2.15] M. C. Ho, K. Uesaka, M. E. Marhic, Y. Akasaka and L. G. Kazovsky , "200-nm-bandwidth fiber optical amplifier combining parametric and raman gain", Journal of Lightwave Technology, vol. 19, no. 7, pp. 977-981, (2001).

[2.16] S. Radic, C. J. McKinstrie, R. M. Jopson, J. C. Centanni, Q. Lin and G. P. Agrawal, "Record performance of parametric amplifier constructed with highly nonlinear fiber", Electronics Letters, vol. 39, pp. 838-839, (2003).

[2.17] K. C. Byron, M. A. Bedgood, A. Finney, C. McGauran, S. Savory and I. Watson, "Shifts in zero dispersion wavelength due to pressure, temperature and strain in dispersion shifted singlemode fibres", Electronics Letters, vol. 28, no. 18, pp. 1712–1714, (1992).

[2.18] J. M. Chavez Boggio, J. D. Marconi and H. L. Fragnito, "Double-pumped fiber optical parametric amplifier with flat gain over 47-nm bandwidth using a conventional dispersion-shifted fiber", Photonics Technology Letters, vol. 17, no. 9, pp. 1842–1844, (2005).

[2.19] M. Gao, C. Jiang, W. Hu and J. Wang, "Two-pump fiber optical parametric amplifier with three-section fibers allocation", Optics and Laser Technology, vol. 38, pp. 186–191, (2006).

[2.20] H. Y. Chen, Z. X. Zhang, M. H. Sang and L. Zhan, "Gain characteristic of a dual-pump fiber-optical parametric amplifier with a highly nonlinear fiber", Laser Physics, vol. 18, no. 8, pp. 983–987, (2008).

[2.21] F. C. Yang, M. C. Ho, M. E. Marhic and L. G. Kazovsky, "Demonstration of two-pump fibre optical parametric amplification", Electroncs Letters, vol. 33, no.2, pp. 1812–1813, (1997).

[2.22] J. M. Chavez Boggio, F. A. Callegari, S. Tenenbaum and H. L. Fragnito, "Demonstration of 26 dB on-off gain of a two-pump fiber optical parametric amplifier", Optical Fibre Communications, paper ThGG18, Anaheim, USA, March 17 - 22 (2002).

[2.23] M. Gao, C. Jiang, W. Hu and J. Wang, “Optimized design of two-pump fiber optical parametric amplifier with two-section nonlinear fibers using genetic algorithm”, Optics Express, vol. 12, pp. 5603-5613, (2004).

[2.24] J. M. Chávez Boggio, P. Dainese and H. L. Fragnito, "64 x 10 Gb/s DWDM system using two-pump fiber optical parametric pre-amplifier", IEEE Laser and Electro-Optics Society Annual Meeting, paper WQ 3, Glasgow, Scotland, UK, (2002).

[2.25] J. M. Chavez Boggio, E. A. M. Fagotto, M. E. Marhic, F. A. Callegari and H. L. Fragnito, “Amplification of 12 x 10 Gb/s WDM signals with negligible FWM crosstalk in a double-pumped fiber optical parametric amplifier”, Optics Communications, vol. 280, no. 2, pp. 468-471, (2007).

[2.26] T. Torounidis, H. Sunnerud, P. Hedekvist and P. A. Andrekson, “Amplification of WDM signals in fiber-based optical parametric amplifiers”, Photonics Technology Letters, vol. 15, pp. 1061-1063, (2003).

[2.27] K. Krastev and J. Rothman, “Crosstalk in fiber parametric amplifier”, European Conference on Optical Communication , paper We.L.3.5, Amsterdam, Netherlands, September 30 - October 4 (2001).

[2.28] F. Forghieri, R. W. Tkach, A. R. Chraplyvy and D. Marcuse, “Reduction of four-wave mixing crosstalk in WDM systems using unequally spaced channels”, Photonics Technology Letters, vol. 6, no. 6, (1994).

[2.29] A. Mussot, E. Lantz, A. Durecu-Legrand, C. Simonneau, D. Bayart, H. Maillotte and T. Sylvestre, “Simple methods for crosstalk reduction in fiber optical parametric amplifiers”, Optics Communications, vol. 275, no. 2, pp. 448-452, (2007).

[2.30] J. L. Blows, “Design strategy for controlling four-wave mixing-induced crosstalk between channels in a fibre optical parametric amplifier”, Optics Communications, vol. 236, no. 1-3, pp. 115-122, (2004).

[2.31] B. P. -P. Kuo, P. C. Chui, K. K. Y. Wong, "A comprehensive study on crosstalk suppression techniques in fiber optical parametric amplifier by modulation format," IEEE Journal of Selected Topics in Quantum Electronics, vol.14, no.3, pp. 659-665, (2008).

[2.32] M. E. Marhic, Y. Park, F. S. Yang, and L. G. Kazovsky, “Broadband fibre optical parametric amplifiers”, Optics Letters, vol. 21, pp. 573-575, (1996).

# Chapter 3 Quasi static analysis of discrete FOPAs

## *3.1 Introduction*

Developments in the required component technologies, such as HNLF with specific dispersive properties and high-power pump sources which allow for high gains over a broad range of wavelengths (and centred at any wavelength) using relatively short lengths of fibre [3.1]-[3.5], have motivated the research on FOPAs that we described in Chapter 2. As we saw, multi-wavelength amplification has also been a topic of active research and studies have focused on optimizing amplifier parameters, such as fibre dispersion and pumping configuration (especially multiple pumps) in order to obtain a flattened gain spectrum for a specific operating condition, i.e., for a fixed number of channels or wavelengths operating at a specific input power [3.6]-[3.9]. However, there have been no detailed reports on their steady-state gain characteristics nor their dynamic response.

In agile, multi-wavelength networks, the number of input channels to an amplifier can vary in response to bandwidth demand or as a result of network reconfiguration. Even if the amplifiers operate near saturation such that the total output power is approximately constant, the gain experienced by each channel will depend on the number of input channels. Channel add/drop will induce time-varying perturbations to surviving wavelengths via transient cross-saturation effects. As a result, it is important to analyze both the quasi-state gain variations and transient responses of FOPAs that accompany changes in amplifier operating conditions such as number of channels, PCIP or TIP, and channel add/drop.

In a packet-switched network, different packets of data arrive at amplifiers after having travelled different paths or experienced different amounts of transmission impairments. As a result, the power level of the input signals (at different wavelengths) will vary on a packet-to-packet basis. These power variations can cause gain transients which, in turn, can degrade system performance. That is why the ability of FOPAs to provide a constant gain under such operating conditions has to be evaluated.

The remainder of this Chapter is organized as follows. In section 3.2, we define the amplifier configuration, simulation model, and the different operating scenarios considered. In section 3.3, we present the results of our simulations. We begin with the steady-state behaviour of FOPAs and examine the dependence of the gain spectrum on the number of WDM channels and the channel spacing. Furthermore, we study the changes in the gain spectrum as a function of PCIP and as a result of channel add/drop. Next, we consider the transient response of the surviving channels following channel add/drop. In section 3.4, we analyse a realistic scenario in a packet switched network wherein the power of the channels varies periodically with the packet period. We investigate the effect of these power variations on a probe channel with constant input power.

## *3.2 Simulation parameters*

Fig. 3.1 illustrates the FOPA under investigation. An array of DFB lasers are coupled together through a WDM coupler and are subsequently coupled into a length of HNLF along with the pump. The pump laser is phase modulated and is afterwards amplified using an EDFA. A BPF at the output of the EDFA is used to eliminate any ASE noise that has been introduced. After the amplification process has taken place throughout the HNLF, the WDM channels are selected by placing a BPF at the output of the amplifier, discarding the pump and the generated idlers.

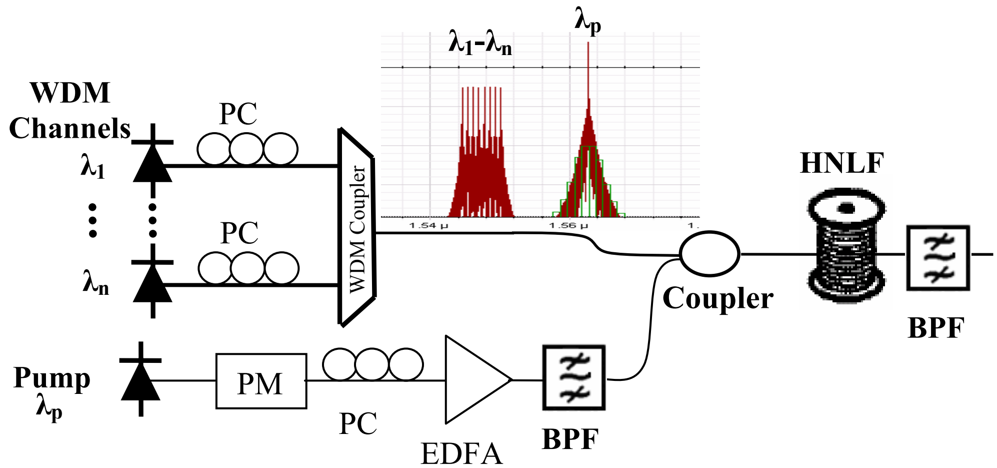


**Fig. 3.1** FOPA topology. PM: phase modulator, HNLF: highly nonlinear fibre, BPF: bandpass filter. The inset shows the position of the pump and WDM channels relative to each other.

Table 3.1 summarizes the parameters of the HNLF and of the pump used in all subsequent simulations unless otherwise stated.

**Table 3.1** FOPA parameters used in simulations

| **Fibre Length** $L$ **(km)** | **Non-Linearity Parameter** $n_2$ **(m$^2$/W)** | **Effective Area** $A_{eff}$ **(μm$^2$)** | **Zero Dispersion Wavelength** $\lambda_0$ **(nm)** | **Dispersion Slope** $S$ **(ps/nm2/km)** | **Pump Power** $P_p$ **(W)** | **Pump Wavelength** $\lambda_p$ **(nm)** |
|---|---|---|---|---|---|---|
| 0.25 | $2.6\times10^{-20}$ | 9.5 | 1559 | 0.03 | 1 | 1560.3 |

Note that in our investigation, the amplifier parameters are not optimized in terms of obtaining a flat gain spectrum. Moreover, it is possible to use a gain flattening filter (GFF) so that each WDM channel receives the same gain. However, the GFF is a purely passive device and hence, the actual dynamics and interactions within the FOPA will not be affected. Only the specific values of the gain variations will differ about the gain value set by the GFF, i.e., if we design the FOPA to provide > 16 dB gain for all channels and then use a GFF so that all channels see the same gain (16 dB), then the gain changes will be centred about this gain. The results and conclusions obtained in our simulations are still applicable.

The WDM signals are not modulated with data; therefore, the results we present pertain to CW operating conditions, as is commonly the case when performing similar studies of other amplifier technologies. We simulate the steady-state and dynamic responses of the FOPA by solving numerically the nonlinear coupled Schrödinger equations using the commercial software package OptiSystem™ (Optiwave). The coupled nonlinear Schrödinger equations are solved by using the symmetrised non-iterative split-step Fourier method.

Since the pump wavelength is longer than the signal wavelengths, simulations show that ignoring stimulated Raman scattering (SRS) will result in an error of less than 1%. We have also chosen to ignore SBS, whose threshold can be increased by broadening the pump spectrum through phase modulation. We also ignore polarization dependent effects for simplicity. In practise polarization controllers are needed for the signals as the FWM processes is polarization dependent. Furthermore, in practise, two orthogonally polarized pumps are lunch into the FOPA in order to eliminate polarization dependent effects. The error tolerance for the simulations is set to approximately 2% to reduce computation time. We have verified the accuracy of the model by comparing our results to other published experimental results and have found them to agree to a great extent. Moreover, Karásek *et al.* have performed a rigorous comparison of experimental and simulation results on parametric amplification using the OptiSystem software, demonstrating the good accuracy of the model [3.10].

**Table 3.2** Amplifier operating conditions considered in this study.

| Number of WDM channels | Spacing between WDM channels (GHz) | Input power per channel (dBm) | **Surviving channels** |
|---|---|---|---|
| 16 | **100,200** | **-30** | All |
| 32 | **50,100** | **-20** | First 1/4 |
| 64 | **50** | **-10** | Last 1/4 |
| | | **-6** | Middle 1/4 |
| | | **-3** | First ½ |
| | | | Last ½ |

Table 3.2 summarizes the different amplifier operating conditions (we only present typical and illustrative results for some of these scenarios). In our study, we investigate the behaviour of FOPAs under the most unfavourable conditions, i.e. we consider the worst-case scenario whereby, all channels are set to be in phase and have exact channel spacings. In this way, FWM and crosstalk are maximized as the newly generated FWM products overlap exactly on other WDM channels. In all cases, the first WDM channel is at 193.1 THz with the remaining channels increasing in frequency. For comparison, we also examine the cases where all of the channels have uniformly distributed random initial phases as well as normally distributed fluctuations in the channel spacing (this would correspond to the case in practical systems where different sources are used for the different channels).

We first consider the steady-state behaviour by examining the impact of channel number, spacing, PCIP, and the impact of channel add/drop on the gain spectrum. For evaluating the dynamic response, we consider the gain transients for a single surviving channel, i.e., in the worst possible case of channel add/drop. The add and drop operations are performed at 9 ns intervals, which is sufficient to allow the transients in the surviving channel to reach a steady state. We also examine the dynamic response for different locations of the surviving channel.

## 3.3 Steady-state and Quasi Steady-state Results

### 3.3.1 Steady-state Analysis

In this part of the investigation we are assuming a steady-state mode of operation. Once we change the operating conditions of the amplifier, we then evaluate the effect these conditions have at the output of the FOPA. In other words, we are examining the gain spectrum before and after channels have been dropped or added, when changing the channel spacing, or when changing the PCIP.

**Effect of PCIP and channel spacing on gain spectrum**

We begin by investigating the impact of increasing uniformly the PCIP on the amplifier gain spectrum. For illustration, we consider two input conditions that span the same total bandwidth, namely 32 × 100 GHz and 64 × 50 GHz.

a)

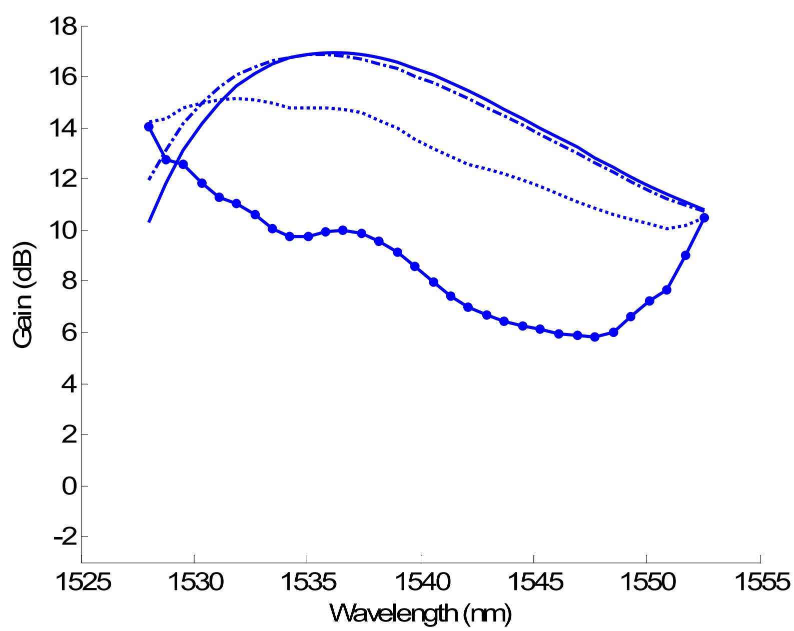


**Fig. 3.2** FOPA gain spectra as a function of PCIP for (a) 32 × 100 GHz system, (b) 64 × 50 GHz system and (c) 32 × 100 GHz with random initial phase and uneven channel spacing. PCIP: -30 dBm (solid), -20 dBm (dash-dot), -10 dBm (dotted), and -6 dBm (solid with dots).

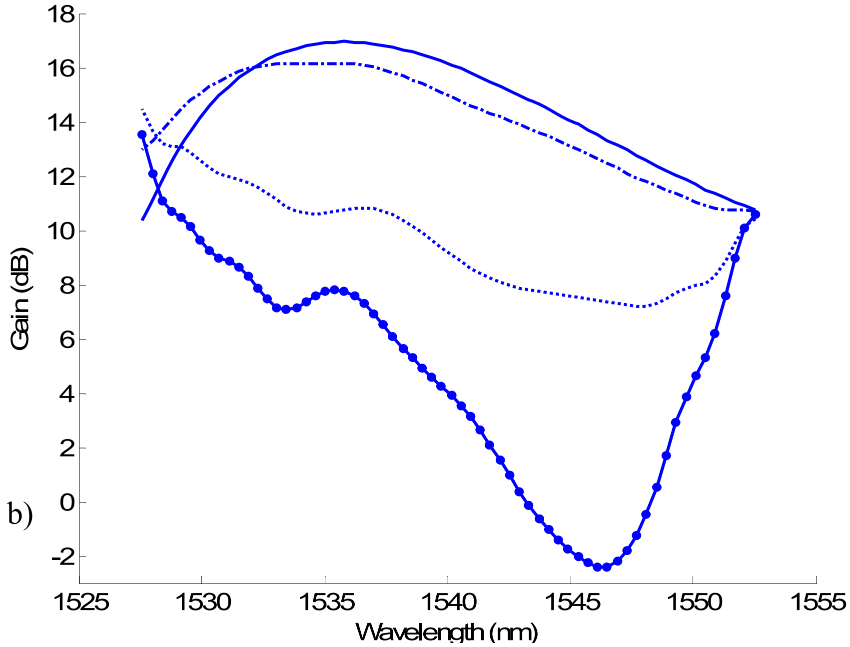


b)

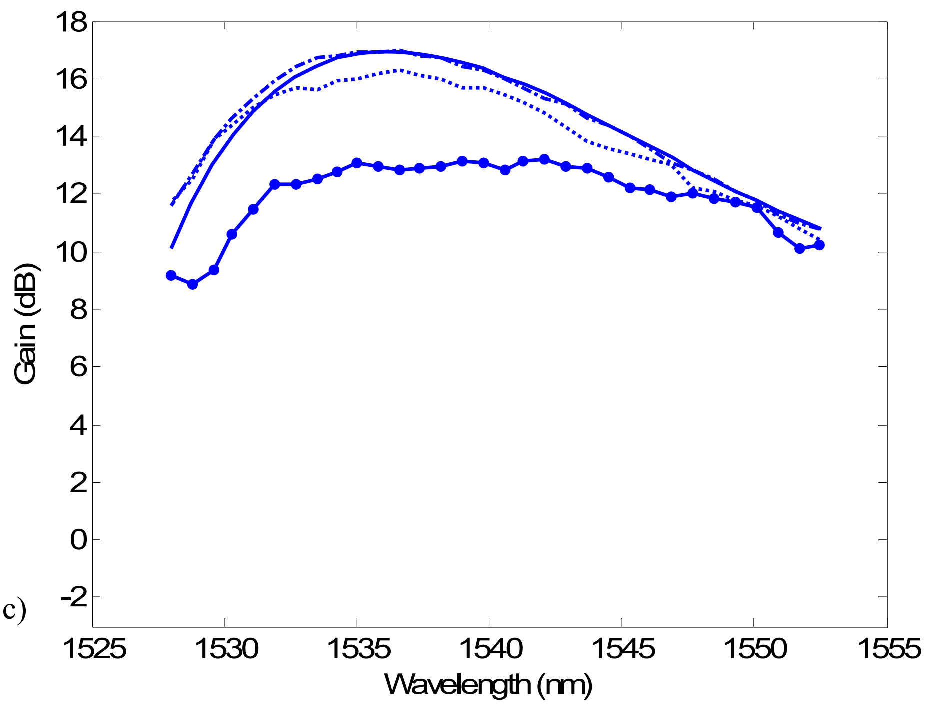


c)

**Fig. 3.2** (Continued) FOPA gain spectra as a function of PCIP for (a) 32 × 100 GHz system, (b) 64 × 50 GHz system and (c) 32 × 100 GHz with random initial phase and uneven channel spacing. PCIP: -30 dBm (solid), -20 dBm (dash-dot), -10 dBm (dotted), and -6 dBm (solid with dots).

Figs. 3.2(a) and 3.2(b) show the corresponding gain spectra for PCIPs ranging from -30 dBm to -3 dBm or -6 dBm. In both cases, most channels experience reduced gain as the PCIP increases from -30 dBm to -20 dBm, except for the shorter wavelengths which experience increased gain. As expected, the reduction in gain is greater for the 64 channel configuration since the pump is depleted faster due to the higher TIP and larger number of interactions between pump and signals. As the PCIP increases further, there are significant changes in the gain spectrum: for both systems, two dips at 1533 nm and 1547 nm appear and become more pronounced as the PCIP is increased beyond -6 dBm. We attribute this behaviour to a transfer of energy between these particular wavelengths and shorter wavelengths (which explains in part the increased gain for shorter wavelengths). These channels behave like pumps as they increase in power. In Fig. 3.2(c), we show the 32 × 100 GHz scenario, but this time all signals have random initial phases and as well as random fluctuations in channel spacing. The fluctuations are chosen according to uniform distributions and the results shown are averaged over 10 simulations comprising different initial phases, but the same channel spacings. As expected, the random phases and channel spacings create the following two effects: first, the strength of the interactions decrease and second, the FWM products do not fall exactly on other WDM channels. Nevertheless, the phenomena observed above still occur but to a lesser degree.

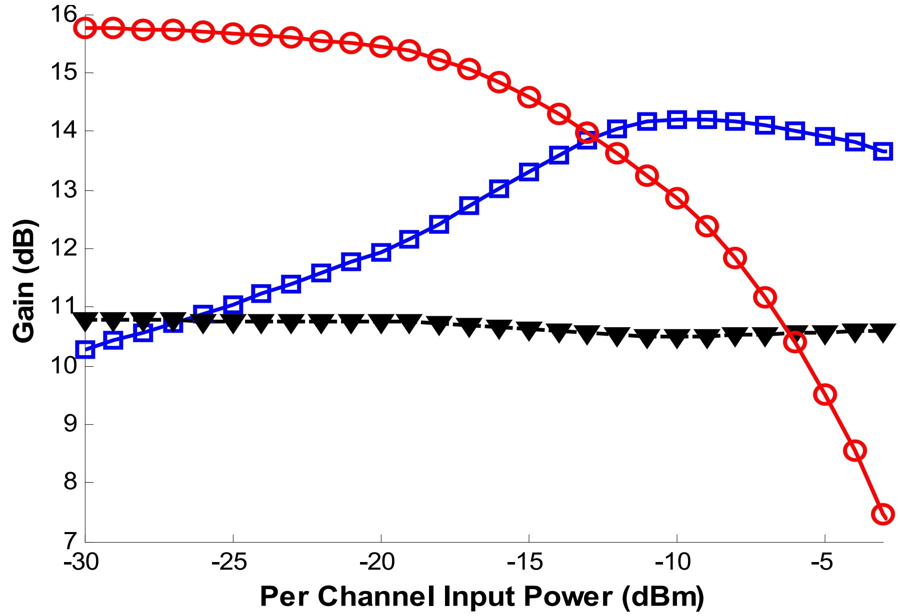


**Fig. 3.3** Gain as a function of PCIP for the WDM channel at the longest wavelength (solid triangles), shortest wavelength (hollow squares), and at midband (hollow circles) of a 32 × 100 GHz system.

Further insight can be obtained by examining the gain variation as a function of PCIP for different channels. For example, we consider the case of 32 × 100 GHz and examine the gain variation for three channels of the gain spectrum, two at the extremes (193.1 THz (1553.6 nm) and 196.2 THz (1529.05 nm)) and one at midband (194.6 THz (1541.62 nm)). As shown in Fig. 3.3, only the channel at midband exhibits the typical amplifier behaviour of decreasing gain with increasing PCIP. On the other hand, the extreme channels exhibit a more unexpected response. The longest wavelength has a relatively constant gain and is independent of the PCIP. Conversely, the shortest wavelength first increases in gain, peaks for a PCIP of around -10 dBm, then decreases due to saturation. As mentioned above, this behaviour is a result of the transfer of energy from middle to shorter wavelengths (i.e., channels far from the pump). This also demonstrates the fact that different wavelengths saturate at different rates and thus in

FOPAs, we can not define saturated or small signal regimes of operation for the whole amplification band in the same time, in accordance with [3.11].

**Effect of channel spacing and number of channels**

In order to make a direct and fair evaluation of the effect of channel spacing we simulate the following scenario: we change the number of channels and the channel spacing, while we keep the TIP and the total bandwidth constant.

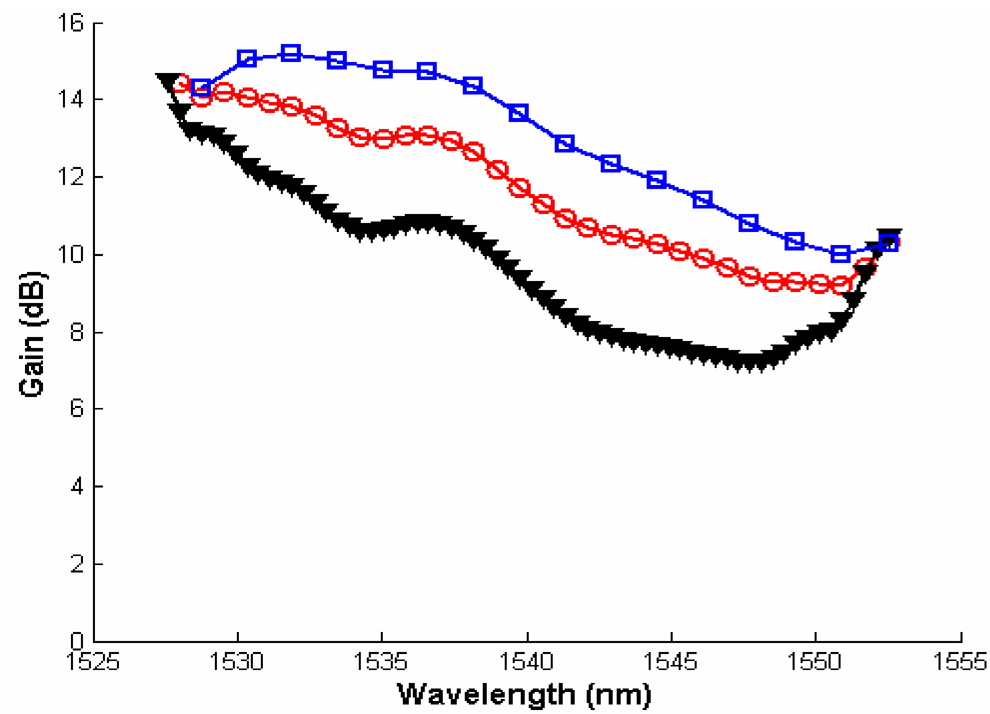


**Fig. 3.4** Gain spectrum of FOPA for 16 channels spaced at 200 GHz, 32 channels spaced at 100 GHz and 64 channels spaced at 50 GHz, preserving the same TIP (6.4 mW) and bandwidth (3.1 THz).

Fig. 3.4 illustrates the impact of channel spacing on the gain spectrum. Three configurations are considered, each spanning roughly the same bandwidth – (16-1)×200 GHz, (32-1)×100 GHz and (64-1)×50 GHz – and the same total input signal power of 6.4 mW – 16 × -4 dBm, 32 × -7 dBm and 64 × -10 dBm.  We consider also the worst case scenario where all channels are in phase and the spacings amongst them are exact.

The more sparsely spaced configuration, 16×200 GHz with a PCIP of -4 dBm, exhibits the largest gain: the peak gain is about 1.5 dB greater than the 32 channel configuration and more than 3.5 dB greater than the 64 channel configuration. This behaviour is expected due to the increase of the FWM interactions as signal spacing becomes narrower. In other words, when the spacing between two optical signals travelling in an optical fibre decreases, more FWM tones are generated [3.12], which deplete the pump and leave less power available to the WDM signals.

In the next scenario, we keep the TIP and the channel spacing constant and change the number of channels and the PCIP.

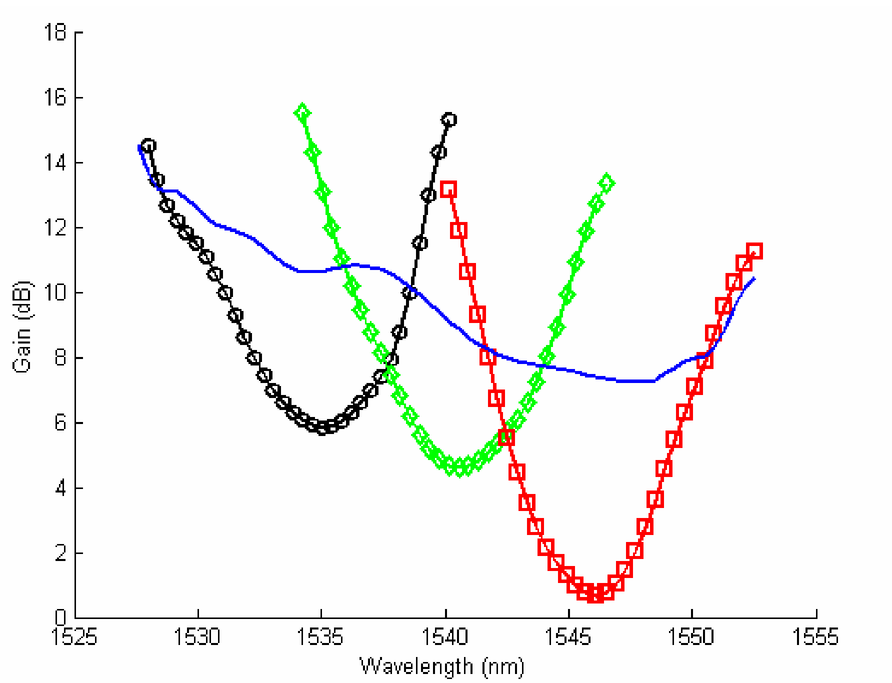


**Fig. 3.5** Gain spectrum when 64 channels with a PCIP of -10 dBm are present (blue solid line). The first 32 channels (black circles), the middle 32 channels (green diamonds) and the last 32 channels are present (red squares) with a PCIP of -7 dBm. In all cases the channel spacing is 50 GHz.

In the scenario presented in Fig. 3.5 three different configurations with 32 channels, having the same TIP, are presented: the channels occupy the first half, the middle half and the last half of the total spectrum. The PCIP is set at -7 dBm. In the same figure, the gain spectrum is shown for the scenario where all 64 channels are present in the amplifier. In this latter case the PCIP is set to be -10 dBm and thus equalling the TIP of the other scenarios. Clearly, the "**V**" shaped gain spectrum we observed in Fig. 3.2(b) is repeated here as well for all three configurations. Here, it should also be noted, that as it was shown in [3.13], one specific wavelength exists at which all pump power is symptotically converted to the signal and idler. Interestingly, this differs from the phase-matching condition $\Delta\beta = -2\gamma P_p$, which gives the wavelength with the largest initial gain. The signal wavelength yielding total pump conversion lies approximately halfway between the pump wavelength and the maximum-gain wavelength. Therefore, the transfer of energy from signal to signal also depends on their position, relative to the wavelength of maximum conversion.

The gain tilt between the three surviving bands that we observe is due to the dispersion slope. When the dispersion slope is set to zero, the "**V**" shaped gain spectrum becomes symmetrical for all cases. As noted before, the middle channels in every case, act as pumps in the newly formed gain spectrum losing power to the channels in both sides. This phenomenon clearly illustrates how the FWM interactions are stronger amongst neighbouring channels. In all three 32 channel scenarios, the extreme channels are increasing their gain compare to the case where all 64 channels are present, even if their PCIP is increased and the TIP remains constant. These observations are consistent with the results presented in Fig. 3.2.

### 3.3.2 Effect of Channel Add/Drop

Next, we analyze the impact of channel drop on the gain spectrum for the case of $64 \times 50$ GHz and a PCIP of -20 dBm.

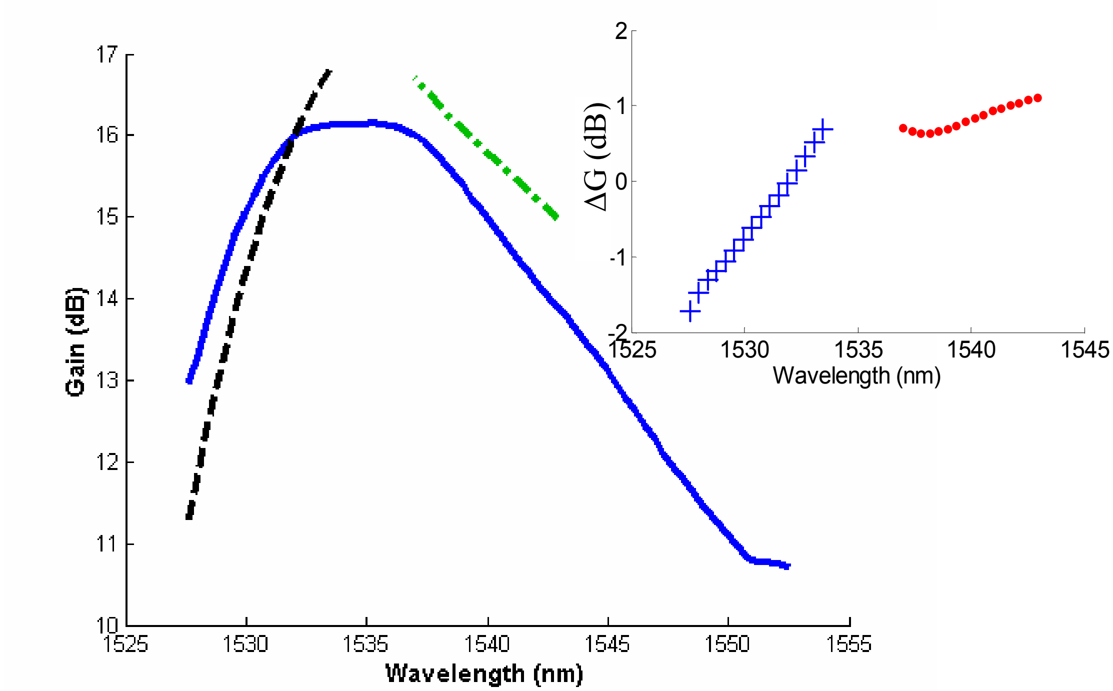


**Fig. 3.6** FOPA gain spectrum for a 64 × 50 GHz system with a PCIP of -20dBm when all channels are present (solid line), only the middle 16 channels survive (dotted-dashed line), and only the first 16 channels survive (dashed line). The inset shows the gain variation ΔG (in dB) relative to the case when all channels are present: the circles (crosses) correspond to the case when the middle (first) 16 channels survive.

Fig. 3.6 shows the steady-state gain spectrum when all 64 channels are present [same as in Fig. 3.2(b)], when only the middle 16 channels of the system survive, and when only the 16 channels at the shortest wavelengths survive. When the first and last 24 channels are dropped (48 channels dropped in total), there is more pump power available and as a result, the middle 16 surviving channels experience an increase in gain of ≈ 1 dB. On the other hand, quite unexpectedly, when the 48 channels at longer wavelengths are dropped, some of the surviving channels experience a *decrease* in gain (a maximum of -1.8 dB for the shortest wavelength) while others increase in gain. This is due to the fact that the transfer of energy from longer to shorter wavelengths no longer takes place since the former have been removed; this corroborates the results illustrated in Fig. 3.2 and Fig. 3.3.

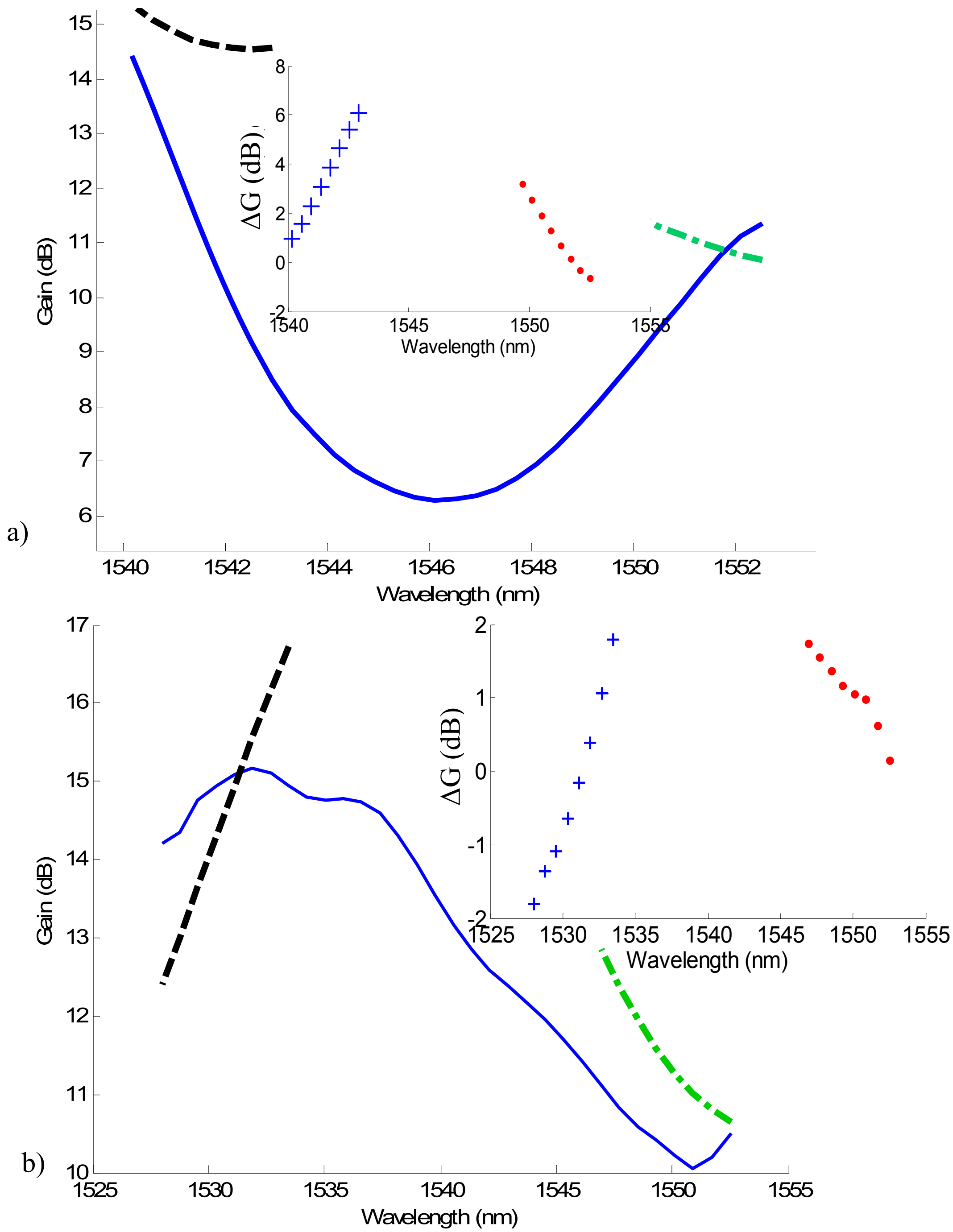


**Fig. 3.7** FOPA gain spectrum for (a) 32 × 50 GHz and (b) 32 × 100 GHz systems with a PCIP of -10 dBm when all 32 channels are present (solid line), the first 8 channels survive (dashed lines), and the last 8 channels survive (hollow squares). The inset shows the gain variation ΔG (in dB) relative to the case when all channels are present: the circles (crosses) correspond to the case when the last (first) 8 channels survive. (c) is similar to (b), but the channels have random initial phases.

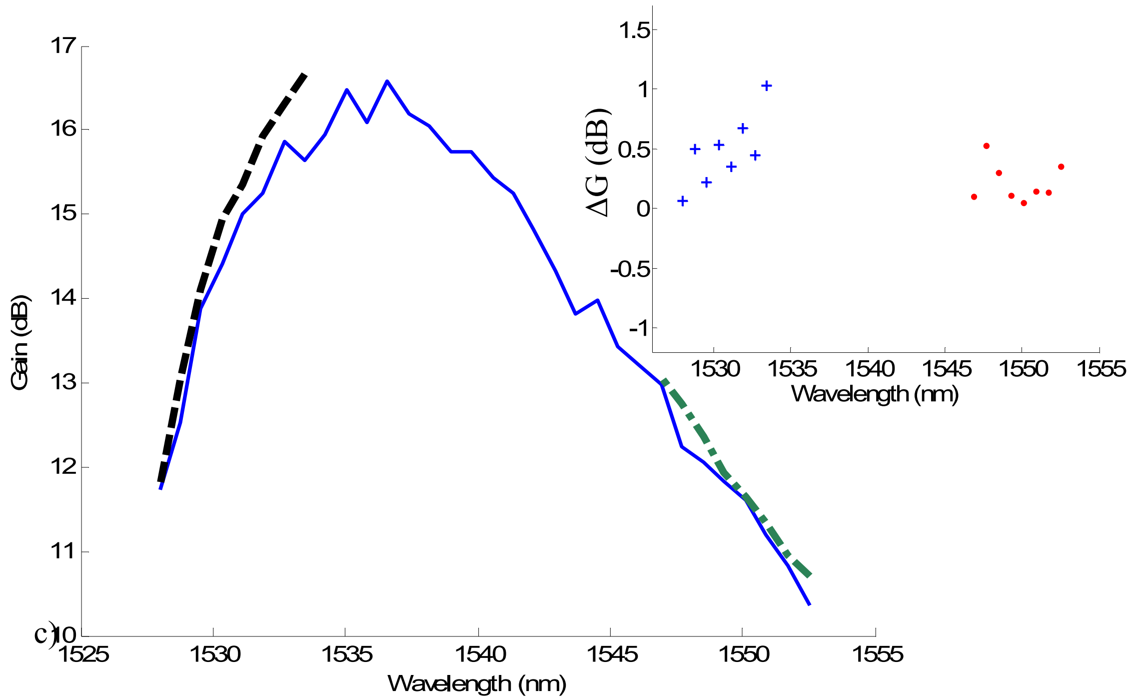


**Fig. 3.7** (Continued) FOPA gain spectrum for (a) 32 × 50 GHz and (b) 32 × 100 GHz systems with a PCIP of -10 dBm when all 32 channels are present (solid line), the first 8 channels survive (dashed lines), and the last 8 channels survive (hollow squares). The inset shows the gain variation ΔG (in dB) relative to the case when all channels are present: the circles (crosses) correspond to the case when the last (first) 8 channels survive. (c) is similar to (b), but the channels have random initial phases.

We also consider the impact of channel drop in two systems involving 32 channels with a PCIP of -10 dBm. The first has a channel spacing of 50 GHz while the second has a spacing of 100 GHz (see Fig. 3.7). In this example, we examine the steady-state gain spectrum when all channels are present and when only the 8 channels at the shortest or longest wavelengths survive. The results presented in Fig. 3.7(b) are interesting for two reasons. First, there is a similar behaviour to that observed in Fig. 3.6 whereby some of the shorter wavelengths experience a decrease in gain, despite the decrease in the number of channels. This provides further confirmation of the transfer of energy between longer and shorter wavelengths. Second, by comparing Fig. 3.7(a) and Fig. 3.7(b), we see that when keeping the PCIP (and hence TIP) constant, a larger channel spacing appears to increase the robustness of the amplifier to channel add/drop since the peak-to-peak variations in gain ($\Delta G$) are smaller. Once again, as shown in Fig. 3.7(c), when comparing the above results to the case where the channels have random initial phases, the behaviour is very similar with $\Delta G$ varying substantially over the amplifier bandwidth (though in this case, it is never negative).

The above results highlight the complex nature of the nonlinear FWM interactions between the channels and the pump present in the FOPA which make the prediction of changes in gain due to changes in amplifier operating conditions difficult. We stress that for the worst case scenario (all signals are in-phase and have exact channel spacings), all the above hindrances manifest themselves at their strongest. Even when we consider typical cases where the channels have random phases and fluctuations in the channel spacing, the phenomena are present, but to a reduced degree.

For EDFAs, the signal gain depends on the average inversion level and hence changes to the gain can be well predicted. For FRA, even if Raman interactions amongst all signals (pump and WDM channels) exist, they are easier to predict since the transfer of energy always occurs from shorter to longer wavelengths in a manner dictated by the total gain coefficient "seen" at a particular wavelength from all shorter wavelengths.

Based on the above results, we draw the following two conclusions. First, there is a transfer of energy from longer to shorter wavelengths (for the case where the pump is located on a longer wavelength than the channel band). This is explained by the fact that the signals are increasingly acting as pumps themselves, transferring energy in a classical "two-lobe" fashion to both their sides. A consequence of this transfer is that the gain of shorter wavelengths decreases when the longer wavelengths are dropped. This also demonstrates that the midband channels saturate with a faster rate than the ones positioned in the two edges. This behaviour is unique to FOPAs and contrasts EDFAs or FRAs in which the gain is expected to increase when fewer channels are present. Second, the gain is a strong function of the number of channels and channel spacing. For the same PCIP (or TIP), increasing the channel spacing can result in smaller gain variations following channel add/drop. The above observations and trends are based on investigation of all the scenarios mentioned in Table 3.2.

### 3.3.3 Dynamic Response

Next, we evaluate the changes in the gain that channels receive as a function of time during the add/drop operations. As explained before, when the number of channels present into the amplifier changes, so does the gain. Before, we saw the steady-state gain variations of the surviving channels after a number of channels have been dropped. In order to simulate the add/drop of channels, we use an amplitude modulator (AM) with its extinction ratio set to infinity (not shown in Fig. 3.1)

Fig. 3.8(a) and Fig. 3.8(b) show the gain variation as a function of time for a single surviving channel at the longest wavelength (193.1 THz) in the 32 × 50 GHz and 64 × 50 GHz systems, respectively, during channel add/drop. The rise and fall times of the gain excursions are essentially instantaneous as the transition time for the FWM phenomenon is on the scale of femtoseconds.

Ostensibly, these times are independent of the amplifier operating conditions as well as the amplifier length. Furthermore, no overshoots nor undershoots following channel drop or add, respectively, are observed. This is similar to the dynamic behaviour of non gain-controlled EDFAs and FRAs [3.14]-[3.17]. In earlier studies on EDFA or

FRA gain transients, the excursions were found to depend on the number of channels dropped. Moreover, the time required to reach steady-state was dependent on the number of channels dropped as well as the PCIP.

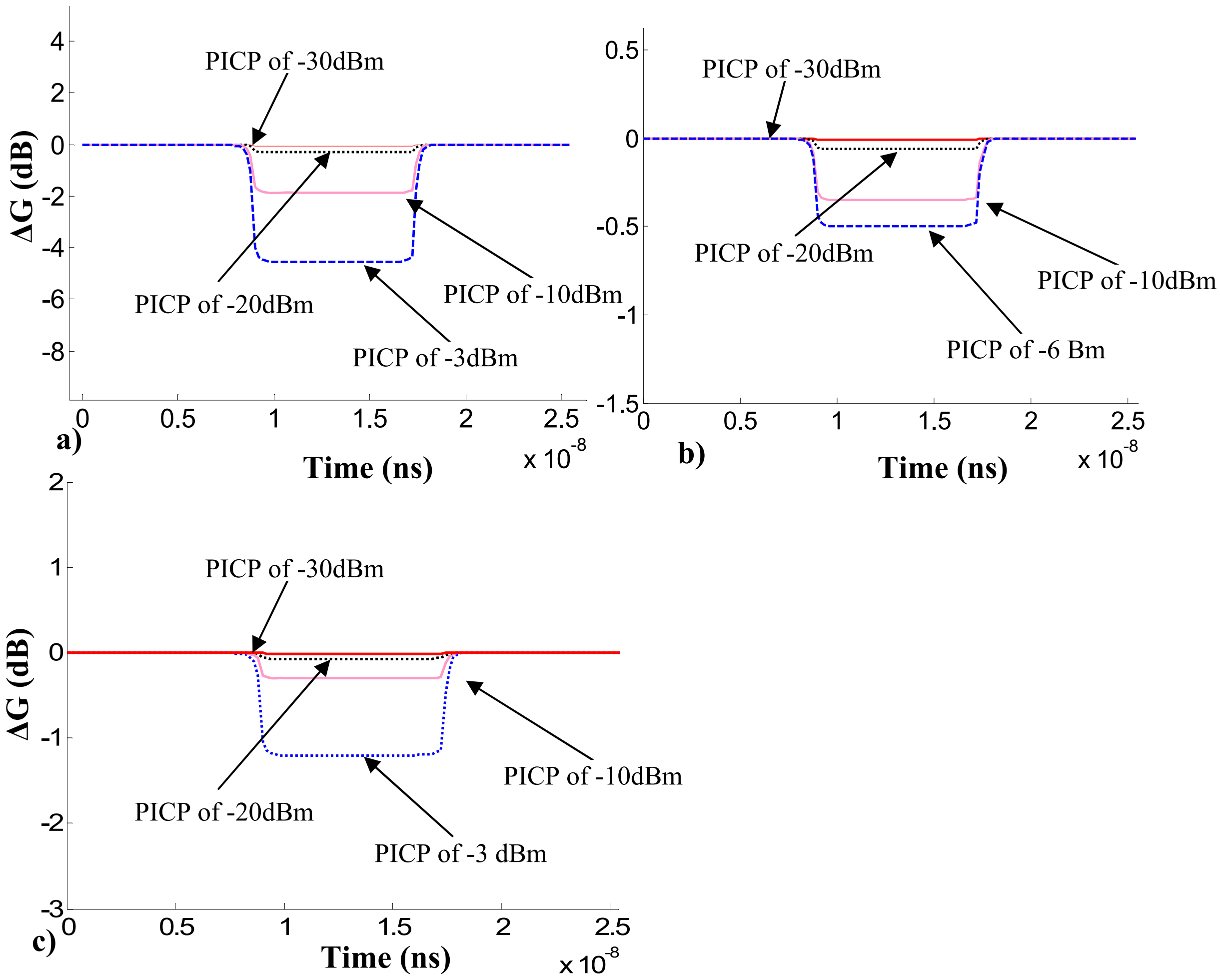


**Fig. 3.8** Gain change for the surviving channel at 193.1 THz when (a) 31 and (b) 63 channels are added (9 ns after the reference time) and then dropped (9 ns later). c) is similar to (a) but the signals have random initial phases and exhibit variations in channel spacing.

In Fig. 3.8(c), we show the results for a system similar to that in Fig. 3.8(a) where the signals have random initial phases and fluctuations in channel spacing. As before, gain excursions still occur though their impact is less significant: the excursions for -30 dBm, -20 dBm, -10 dBm, and -3 dBm input powers are reduced from -0.06 dB, -0.29 dB,

-1.87 dB, and -4.56 dB to -0.01 dB, -0.07 dB, -0.3 dB, and -1.2 dB, respectively. Based on our observations in section 3.3.2, we should expect the above gain excursions to depend on the position of the surviving channel. Essentially, as analysed in Fig. 3.6 and Fig. 3.7, when add/drop operations occur the gain varies in a different manner for each part of the channel band. This is why in our study we also consider the impact of the location of the surviving channel on the peak gain excursion. Table 3.3 summarizes the peak gain excursions experienced by the surviving channel following addition of the remaining channels to the amplifier.

**Table 3.3** Peak gain excursions ($\Delta G$) for the surviving channel at the first (194.65 THz), middle (193.9 THz) and last (194.65 THz) channel for PCIPs of -30 dBm, -20 dBm, -10 dBm and -3 dBm, following the addition of channels for (a) 32 × 50 GHz and (b) 64 × 50 GHz systems. A negative $\Delta G$ signifies a decrease in gain.

| PCIP (dBm) / Surviving Channel Frequency (THz) | **-30** | **-20** | **-10** | **-3** |
|---|---|---|---|---|
| **193.1** | -0.06 dB | -0.29 dB | -1.87 dB | -4.56 dB |
| **193.9** | -0.11 dB | -1.03 dB | -7.33 dB | -11.57 dB |
| **194.65** | 0.02 dB | 0.14 dB | 0.57 dB | -2.15 dB |

| PCIP (dBm) / Surviving Channel Frequency (THz) | **-30** | **-20** | **-10** | **-3** |
|---|---|---|---|---|
| **193.1** | -0.01 dB | -0.06 dB | -0.35 dB | -0.5 dB |
| **194.6** | -0.14 dB | -1.78 dB | -6.6 dB | -12.6 dB |
| **196.25** | 0.03 dB | 0.22 dB | -0.2 dB | -1.6 dB |

While each channel experiences a different gain excursion, depending on its position in the amplification band, those for the midband channel are substantially larger than for the channels positioned at the extremes. Moreover, even for the shortest wavelength channel that experiences a positive $\Delta G$ (i.e., increase in gain) when channels are added (due to the phenomena explained in section 3.3.1), further increases in PCIP will result in a saturation and $\Delta G$ eventually becomes negative. In addition, in the simulations we performed for scenarios with larger channel spacings (100 GHz and 200 GHz), the gain excursions diminish. All of these results are consistent with those observed from the steady-state analysis.

### 3.3.4 Summary

In summary, we have investigated the performance of FOPAs within the context of agile, multi-wavelength systems. In particular, we examined the steady-state gain variations and transient responses due to variations in amplifier operating conditions such as PCIP or as a result of channel add/drop. The gain spectrum depends strongly on the number of input signals and any changes as a result of variations in PCIP are irregular and not predictable due to the complex nature of the nonlinear FWM interactions. The gain tilt depends on various parameters such as the position of the surviving channels and the TIP. Furthermore, we have shown that the gain spectrum is a strong function of channel spacing and found that more sparsely spaced configurations are more robust to channel add/drop. We showed that the gain excursions observed in the case of channel add/drop strongly depend on the position of the surviving channel. The rise and fall times are very short and independent of the PCIP and there are no overshoots nor undershoots during channel add/drop.

All the above observations pertain to the worst case scenario where all signals are in-phase and have exact channel spacings. Nevertheless, when considering a typical scenario where the channels have random phases and exhibit fluctuations in channel spacing, even if the magnitude of deleterious effects are reduced, the main conclusions still hold and remain as serious impediments to the functionality of the amplifiers. FOPAs exhibit a complex behaviour and constructing a complete model that can a priori describe the amplifier's behaviour would be very tedious process when operating under dynamic conditions and thus, their deployment in agile, multi-wavelength networks will require careful consideration. Techniques that have been previously utilized in other amplifier technologies such as gain clamping will have to be investigated in order to mitigate the aforementioned problems. The concept of gain clamping is explained and investigated in Chapter 5.

## *3.4 Statistical analysis of a packet based network*

In agile all-photonic networks, different packets of data arrive at amplifiers after having travelled different paths or experienced different amounts of transmission impairments [3.18]. As a result, the power level of the input signals (at different wavelengths) will vary on a packet-to-packet basis. These power variations can cause gain transients which, in turn, can degrade system performance.

In this section, we use numerical simulations to study the gain excursions that occur when the powers of the signals input to a multi-channel FOPA vary in a random fashion on a packet-to-packet basis. We obtain the statistical nature of the corresponding gain variations and determine whether the amplifier is able to provide the required gain in such a dynamic environment.

### 3.4.1 Simulation description

Our objective is to simulate a realistic scenario in a packet-switched network wherein the power of the channels varies periodically. We use 4 WDM channels of which 3 randomly vary in power with time and one remains constant (we will call it the probe channel). At the output of the system we monitor the induced gain excursions on the probe channel (either the first or the third channel).

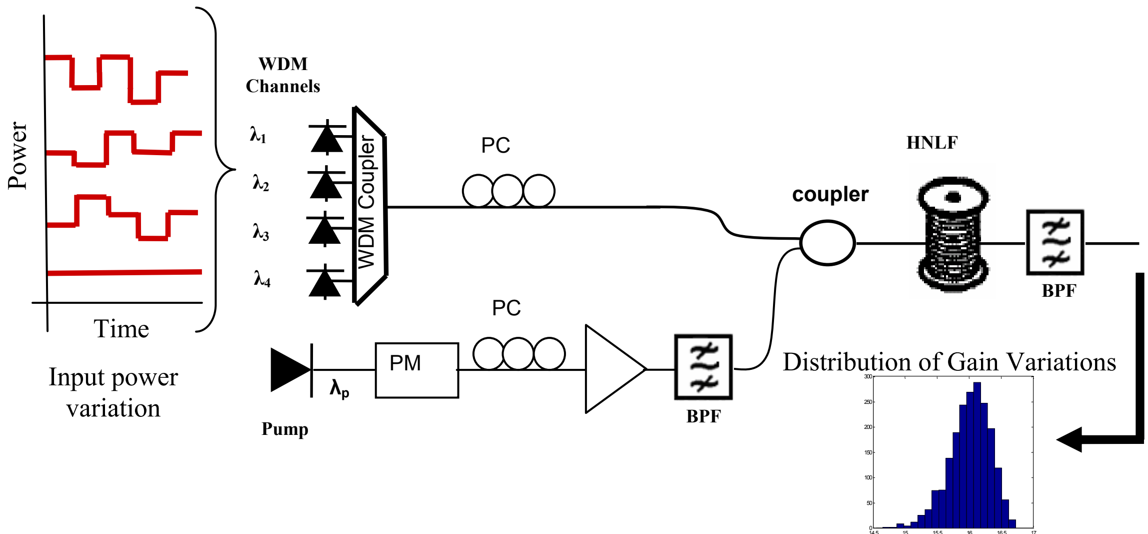


**Fig. 3.9** Schematic of FOPA system under study. PC: polarization controller; PM: phase modulator; BPF: bandpass filter.

The network in which the amplifier is designed to operate has an inter-amplifier span of 80 km. With an attenuation of 0.2 dB/km for a standard SMF, each amplifier has to provide 16 dB of gain. The FOPA is based on the same configuration described in Table 3.1, except that $P_p$ is increased to 31.5 dBm. As before, we assume that the signals are not modulated with data, the signals are in phase, the packets at each wavelength are aligned in time (to reduce simulation time, we use a packet duration of only 100 ns, but this is long compared to the amplifier response time), and the channel spacing is exact. These assumptions correspond to a worst-case scenario.

Fig. 3.9 shows the FOPA and the system under study: at the input of the amplifier we have the three varying channels and the one probe channel while in the output we have the resulting variation of the gain of the probe channel. As the TIP changes the load of the amplifier changes as well and as a result the gain provided to the probe channel will vary accordingly.

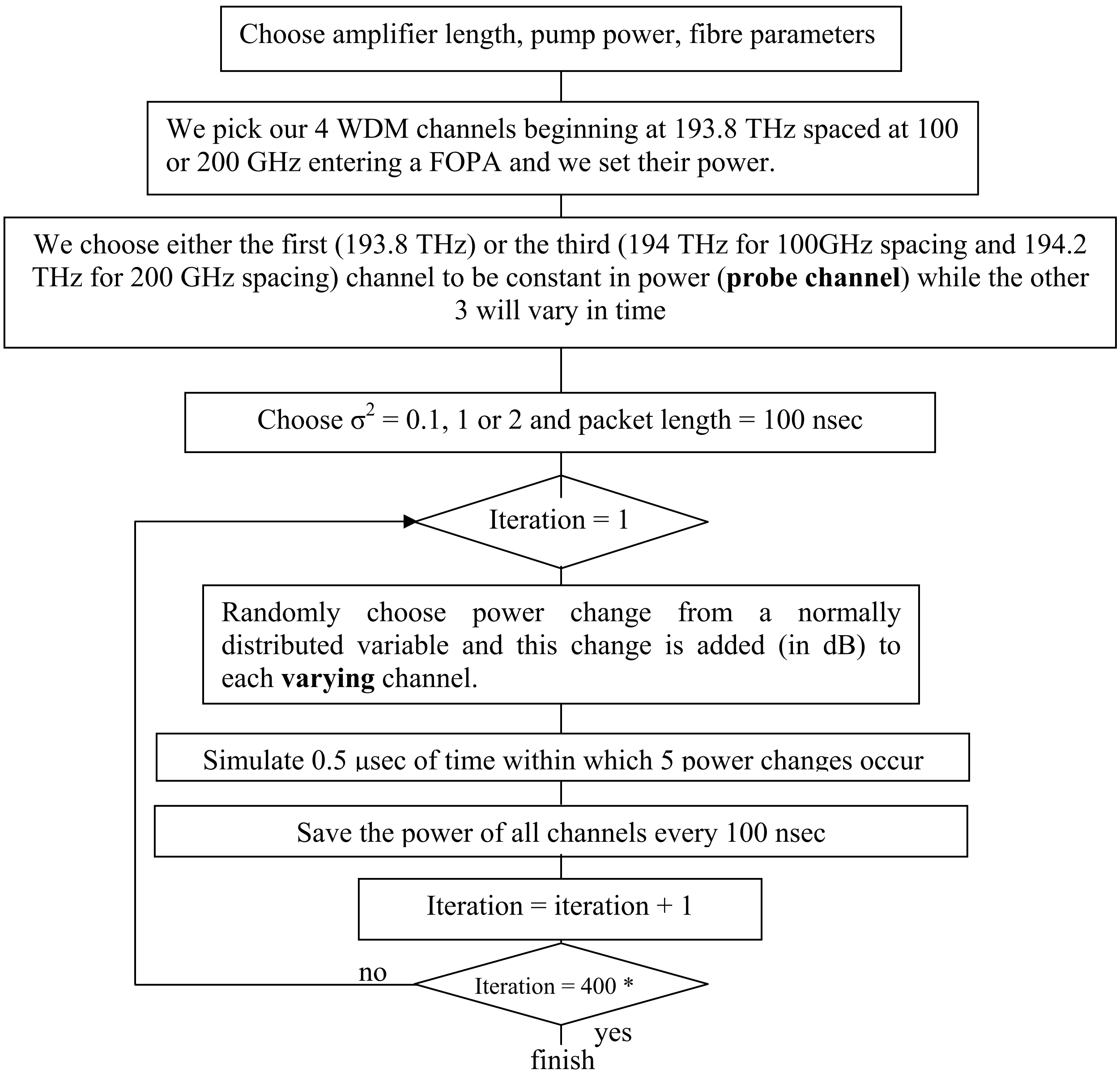


**Fig. 3.10** Flow chart of the simulation of our packet-switched network.

The flow chart shown in Fig. 3.10 describes in detail the steps followed in the simulations. The power of the three other channels fluctuates according to a normal distribution with a defined mean (μ) and variance ($\sigma^2$). We then examine the power variations of the probe channel. First, we can see the variation over the target gain of 16 dB and find out how often our amplifier falls short of that goal. We can also plot the maximum deviation (negative or positive) as a function of the position of the probe channel position, the channel spacing, and the mean and $\sigma^2$ (PCIP) of the three other channels. Moreover, we can extract the histogram that tells us the distribution of the probe channel gain variation as a function of the aforementioned variables.

In total, 2000 packets (or 2000 power changes) are simulated for each scenario. As 5 packets are simulated at a time, a total of 400 iterations is required. The way we define the change in power of the three varying channels is as follows:

$$\textit{New power value} = \textit{mean power value} + \sqrt{\sigma^2} \times (\textit{random value from normal distribution})$$

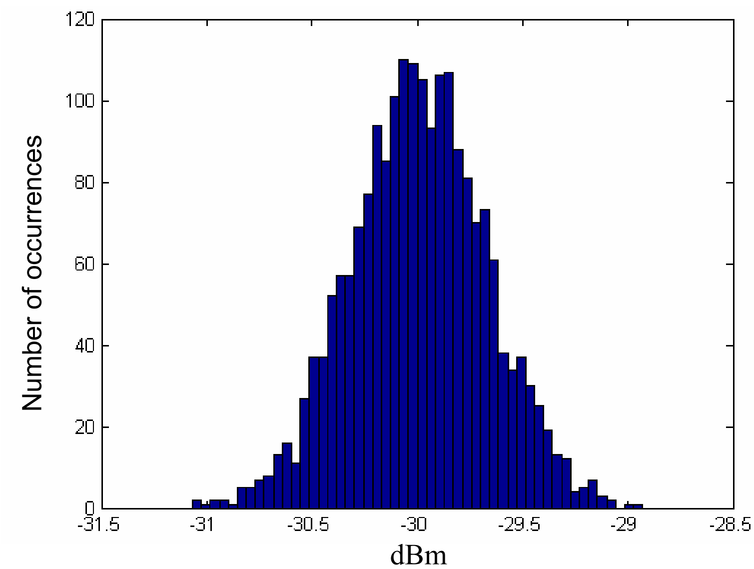


**Fig. 3.11** Output power distribution (in dBm) for the three varying channels. The histogram is built by separating the values in 50 different groups

In Fig. 3.11, we show the histogram of 2000 channel output powers, with $\mu$ = -30 dBm and $\sigma^2$ = 0.1. All the scenarios that are to be simulated are tabulated in Table 3.4.

**Table 3.4** Simulated scenarios for statistical analysis of a packet-switched network

| |
|---|
| Vary the channel spacing for 100 GHz or 200 GHz. |

| |
|---|
| Vary the position of the channel (first or third). |
| Vary the PCIP: -3 dBm (near saturation), -30 dBm (small-signal regime) |

The variance of the Gaussian distribution of the input power for the three varying channels is set to be 0.1 dB$^2$, 1 dB$^2$ and 2 dB$^2$ according to the following:

$$f(x;\mu,\sigma) = \frac{1}{\sigma\sqrt{2\pi}} \exp\left(-\frac{(x-\mu)^2}{2\sigma^2}\right).$$

### 3.4.2 Results

In order to quantify the effect of input power variation according to a Gaussian distribution we monitor the probe channel output power distribution and calculate its four first statistical moments: mean, variance, skewness and kurtosis (see Appendix I). To demonstrate the behaviour of the system under such conditions, we present two of the scenarios described in Table 3.4. The signal we concentrate on is the third WDM channel at a frequency of 194 THz (the channels are spaced at 100 GHz) while the PCIP is -3 Bm.

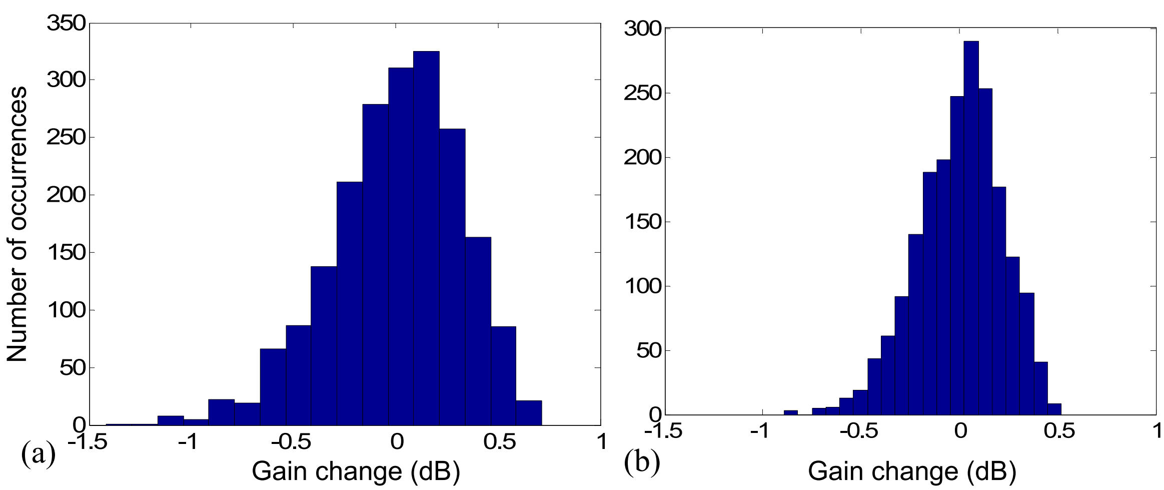


**Fig. 3.12** The gain variation (in dB) distribution of the probe channel, over its mean value as a result of the gain fluctuation caused by the input power changes over 2000 packets with a) $\sigma^2 = 2$ and b) $\sigma^2 = 1$.

In both cases the mean gain is very similar, 16.01 dB in (a) and 16.04 dB in (b) as expected. However, when taking a look at the higher order moments of each case we find out that in a) the variance is 0.10, its skewness (third statistical moment) $-2.31\times10^{-2}$ and its kurtosis (fourth statistical moment) $4.33\times10^{-2}$; while in (b) the variance is less than half and equals to 0.05, its skewness is about 20% ($-4.59\times10^{-3}$) of the one in (a) and its kurtosis is $7.25\times10^{-3}$. The skewness for both distributions is negative as seen in the graph, as long as the tail extends out towards more negative values of $\Delta G$. The difference in variance is also to be expected as a greater variance in the input power will induce a greater fluctuation on the gain of the probe channel. The interesting observation is that while the input powers of the three varying channels follow a Gaussian distribution, that of the probe channel follows a negatively skewed.

The skewness of the two distributions shows that for case a) the asymmetry of the function is 5 times higher than that in case b). As for the kurtosis, both cases are leptokurtic in comparison to a normal distribution with case b) being closer to a Gaussian distribution (zero 4th moment).

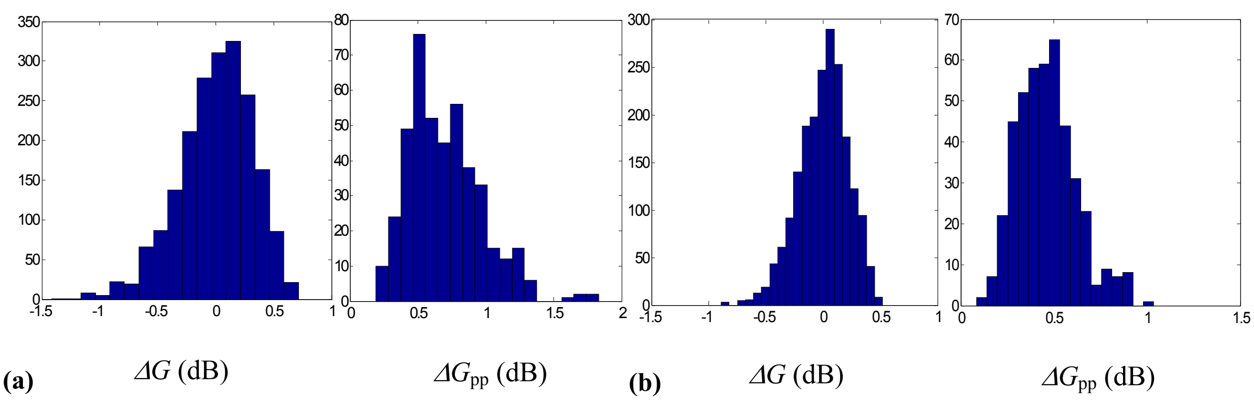


**Fig. 3.13** Typical histogram (distribution) of the gain variation $\Delta G$ in the probe channel from its target value as a result of the fluctuations in the channel input powers for (a) $\sigma_i^2 = 2$ dB$^2$ and (b) $\sigma_i^2 = 1$ dB$^2$.

The above statistical observations translated into physical terms reveal certain properties for our system. First, a larger $\sigma^2$ means that the output power is changing over its average value more, indicating larger gain excursions. Second, observing a negative skewness is explained by the fact that the amplifier can only provide a specific maximum gain to a single channel, so long as there are other signals present in the amplifier. This is due to the extra FWM tones that are generated which drain the pump power as well as the power transferred to the WDM channels. A positive skewness would indicate the opposite; that is, that the gain provided can not fall under a specific value.

Finally, a higher kurtosis means more of the variance is due to infrequent extreme deviations, as opposed to frequent modestly-sized deviations. Therefore, for case (a) which has a 6 times higher kurtosis than case (b), the probe channel is experiencing mostly small-sized deviations but at the same time, the infrequent extreme deviations are larger. Correspondingly, in case (b), the probe channel is experiencing many mid-sized deviations and a lot less extreme gain deviations.

Furthermore, Fig. 3.13 shows typical histograms for the distribution of the gain variations ($\Delta G$), i.e. difference between the target gain of 16 dB and the FOPA gain for the probe channel averaged over 5 packets, and for the distribution of the peak-to-peak gain variations ($\Delta G_{pp}$), also over 5 packets, for different values of $\sigma_i^2$ when the FOPA operates near saturation with a channel spacing of 100 GHz and the probe channel is the third channel. Clearly, the random power fluctuations at the input cause variations in gain from the target value of 16 dB. As expected, these variations, as well as the peak-to-peak gain variations, are larger when $\sigma_i^2$ is greater.

Table 3.5 summarizes the characteristics of the distribution of $\Delta G$ in the probe channel for different scenarios both for 100 GHz and 200 GHz channel spacings.

**Table 3.5** Statistical moments of several system configurations

| **100 GHz spacing** | | | **200 GHz spacing** | | |
|---|---|---|---|---|---|
| **Configuration** $\sigma_i^2$, PCIP (dBm), probe channel | $\boldsymbol{\sigma_p^2}$ **(dB$^2$)** 2nd statistical moment | **Skewness** 3rd statistical moment | **Configuration** $\sigma_i^2$, PCIP (dBm), probe channel | $\boldsymbol{\sigma_p^2}$ **(dB$^2$)** 2nd statistical moment | **Skewness** 3rd statistical moment |
| 1, -3, 1st | $2.95\times10^{-2}$ | $-2.52\times10^{-3}$ | 1, -3, 1st | $1.27\times10^{-2}$ | $-4.53\times10^{-4}$ |
| 1, -3, 3rd | $4.70\times10^{-2}$ | $-4.59\times10^{-3}$ | 1, -3, 3rd | $1.03\times10^{-1}$ | $-1.21\times10^{-2}$ |
| 1, -30, 1st | $3.75\times10^{-7}$ | $-1.14\times10^{-10}$ | 1, -30, 1st | $3.26\times10^{-7}$ | $-1.08\times10^{-10}$ |
| 1, -30, 3rd | $1.19\times10^{-7}$ | $-9.32\times10^{-12}$ | 1, -30, 3rd | $9.28\times10^{-8}$ | $-7.78\times10^{-12}$ |
| 2, -30, 1st | $1.01\times10^{-6}$ | $-7.96\times10^{-10}$ | 2, -30, 1st | $9.89\times10^{-7}$ | $-5.48\times10^{-10}$ |
| 2, -30, 3rd | $1.97\times10^{-6}$ | $-1.98\times10^{-9}$ | 2, -30, 3rd | $2.01\times10^{-6}$ | $-2.98\times10^{-9}$ |

First, we note that the distribution has a negative skewness at all instances. This signifies that the FOPA tends to undershoot its nominal gain when there are fluctuations in the input powers. Second, the middle channels are generally more prone to gain excursions than those located at the extremes, especially in near saturation; this agrees with the observations in section 3.3 for the steady-state gain variations occurring as a result of channel add/drop. Third, as expected, for larger values of $\sigma_i^2$, the variance of the distribution of $\Delta G$ (denoted $\sigma_p^2$) is larger and the FOPA is more prone to fail in providing the required gain. Finally, for increased channel spacing, the gain variation is smaller for the first channel while it is larger for the third channel when operating close to saturation. However, it stays virtually the same when operating in the small-signal regime.

As discussed in section 3.3.2, channels that are positioned in the middle of the channel band, undergo larger gain changes when the operating conditions of the amplifier change (number and/or power of channels). This is due to the fact that signals experience stronger FWM interactions with their neighbouring signals than with the ones located further. In other words, when a channel is positioned in the middle of the channel band more interactions take place, which means that the factors affecting its output power are more. Therefore, the variation of the output power is larger as well.

Moreover, the expected decrease in gain variations for an increased channel spacing, only happens near saturation (PCIP of -3 dB). Evidently, in the small-signal regime, the amplifier has enough pump power to keep providing the same amount of gain even when the operating conditions change on a packet to packet basis. On the other hand, near saturation, the amplifier can not supply more power and this is why the increase of the channel spacing partly alleviates the problem, as expected based on the analysis we made in section 3.3.2.

### 3.4.3 Conclusion

In summary, the target gain is not achieved more than 50% of the time when $\sigma_i^2 >$ 1 dB$^2$ when the FOPA operates near saturation; moreover, $\Delta G_{pp}$ can exceed 1 dB. However, when operating in small-signal or for small input power fluctuations (e.g. $\sigma_i^2 =$ 0.1 dB$^2$), the variation is insignificant and the target gain is always achieved. Thus, when FOPAs operate in a dynamic network close to saturation or when the power fluctuations on packet-to-packet basis are substantial, the WDM channels suffer from significant gain excursions that can degrade overall amplifier performance. This study in conjunction with the results discussed in the previous sections of Chapter 3, reaffirms the need for control of this dynamic behaviour if FOPAs are to be deployed in agile photonic networks.

**References**

[3.1] M. C. Ho, F. S. Yang, M. E. Marhic and L. G. Kazovsky, “Optical parametric amplification in a high-nonlinearity fiber”, Conference of Lasers and Electro-Optics, paper CFA6, San Francisco, May 3 - 8 (1998).

[3.2] J. Hansryd, P. A. Andrekson, M. Westlund, J. Li and P. O. Hedekvist, “Fiber-based optical parametric amplifiers and their applications”, IEEE Journal of Selected Topics in Quantum Electronics, vol. 8, no. 3, pp. 506-520, (2002).

[3.3] M. N. Islam and O. Boyraz, “Fiber parametric amplifiers for wavelength band conversion”, IEEE Journal of Selected Topics in Quantum Electronics, vol. 8, no. 3, pp. 527-537, (2002).

[3.4] S. Radic, C. J. McKinstrie, A. R. Chraplyvy, G. Raybon, J. C. Centanni, C. G. Jorgensen, K. Brar and C. Headley, “Continuous-wave parametric gain synthesis using nondegenerate pump four-wave mixing”, Photonics Technology Letters, vol. 14, no. 10, pp. 1406-1408, (2002).

[3.5] K. K. Y. Wong, K. Shimizu, M. E. Marhic, K. Uesaka, G. Kalogerakis and L. G. Kazovsky, “Continuous-wave fiber optical parametric wavelength converter with +40 dB conversion efficiency and a 3.8-dB noise figure”, Optics Letters, vol. 28, no. 9, pp. 692-694, (2003).

[3.6] C. J. McKinstrie, S. Radic and A. R. Chraplyvy, “Parametric amplifiers driven by two pump waves”, IEEE Journal of Selected Topics in Quantum Electronics, vol. 8, no. 3, pp. 538-547, (2002).

[3.7] K. Y. Wong, M. E. Marhic, K. Uesaka and L. G. Kazovsky, “Polarization-independent two-pump fiber optical parametric amplifier”, Photonics Technology Letters, vol. 14, no. 7, pp. 911-913, (2002).

[3.8] L. Provino, H. Maillotte, E. Lantz, T. Sylvestre and J. M. Dudle, “Broadband and nearly flat parametric gain in single-mode fibers”, Conference of Lasers and Electro-Optics Europe, paper Ctul2, Nice, France, September 10 - 15 (2000).

[3.9] J. M. Chavez Boggio, J. D. Marconi and H. L. Fragnito, “Double-pumped fiber optical parametric amplifier with flat gain over 47-nm bandwidth using a conventional dispersion-shifted fiber”, Photonics Technology Letters, vol. 17, no. 9, pp. 1842-184, (2005).

[3.10] M. Karásek, J. Kaňka and J. Radil, “Parametric amplification and multiple wavelength conversion in HNLF: experimentation and modelling”, Trans-European

Research and Education Networking Association, paper TNC06, Catania, Italy, May 15-18 (2006).

[3.11] K. Inoue and T. Mukai, “Signal wavelength dependence of gain saturation in a fiber optical parametric amplifier”, Optics Letters, vol. 26, no. 1, pp. 10-12, (2001).

[3.12] F.A. Callegari, J.M. Chavez Boggio and H.L. Fragnito, “Mixing of signals in two-pump fiber optic parametric amplifiers and wavelength converters”, Optical Fiber Communication Conference, paper MF18, Sunnyvale, USA, February 23 - 27 (2004).

[3.13] P. Kylemark, H. Sunnerud, M. Karlsson, P. A. Andrekson, “Semi-analytic saturation theory of fiber optical parametric amplifiers”, Journal of Lightwave Technology, vol. 24, no. 9, pp. 3471-3479, (2006).

[3.14] E. Desurvire, “Analysis of transient gain saturation and recovery in Erbium-doped fiber amplifiers”, Photonics Technology Letters, vol. 1, no. 8, pp. 196-199, (1989).

[3.15] A. K. Srivastava, Y. Sun, J. L. Zyskind and J. W. Sulhoff, “EDFA transient response to channel loss in WDM transmission system”, Photonics Technology Letters, vol. 9, no. 3, pp. 386-388, (1997).

[3.16] M. Karásek and M. Menif, “Channel addition/removal response in Raman fiber amplifiers: modelling and experimentation”, Journal of Lightwave Technology, vol. 20, no. 9, pp. 1680-1687, (2002).

[3.17] L. L. Wang, B. C. Hwang and L. M. Yang, “Gain transients in copumped and counterpumped Raman amplifiers”, Photonics Technology Letters, vol. 15, no. 5, pp. 664-666, (2003).

[3.18] L. G. Mason, A. Vinokurov, N. Zhao and D. Plant, “Topological design and dimensioning of agile all photonic networks”, Journal of Computer Networks, vol. 50, no. 2, pp. 268-287, (2006).

# Chapter 4 Dynamic analysis of discrete FOPAs

## *4.1 Introduction*

In this chapter we will consider FOPAs in a non-static environment. Specifically, in section 4.2 we will examine the BER performance of FOPAs using modulated WDM channels. We will present and compare several modulation formats in order to evaluate the most suitable format for use in FOPAs.

As we have already mentioned in Chapter 2, channel crosstalk along with XGM, are two of the main hindrances FOPAs face. As we know, the FWM process takes place on a femtosecond level. For this reason, XGM in FOPAs will occur on a bit level. This fact makes it obvious that the modulation format used by the amplified channels is of great importance for the performance of the amplifier. OOK modulated channels will most likely suffer from XGM-generated performance degradation. In this Chapter, we investigate whether other formats such as RZ-DPSK, whose power is pattern independent, can reduce crosstalk.

## *4.2 Modulation Formats in FOPAs*

So far in our investigation, we have assumed constant wave (CW) operation for all the WDM channels present in the amplifier. Studying the behaviour of the amplifier under this condition is sufficient when looking into the static and quasi-static properties of the system. Characteristics such as gain-tilt, gain spectrum changes, gain excursions can be adequately described using CW channels. However, in order to examine an optical communications system in its entirety, channels modulated with data have to be included.

In this section, we will examine the performance of several modulation formats within the context of FOPAs.

In transmission systems, it is required that the optical data stream experiences the same gain, regardless of being "0" or "1". When using RZ or NRZ modulation, due to pump depletion, the gain of the FOPA saturates instantaneously for high input signal peak powers. This means that the gain saturates not only as an average, like in an EDFA with a significantly longer gain saturation time constant (in the order of ms), but on a bit level, which can result in a "1" bit experiencing less gain than a "0" bit. This effect is even more distinct in a multi-channel system since the total input signal power to the FOPA varies substantially and saturates the gain at high input power (see Fig. 4.1).

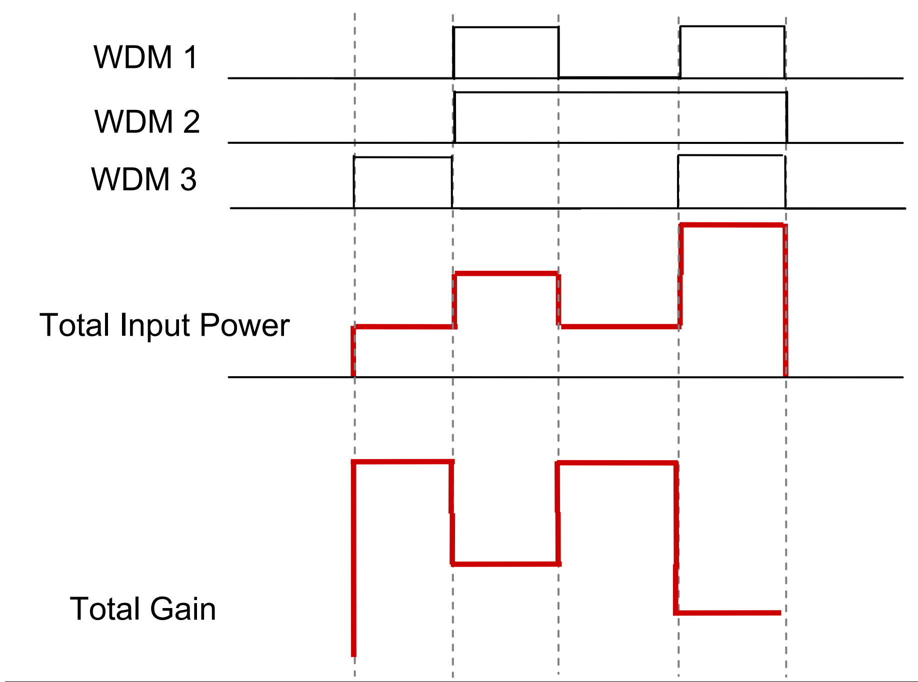


**Fig. 4.1** Cross gain modulation (XGM) on a bit-level in FOPAs.

In other words, the input power of one channel saturates the gain of another channel. Therefore, when multiple channels are present in the amplifier, the gain received from each channel decreases whenever the "1s" of two or more channels are overlapping.

Moreover, FWM interactions amongst all signals will manifest as an increased intensity of noise, further deteriorating the performance of the system. In particular, every pair of signals, through FWM interaction, will generate a third signal (their idler) which in turn will interact with every other signal. Of course, the FWM effect is mainly occurring amongst neighbouring channels, while XGM is a phenomenon that affects all channels, independently of their position in the gain spectrum.

### 4.2.1 Investigation

Our study concentrates on measuring the channel BER at the output of the amplifier as a function of several system parameters. Specifically, we investigate how modulation format, PCIP, channel spacing, bit-rate and position can affect the signal quality. Moreover, we quantify the impairments that limit the performance of FOPAs, such as XGM and FWM, as a function of the number of channels being used and explore possible limitations of using FOPAs in WDM systems. The final objective of this study is to determine whether a specific modulation technique is more advantageous when used in FOPAs. Particularly, we investigate whether DPSK modulation could mitigate such problems since the input power of such a modulation format is constant.

We first examine the traditionally used NRZ (section 4.2.3) and RZ (section 4.2.4) modulation formats to understand how each of the aforementioned parameters is affecting their performance. Next, we introduce the DPSK format and investigate whether this modulation format can alleviate the problems associated with amplitude shift keying modulation formats.

### 4.2.2 Description of the system

The FOPA is set to provide a small signal gain of 16 dB (to compensate the attenuation of ≈ 80 km of standard SMF). In the system under investigation, we consider

1,4 and 8 WDM channels modulated at 10 Gb/s and 40 Gb/s. The channel frequencies start at 193.8 THz, and are spaced by 100 GHz and 200 GHz. A CW laser amplified by an EDFA serves as a pump and is centred at 1562.7 nm with an output power of 30 dBm. The rest of the characteristics of the amplifier are the same as the ones mentioned in Table 3.1.

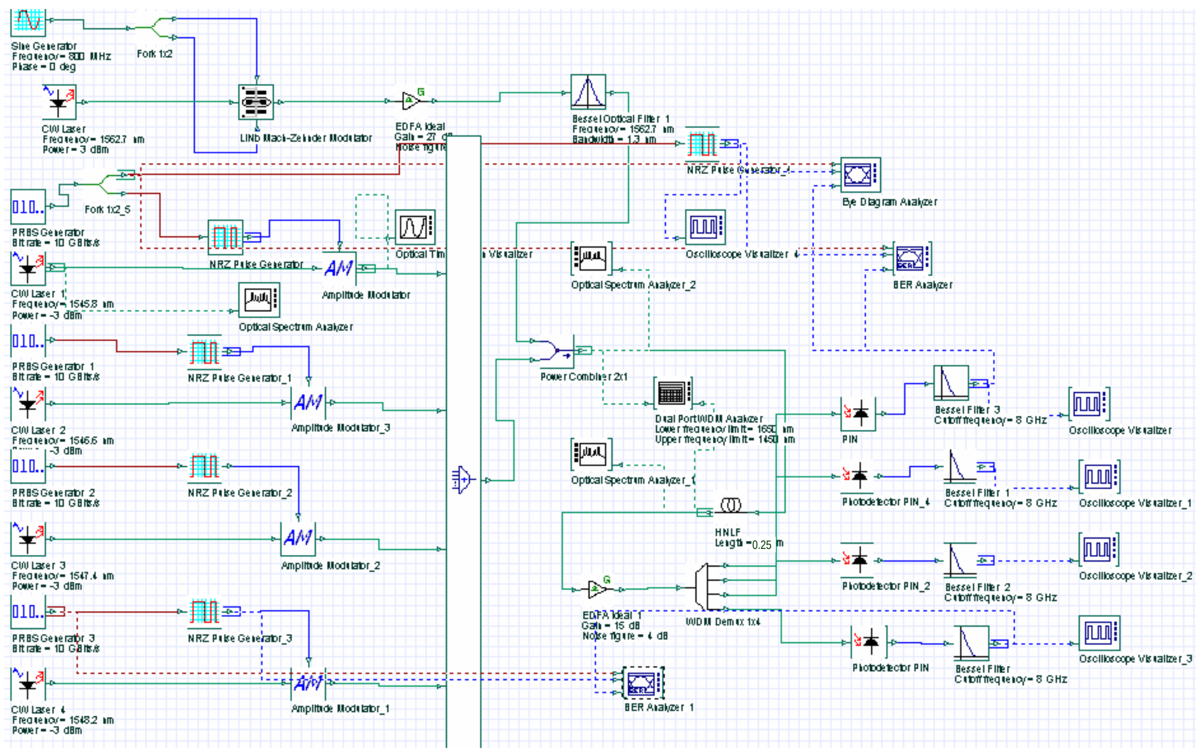


**Fig. 4.2** System topology for a 4 WDM channel, NRZ modulated FOPA.

A generic sketch of the system is shown in Fig. 3.1 while Fig. 4.2 shows the corresponding simulator topology of NRZ modulation in the OptiSystem$^{TM}$ software. Even if SBS is not simulated in this software, the DFB laser used as a pump is phase modulated at 800 MHz in order to simulate more realistically the system's behaviour in a practical application where the pump is phase modulated in order to suppress any undesired SBS.

We also make the following assumptions: the signals have random initial phases and random frequency offsets between 0 and 10 MHz from their exact channel frequencies. Moreover, while the bits of each channel are synchronized, each is fed with a different $2^{11}$-1 Pseudo-Random Bit Sequence (PRBS). After the channels have been externally modulated with different but synchronized PRBS, they are multiplexed and combined with the pump into the FOPA through a pump combiner. The optical spectrum is monitored both at the input and output of the amplifier. The signals are then demultiplexed and detected using a photodetector. Before the photodetector, we place a variable optical attenuator (VOA) in order to vary the Received Optical Power (ROP) and thus determine the receiver sensitivity. The resulting electrical signal passes through a low pass filter at 0.8 the bit-rate, in order to reduce high frequency noise. Finally it is fed into the BER analyser where we calculate the Q-factor and monitor the opening of the eye-diagram. From the Q-factor, we estimate the BER for each Received Optical Power (ROP). Our control parameters are the PCIP (in the case of modulated channels, PCIP refers to the average per channel input power) and channel spacing.

We consider two different PCIPs, one in the critical regime (in this regime, the total input power corresponds to that necessary to achieve a gain 0.5 dB less than the small-signal gain) and one 5 dB lower. For comparison purposes, we set the average input powers for all modulation formats to be the same. For the simulation conditions considered, this corresponds to -5.77 dBm for the first case and -10.77 dBm in the second case; these powers are denoted *P1* and *P2*, respectively. We monitor the BER of the first channel (193.4 THz) and all improvements in receiver sensitivity or power penalties refer to a BER of $10^{-9}$.

As an example, Fig. 4.3 shows the Q-factor and eye-diagrams obtained for a PCIP of -30 dBm and -3 dBm in an NRZ modulation scheme at 10 Gb/s.

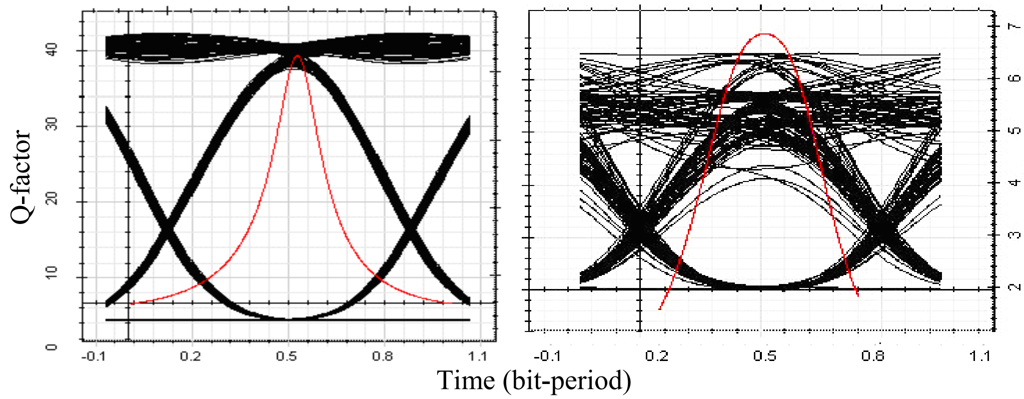


**Fig. 4.3** Q-factor and eye-diagram for a PCIP of -30 (left) and -3 dBm (right) in an NRZ modulation scheme at 10 Gb/s

We can clearly see the deterioration of the Q-factor and the quality of the signal when the PCIP is increased to -3 dBm. This is due to the increase of non-linear effects such as XGM between the signals attributed to the high signal powers present in the amplifier (these diagrams were obtained with a PRBS of $2^8$-1).

### 4.2.3 NRZ modulation

The NRZ modulation format is the simplest and first to be used in optical communications. Simply put, “1”and “0” bits are represented with two different light levels. These levels remain constant during the bit period. The presence of a high-light level in the bit duration represents a binary 1, while a low-light level represents a binary 0. NRZ codes make an efficient use of system bandwidth. However, loss of timing may result if long strings of “1” and “0” bits are present causing a lack of level transitions. Moreover, the NRZ pulses are distorted by some non-ideal phenomena in optical fibres such as dispersion and nonlinear effects, which cause more difficulty in recovering the clock of the bit stream.

The extinction ratio between "1" and "0" bits usually varies from anything between 6 dB and 16 dB. In the following simulations we use a 15 dB extinction ratio. The rise and fall times are usually 25% of the bit period, which corresponds to 25 ps for 10 Gb/s and 6.5 ps for 40 Gb/s.

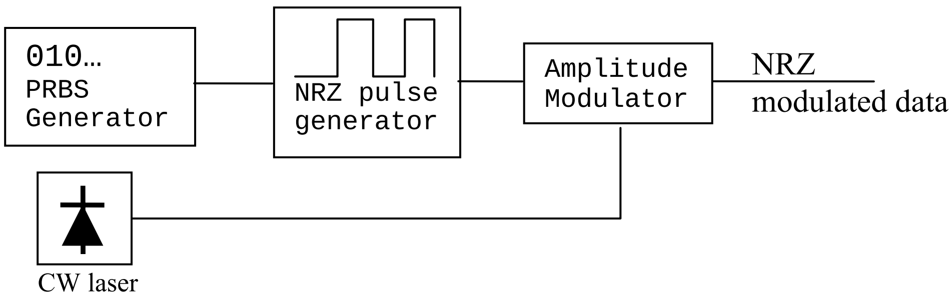


**Fig. 4.4** Non-Return to Zero modulator topology

As seen in Fig. 4.4, in order to make our NRZ modulator, an NRZ pulse generator is fed with a PRBS which in turn feed an amplitude modulator which modulates the output from the CW laser.

First, we compare the impact of different power levels (*P1* and *P2*) for channels modulated at 10 Gb/s and spaced by 100 GHz.

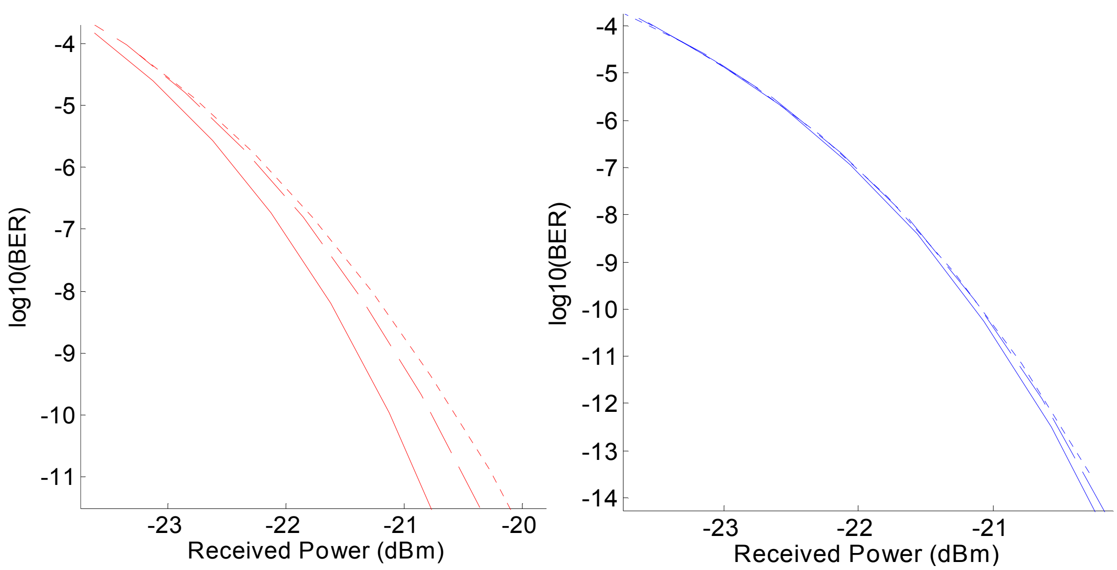


**Fig. 4.5** BER vs. ROP for NRZ modulated channels at 10 Gb/s, spaced at 100 GHz for *P1* (left) and *P2* (right) for 1 (solid), 4 (dashed) and 8 (dotted) WDM channels.

Fig. 4.5 shows that the ROP for a BER of $10^{-9}$ is roughly the same for both PCIPs when only one channel is present. In the case of *P2*, even when 8 channels are added, the BER does not change significantly. However, for *P1*, the system experiences a 0.6 dB power penalty. In this case, the optical power of the signals present in the amplifier, are sufficient to give rise to FWM and XGM. As explained in section 4.2 and illustrated in Fig. 4.3, when the amplifier operates in the small-signal regime (*P2*), there is enough power to supply the same gain to all channels even when several "1" bits coincide at the same time. Conversely, when the amplifier operates close to saturation (as is the case with *P1*) and several "1" bits happen to overlap, the total power into the amplifier increases substantially. In this way, the amplifier cannot provide an equal amount of gain as it does when "0" bits overlap. As a result, the "1" bits are amplified less than the "0" bits and the extinction ratio at the output decreases.

Subsequently, we examine what happens when the channel spacing is increased to 200 GHz while keeping the other parameters the same. As expected from Eq. 2.5 and as has been shown in previous studies [4.1], the effects of FWM and XGM are greatly reduced.

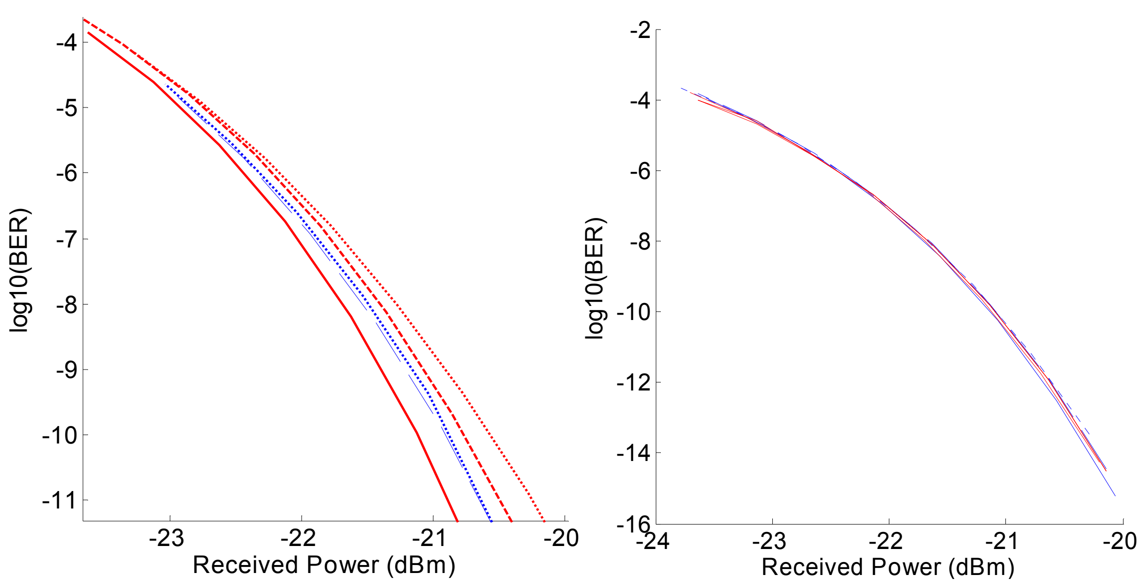

**Fig. 4.6** BER vs. ROP for NRZ modulated channels at 10 Gb/s, *P1* (left) and *P2* (righ) spaced at 100 GHz (red) and 200 GHz (blue) for 1 (solid), 4 (dashed) and 8 (dotted) WDM channels.

Fig. 4.6 shows that the power penalty for introducing 4 or 8 channels to the amplifier is more than halved when 200 GHz channel spacing is employed. Moreover, the power penalty between 4 and 8 channel configurations is minimal. Both these observations are attributed to the same factor. FWM interactions, one of two dominant factors that negatively affect performance, is greatly reduced when the distance between the two signals involved is increased. Moreover, as FWM is more intense between neighbouring signals, the addition of more channels will minimally affect performance when these channels are located far away from the signal under consideration. As expected, for the reasons explained previously, in the case of *P2* no significant difference is observed between 100 GHz and 200 GHz spacing.

Next, we examine the impact of bit rate on the BER performance. We compare 10 Gb/s and of 40 Gb/s for 1, 4 and 8 channels spaced at 100 GHz for *P1*.

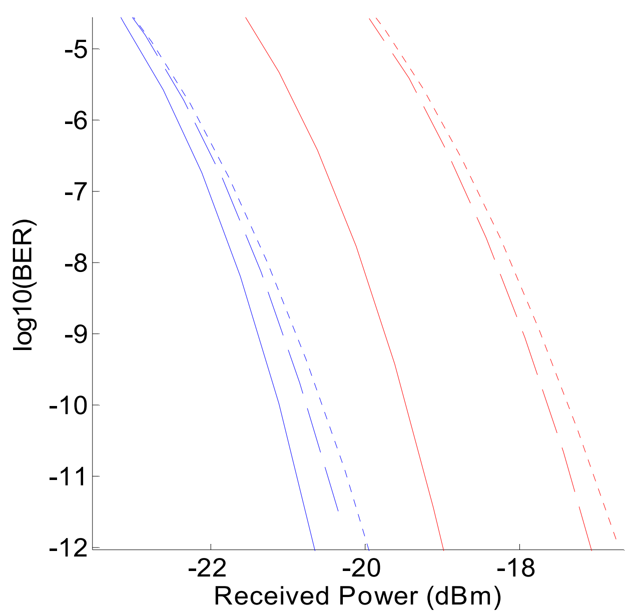

**Fig. 4.7** BER vs. ROP for NRZ modulated channels at 10 Gb/s (blue) and 40 Gb/s (red) *P1* input power, spaced at 100 GHz for 1 (solid), 4 (dashed) and 8 (dotted) WDM channels.

Fig. 4.7 shows that even for the single channel scenario, when the data are modulated at 40 Gb/s, the BER deterioration is 1.8 dB as compared to the 10 Gb/s case. Similarly, as the bit rate is increased from 10 Gb/s to 40 Gb/s we see that the power penalty for adding 4 channels to the system, goes from a mere 0.2 dB to 1.8 dB. Interestingly, for both bit rates, adding 4 more channels (for a total of 8) does not degrade the system performance considerably (less than 0.2 dB in both cases). This again, can be explained using the previous analysis concerning the FWM process and the neighbouring signals.

### 4.2.4 RZ modulation

Compared to NRZ, RZ coding has more frequent transitions of power. More specifically, there is a transition in each transmission of a binary “1” bit. For every bit, the laser is turned on for part of the bit-period while it remains off for the remainder of the period. The percentage of the bit period during which the laser remains on is called *duty cycle* (d.c.). The duty cycle can vary from less than 10% to 67%. Although, RZ offers greater resistance to nonlinear effects at higher bit rates in properly dispersion managed systems and it is easier to recover the clock of the bit stream at the receiver, the disadvantage of RZ coding technique is a larger bandwidth requirement compared to the NRZ coding. In a restricted bandwidth environment, the RZ coding may not be an efficient option.

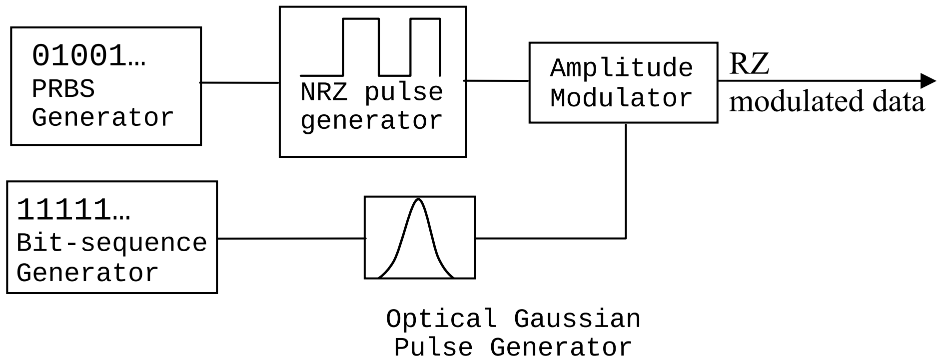


**Fig. 4.8** Return to Zero modulator topology

Fig. 4.8 depicts the RZ modulator block diagram. It is similar to the one that describes the NRZ modulator with the addition of a bit-sequence generator and of an Optical Gaussian Pulse Generator (OGPG) in place of the CW laser. In order to make our RZ modulator, an NRZ pulse generator is fed with a PRBS which in turn feeds an amplitude modulator. The OGPG is fed with a bit-sequence generator that has been set to a constant "1". This way we produce a constant stream of Gaussian pulses with a power and a d.c. defined in the OGPG. This pulse stream is then modulated by the amplitude modulator. The amplitude modulator allows the pulse to propagate in the case of a binary "1" while it extinguishes the corresponding pulse in the case of a binary "0". In the following simulations we use a 15 dB suppression ratio.

Contrary to the NRZ modulation, the "extinction ratio" has to be defined differently as now both "1s" and "0s" are transmitting parts of their bits using the low power level. Therefore, for RZ signals we use the suppression ratio (or contrast ratio), which is the ratio of the average power level of the logic *high* to the average power level in the suppressed level. So basically it is a measure of how much of the falling edge of the previous logical *high* pulse is still present at the beginning of the current pulse within the suppressed region of the signal. Typical values of this measurement can vary between 12 and 30 dB. In the following simulations we use a 16 dB suppression ratio.

We start the discussion of the RZ modulation results by comparing the performance for two different power levels (*P1* and *P2*) with a 100 GHz channel spacing and with a duty cycle of 0.5.

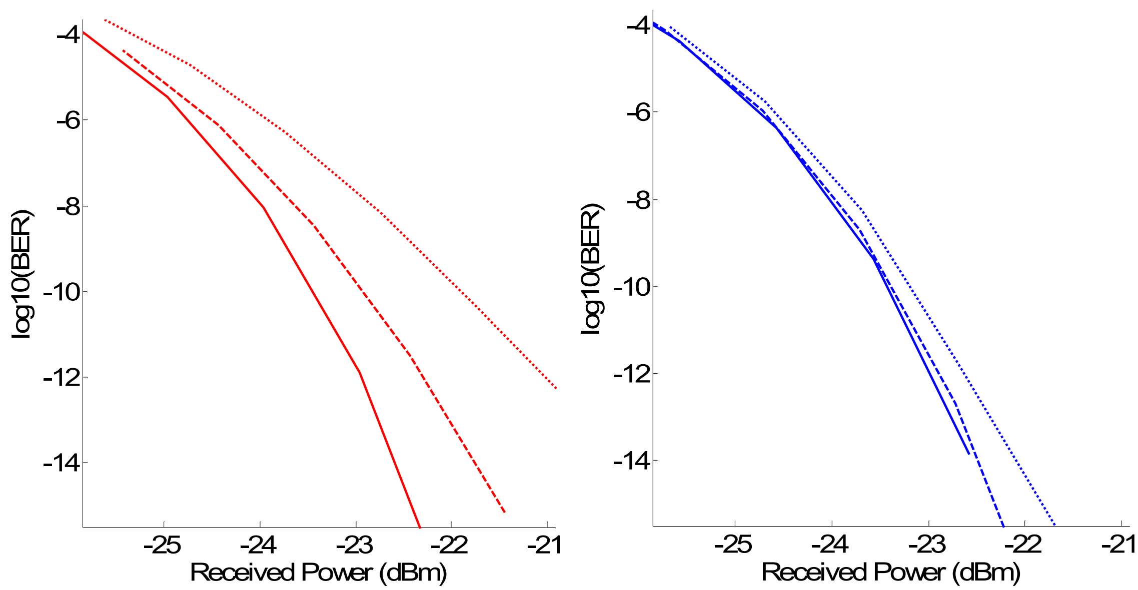


**Fig. 4.9** *P1* (left, red) vs. *P2* (right, blue) for RZ modulated signals at 10 Gb/s with a 0.5 d.c.. for 1 (solid), 4 (dashed) and 8 (dotted) WDM channel.

Similarly as in the NRZ case, Fig. 4.9 shows that the ROP for a BER of $10^{-9}$ is roughly the same for both PCIPs when only one channel is present. In the absence of other channels, FWM and XGM do not affect the performance of the system. In the case of *P2*, even when 8 channels are added the power penalty does not exceed 0.2 dB. Conversely, for *P1* the system experiences a 1.5 dB power penalty when 8 WDM channels are present into the amplifier. It is apparent that an increased input power also gives rise to stronger FWM interactions that decrease the performance of the FOPA. Again, as was the case for NRZ, when operating in the small-signal regime (*P2*), the amplifier can provide equal gain to the channels independently of them containing "1" or "0" bits at the same time slot. On the contrary, when operating close to saturation (*P1*), XGM becomes a serious problem and considerably affects the amplifier's performance. We also see that for *P1*, the power penalty increases almost linearly with the number of channels. This indicates that in a 32 or 64 WDM channel system the power penalty could be very high. In the light of these results, it is becoming apparent that OOK modulation formats suffer significantly from XGM, especially when operating close to saturation.

Next, we consider the same scenario but with a much shorter d.c. of 12.5%.

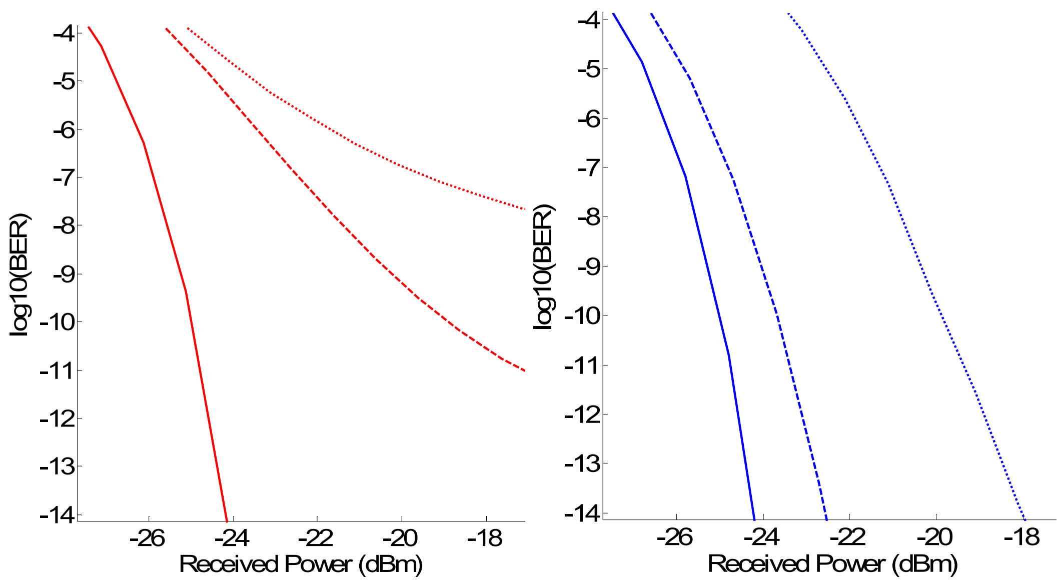


**Fig. 4.10** *P1* (left, red) vs. *P2* (right, blue) for RZ modulated signals at 10 Gb/s with a 0.125 d.c.. for 1 (solid), 4 (dashed) and 8 (dotted) WDM channels.

Fig. 4.10 depicts the BER curves for RZ modulation with a 0.125 d.c., for both *P1* (red) and *P2* (blue) for the cases of 1 (solid line), 4 (dashed) and 8 (dotted) channels. Interestingly, while for the single channel case the required receiver sensitivity is improved compared to the case of a longer d.c. (50%), when more channels are added to the amplifier, the short d.c. scheme dramatically loses the advantage (a more thorough comparison for different d.c. is presented later in this section). More specifically, the power penalty for *P2* is 1 dB for 4 channels and almost 5 dB for 8 channels. This can be explained mainly by the very high peak powers (1 dBm and 6 dBm for *P2* and *P1* respectively) required in order to achieve the same average powers as before. In other words, in low duty cycles, the peak powers are dramatically increasing, which gives rise to stronger nonlinear interactions, mainly FWM, but also Self-Phase Modulation (SPM) and Cross-Phase Modulation (XPM)), and XGM. Another interesting aspect of these results is the noise floor that the BER curves approach in the case of *P1*. For the case of 8 channels the noise floor is reached at around $10^{-8}$. Evidently, when operating close to saturation and many channels with very high peak powers are present inside the amplifier, the FWM interactions and the XGM deteriorate the eye-diagram so much, that they do not allow the BER to improve any further than this value even when the ROP is increased significantly.

Next, we look into the effect of channel spacing and compare the BER for a 100 GHz and 200 GHz channel spacing. The bit rate is 10 Gb/s and the d.c is 0.125.

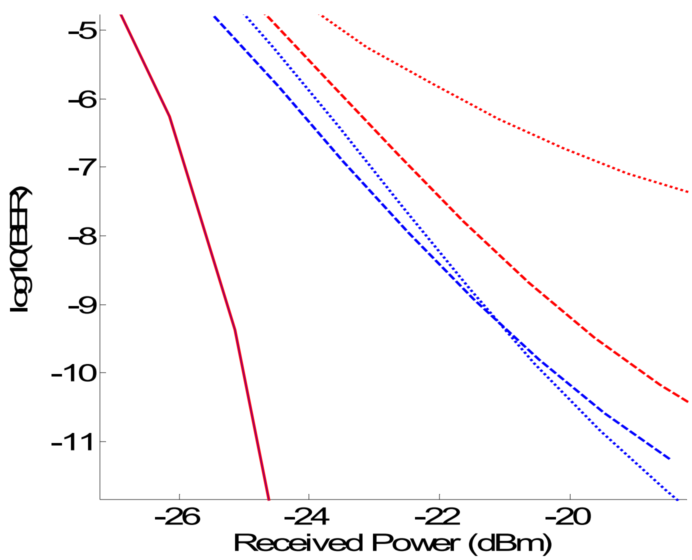


**Fig. 4.11** 100 GHz (red) vs. 200 GHz (blue) channel spacing for *P1,* with RZ modulated signals at 10 Gb/s with a 0.125 d.c., for 1 (solid), 4 (dashed) and 8 (dotted) WDM channel (1 channel configurations are exactly the same both for 100 GHz and 200 GHz spacing).

As Fig. 4.11 shows, when increasing the channel spacing to 200 GHz, the power penalty is decreased by 1 dB for the 4 channel configuration; a result expected by our previous analyses on the effect of channel spacing. Moreover, for the 8 channel configuration we can now achieve error-free operation (BER of $10^{-9}$) whereas with 100 GHz spacing a noise floor was reached at a BER of $10^{-8}$. However, the power penalty compared to the single channel case is still close to 4 dB for both the 4 and the 8 channel configurations.

The argument presented in the NRZ study when comparing the performance of different channel spacings, is further strengthened with these results. FWM interactions are diminished when the distance between the signals involved increases. As before, the addition of more channels will not considerably affect performance when these channels are located far away from the signal under consideration. This is why again, when 200 GHz spacing is used, further adding channels (from 4 to 8) does not affect the performance of the system, while when using a 100 GHz spacing the power penalty for adding more channels, is very substantial.

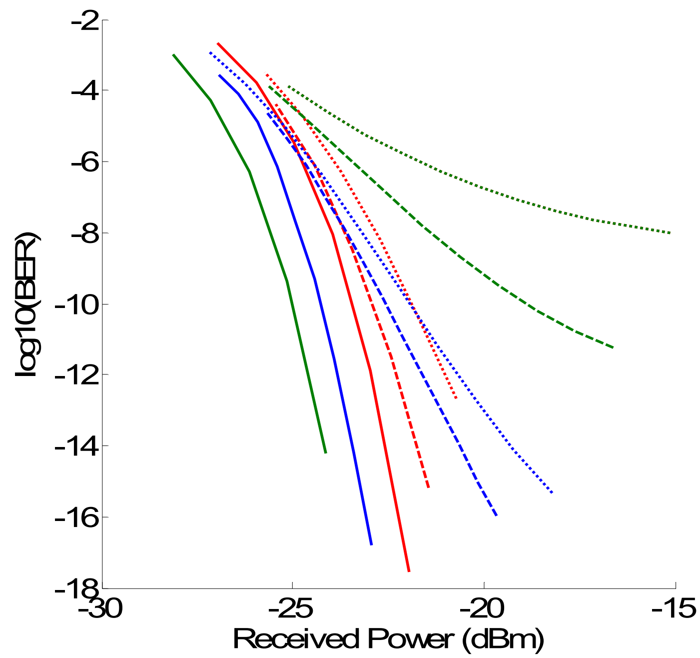


**Fig. 4.12** 100 GHz channel spacing for *P1***,** with RZ modulated signals at 10 Gb/s for 1 (solid), 4 (dashed) and 8 (dotted) WDM channels configuration for a d.c. of 0.125 (green), 0.25 (blue) and 0.5 (red).

Fig. 4.12 summarizes the results for all the RZ modulation configurations of different duty cycles and numbers of channels. Interestingly, the best performing d.c. varies depending on the number of channels present in the amplifier. First, for a single channel configuration the 0.125 d.c. is performing the best. This is because in the absence of other channels, the higher the peak power of the signal, the better the extinction ratio will be. However, when we move on to a 4 channel system the 0.25 and the 0.5 d.c. setups perform equally well for a BER of $10^{-9}$ while the 0.125 d.c. is by far the worse. Again, the strength of the 0.125 d.c. configuration (its high peak power), now becomes its weakness, increasing the nonlinear interactions (FWM, SPM and XPM) and thus degrading the signal quality. Finally, for the 8 channel configuration the 0.25 d.c. is marginally better while the 0.125 d.c. remains by far the worst performing modulation. Overall, one can say that the 0.25 d.c. is the best compromise for good performance for all numbers of channels as it is well balanced between the higher received power at the photodiode and the increased generation of nonlinear effects. Here we should also note that the advantage of the higher peak power is also reduced due to the increased shot noise generated by a higher amplitude pulse.

Next, we quantify the degradation in system performance when the bit rate is increased from 10 Gb/s to 40 Gb/s. We study the *P1* case with the channel spacing set to 100 GHz and the duty cycle at 0.5.

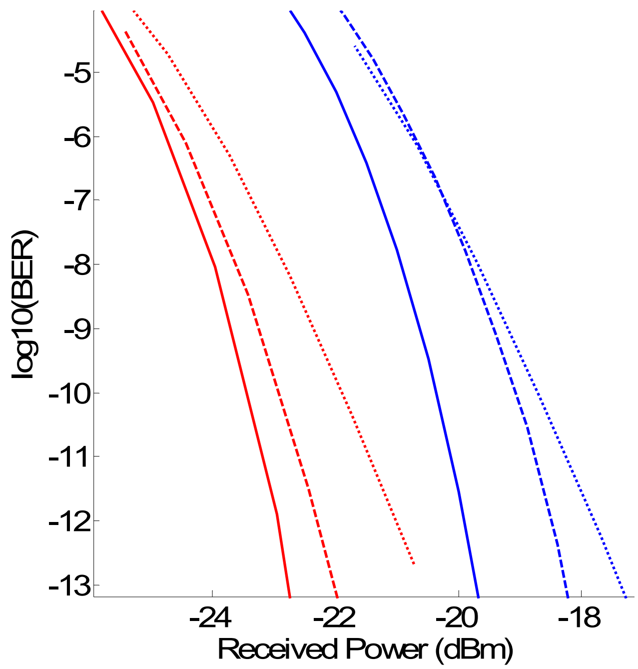


**Fig. 4.13** 40 Gb/s (blue) vs. 10 Gb/s (red) for *P1* with 100 GHz spacing and 0.5 d.c.for 1 (solid), 4 (dashed) and 8 (dotted) WDM channels

Fig. 4.13 shows that the 40 Gb/s scheme has higher receiver sensitivity requirements. The power penalty even in the single channel configuration, reaches 2.9 dB. This is an indication that the performance degradation in 40 Gb/s is not dominated by nonlinearities. Rather, the deciding factor is dispersion within the amplifier. In addition, the higher spectral width of 40 Gb/s pulses means that the peak power is much lower (as the power distribution in the spectrum is wider). The power penalty for the 8 channels configuration is slightly higher and reaches 3.2 dB. Also, the power penalty for doubling the channels from 4 to 8 seems to be less stringent for the 40 Gb/s configuration than for the 10 Gb/s one (0.1 vs. 1.1 dB), again for the same reason explained above.

### 4.2.5 Phase Shift Keying – Differential Phase Shift Keying

Phase-Shift Keying (PSK) is a modulation format that transmits data by modulating the phase of a signal. Every modulation scheme uses a finite number of distinct signals (of different frequency or amplitude) to represent binary data. PSK uses a finite number of different phases to represent binary bits. Each phase encodes an equal number of bits. Each pattern of bits forms the symbol that is represented by the particular phase. The demodulator, which is designed specifically for the symbol-set used by the modulator, determines the phase of the received signal and maps it back to the symbol it represents, thus recovering the original data.

In the case of DPSK, instead of using the bit patterns to set the phase of the wave, we merely change it by a specified amount. In order to demodulate the data we only have to detect changes in the phase of the received signal between successive bits; hence, the name DPSK. An important advantage of DPSK is the simplicity of its implementation over the ordinary PSK since there is no need for the demodulator to have a copy of the reference signal to determine the exact phase of the received signal (non-coherent scheme detection).

In RZ-DPSK, successive RZ pulses are modulated with different phases (the phase changes when there is a “1” and remains the same when we have a “0” or the opposite as shown in Fig. 4.14).

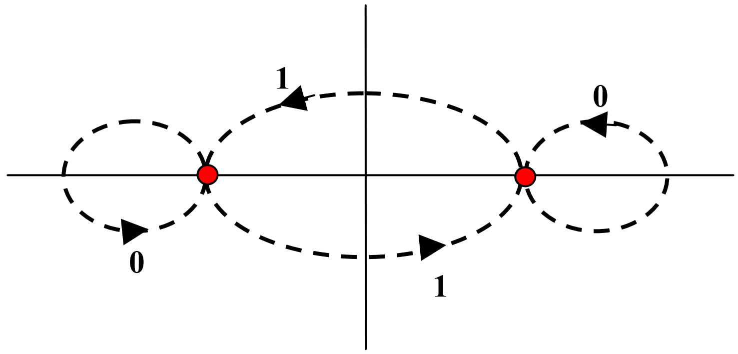


**Fig. 4.14** Finite State Machine diagram for DPSK modulation format.

Apart from improved receiver sensitivity DPSK offers [4.2], as the average power remains constant for every bit-period the signal becomes considerably more immune to non-linear effects and XGM compared to NRZ, RZ and NRZ-DPSK modulation formats while its spectrum has no carrier component [4.3].

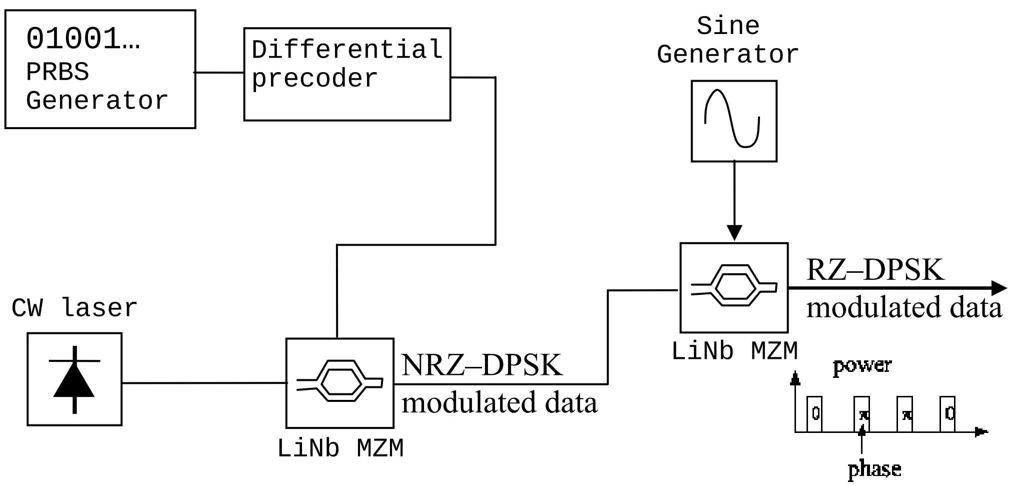


**Fig. 4.15** RZ-DPSK modulator topology. MZM : Mach-Zehnder modulator.

An RZ-DPSK modulator can be constructed using either a single [4.4] or double step [4.5] design. In our case, we adopt the latter design (see Fig. 4.15) as it is more commonly used in practise. We use 2 Mach-Zehnder modulators: one modulator performs phase modulation and is driven by a full bit-rate NRZ data stream, while the other modulator, biased at null, is used in order to generate an RZ pulse train and is driven with a half bit rate sine wave [4.6]. Essentially, in the first stage of the transmitter the phase information is modulated into our signal while the second stage modulates the intensity of the signal into successive RZ pulses. As is the case in RZ modulation, the RZ pulses are characterized by their duty cycle which is the percentage of the bit period during which the laser remains on. In our study of RZ-DPSK, a 33% duty cycle is always used.

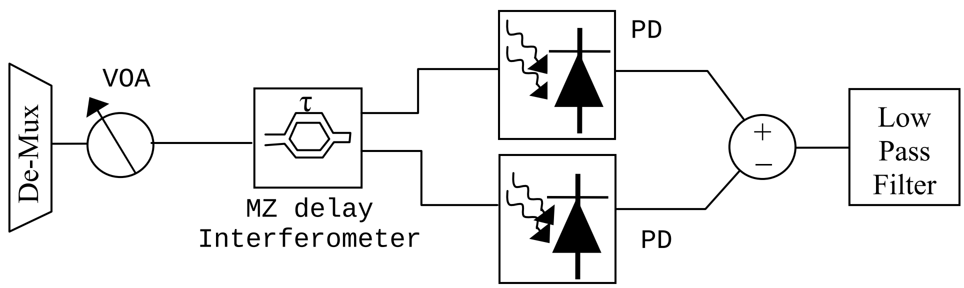


**Fig. 4.16** RZ-DPSK receiver using differential detection.

The structure of a balanced DPSK receiver is shown in Fig. 4.16. After the incoming optical signal has been demultiplexed, it passes through a 1-bit delay interferometer which optically demodulates the data and converts them into two intensity modulated, logically conjugated signals. On the one branch we have constructive interference and on the other one destructive interference. The signals are detected with the use of two photodiodes and subsequently subtracted. The difference of the two signals is then electrically filtered. Each delay interferometer output port carries the full information and could be used for direct detection by itself. However, by subtracting the two signals and using differential detection we gain 3 dB in receiver sensitivity.

First, we investigate the effect of increasing the number of channels and the deterioration of system performance through XGM and FWM when using RZ-DPSK modulation. The case under consideration is for *P1* while the channels are spaced by 100 GHz and modulated at 10 Gb/s.

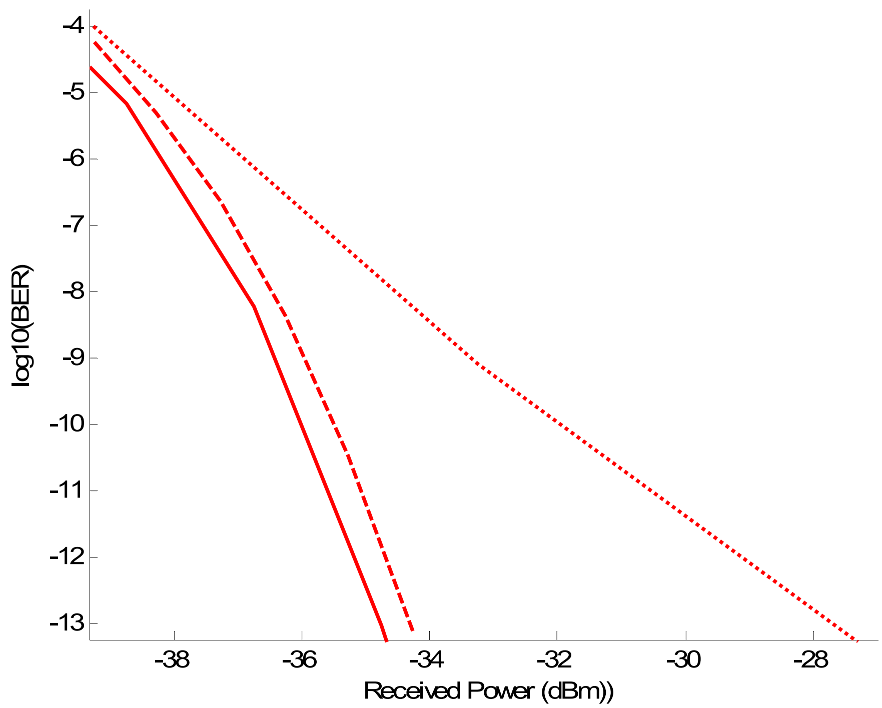


**Fig. 4.17** BER performance at 10 Gb/s for *P1* with 100 GHz spacing for 1 (solid), 4 (dashed) and 8 (dotted) WDM RZ-DPSK modulated channels

As we see in Fig. 4.17, the degradation of system performance is minimal when going from 1 to 4 channels (0.5 dB). However, when 4 more channels are added to the system, the increase in TIP takes a heavy toll on the performance bringing the power penalty to more than 3 dB.

It has been demonstrated that the use of RZ-DPSK modulation format can suppress XGM because of its constant intensity nature [4.8]. Therefore, the main contributing factors for the deterioration of the performance in the 8 channel configurations must be the FWM and other nonlinear effects. A more analytical discussion on the physical causes for the behaviour of RZ-DPSK will be given in the next section, where all the modulation formats we consider are compared.

Next, we examine the BER performance when increasing the bit rate to 40 Gb/s and comparing *P1* with *P2*. The channel spacing is 100 GHz.

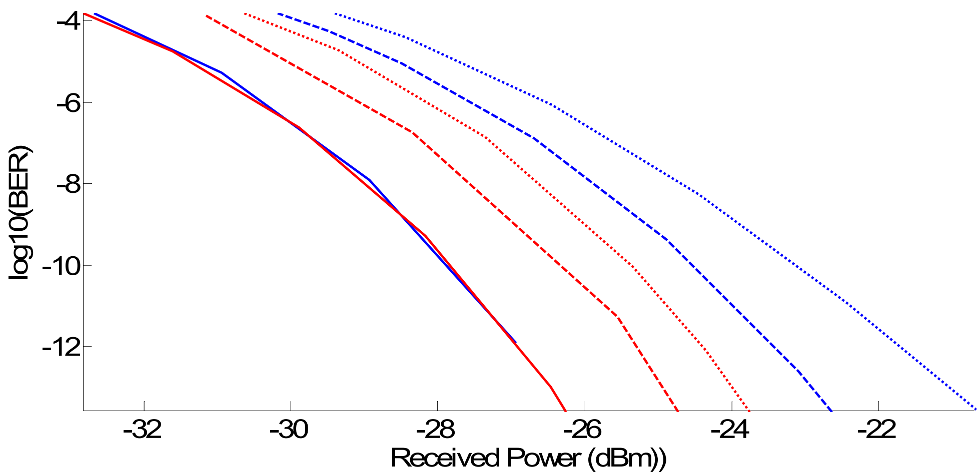


**Fig. 4.18** BER performance at 40 Gb/s for *P1* (blue) and *P2* (red) with 100 GHz spacing for 1 (solid), 4 (dashed) and 8 (dotted) WDM RZ-DPSK modulated channels.

Things are only slightly different when we look at the 40 Gb/s configuration. As shown in Fig. 4.18 the reduction of the system's sensitivity reaches 1.5 dB and 2 dB when 4 and 8 channels are present into the amplifier for *P2*, but increases significantly to 3.3 dB and 4.5 dB for *P1*. Nevertheless, as we will see more analytically in the next section, while RZ-DPSK is not immune to performance degradation due to FWM and XGM when more channels are added, the performance of RZ-DPSK is considerably better than any other modulation format.

Based on the results presented in Fig. 4.17 and Fig. 4.18, we plot the BER curves for both *P1*and *P2* when 8 channels are present in the amplifier for the two different bit rates.

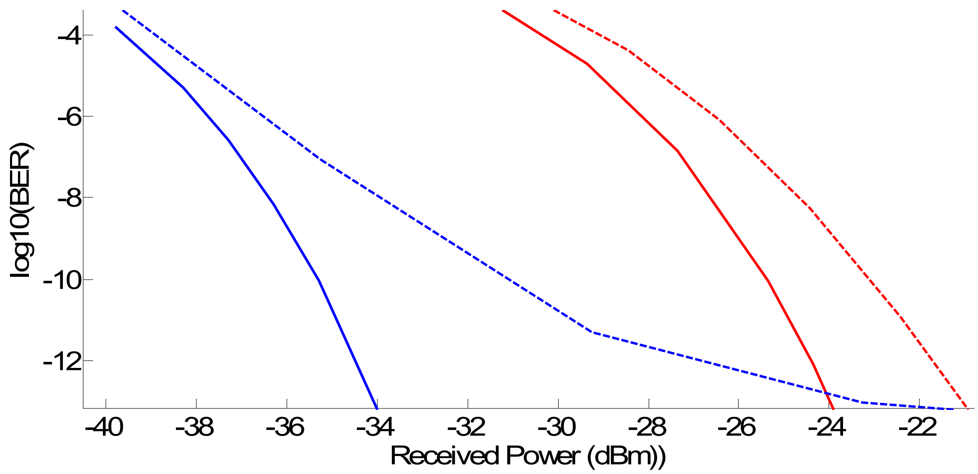


**Fig. 4.19** BER performance at 10 Gb/s (blue) and 40 Gb/s (red) for *P1* (dashed) and *P2* (solid) with 100 GHz spacing.

As we see in Fig. 4.19, the performance considerably deteriorates when the PCIP is increased for both bit rates. The degradation is around 2.5 dB in both cases. Now, comparing the 10 Gb/s with the 40 Gb/s configuration, we see that the system is very sensitive to the bit period and at 40 Gb/s when 8 channels are present in the system, the power penalties are similar to the ones seen in other modulation formats. This serves as a strong indicator that even if XGM is not the dominant degrading factor acting in the amplifier, nonlinear phenomena such as FWM are still affecting the quality of the signals in a significant way.

For reasons that have been previously discussed, the channel spacing is a very important factor for FWM. As it was previously shown, increasing the channel spacing from 100 GHz to 200 GHz significantly reduces the FWM effects and improves performance. This is expected to be the case when RZ-DPSK is employed as well.

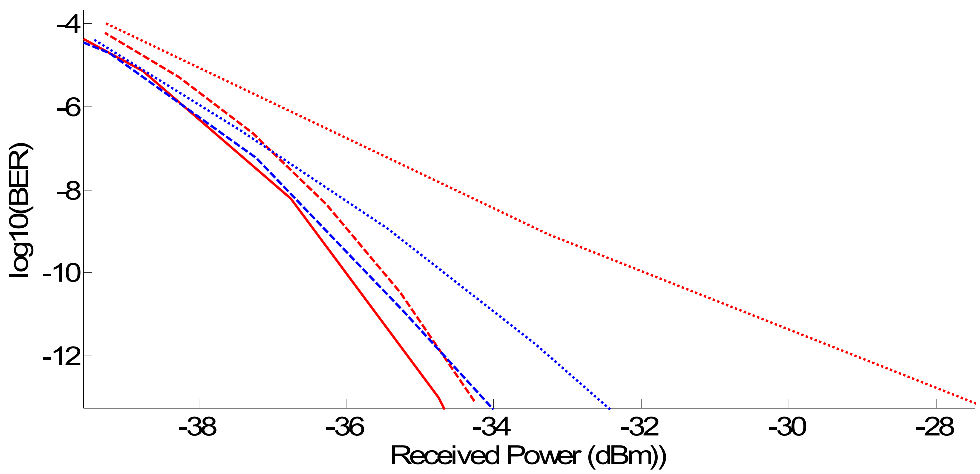


**Fig. 4.20** BER performance at 10 Gb/s for *P1* with 100 GHz (red) and 200 GHz (blue) spacing for 1 (solid), 4 (dashed) and 8 (dotted) WDM RZ-DPSK modulated channels.

Clearly, as seen in Fig. 4.20, when the signals are spaced at 200 GHz, the performance of the 8 channel system is similar to the one obtained for a 4 channel system spaced at 100 GHz. As the FWM crosstalk for a particular channel is dominated by the contribution from its closest neighboring channels, it seems that the degradation due to FWM, is similar for 4 channels spaced at 200 GHz and for 8 channels spaced at 100 GHz.

### 4.2.6 Modulation Format Comparison

First, we compare the 8 channel configurations for all RZ configurations (different d.c.) with NRZ. We do so to determine which of the ASK modulation formats (NRZ or RZ) performs better when used in a network employing FOPAs. We use the results obtained for *P1*, 8 channels and 100 GHz spacing.

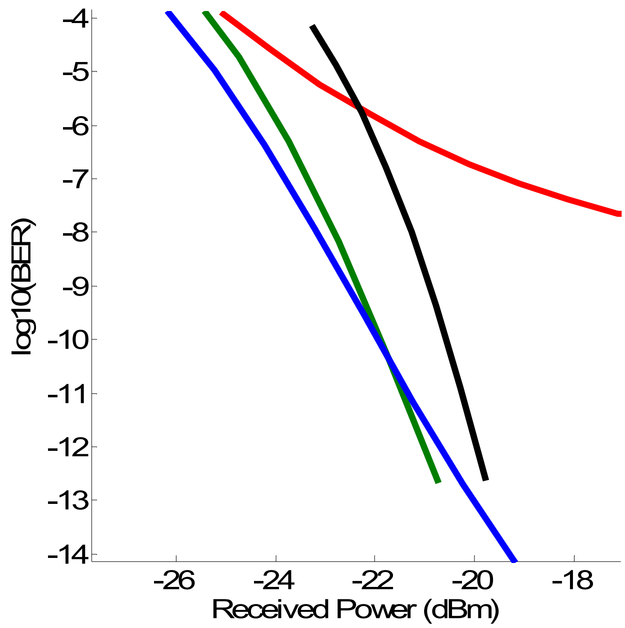


**Fig. 4.21** RZ 0.25 d.c. (blue), RZ 0.5 d.c. (green), NRZ (black) and RZ 0.125 d.c. (red) for 100 GHz spacing, *P1* at 10 Gb/s.

The best performing format as seen in Fig. 4.21 (albeit marginally) is for RZ 0.25 d.c. followed closely by RZ with 0.5 d.c. (0.15 dB of power penalty). The NRZ gives a power penalty of 1.6 dB while the RZ 0.125 d.c. as we previously showed, cannot even provide a BER of $10^{-9}$. Therefore, for a carefully selected d.c. RZ can provide much better performance than the NRZ when used in FOPAs.

As previously discussed, the pulse width of an NRZ modulated signal occupies the whole bit period. On the other hand, for RZ modulated signals, this is reduced to a fraction of the bit period which is determined by the d.c. This way, the portion that signal pulses of different channels overlap in time, decreases. Consequently, the efficiency of the FWM process between channels, also decreases.

Finally, we compare 8 channels configurations, for both *P1* and *P2*, modulated with RZ-DPSK, NRZ and RZ at 40 Gb/s. For the RZ case, we pick the best performing configuration (d.c. of 0.25). To show the striking difference in performance, we actually allow for the RZ and NRZ to have a 200 GHz channels spacing, while we keep the channel spacing of the RZ-DPSK at 100 GHz. For RZ this corresponds to the best case scenario.

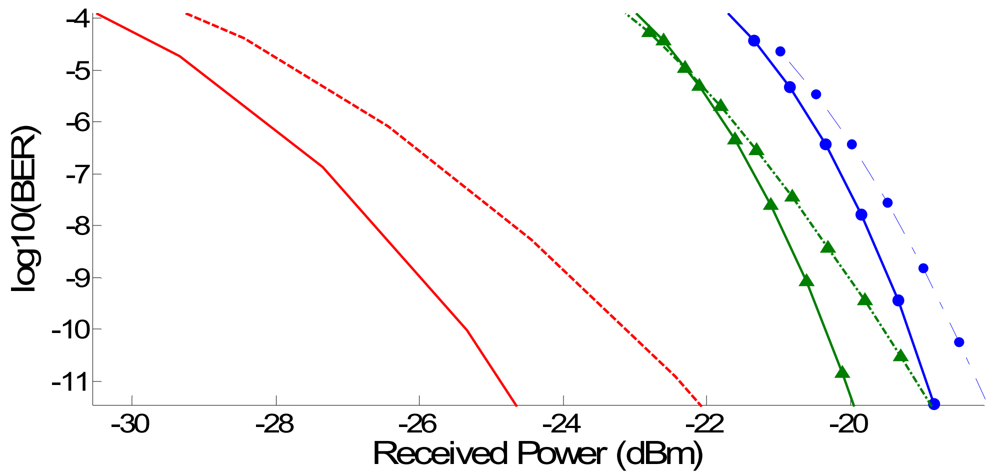


**Fig. 4.22** NRZ (blue circles), RZ with 0.25 d.c. (green triangles) spaced at 200 GHz, vs. RZ-DPSK (red) for 100 GHz spacing, *P1* (dashed) and *P2* (dashed) at 40 Gb/s.

Fig. 4.22 clearly demonstrates the superiority of the RZ-DPSK over RZ and NRZ modulation in the context of FOPAs. The increased sensitivity of the system reaches 6.5 dB for *P2* and 5 dB for *P1* when compared to NRZ. Similarly, the RZ-DPSK performs much better even when compared to the best case scenario for RZ. The increased sensitivity in this case reaches 4 dB for *P1* and 6 dB for *P2*. Many of the physical causes of these results have been explained analytically throughout this chapter.

## *4.3 Conclusion*

Optical DPSK modulation can be advantageous for several reasons: First, the optically pre-amplified quantum limited DPSK receiver gives ~ 3 dB better sensitivity compared to NRZ modulation when using differential data detection. Second, for the same average power, the peak power in DPSK is 3 dB less than in NRZ. Finally, the optical power is more evenly distributed in a DPSK signal than in NRZ since power is present in every bit slot. The latter two points imply that DPSK can be more resilient to fibre nonlinear effects.

Furthermore, RZ modulation has the broadest optical spectrum (about twice as wide as the NRZ modulation). The DPSK spectrum is similar to NRZ, except for the lack of a carrier. DPSK modulation has a lower peak power compared to NRZ, and thus, creates reduced nonlinear effects. Moreover, the DPSK 3 dB advantage in receiver sensitivity makes it possible to lower the launch power of WDM channels to further reduce nonlinear effects, or to use the extra margin for other link impairments such as dispersion and linear crosstalk.

These results also confirm that the FWM crosstalk for a particular channel is dominated by the contribution from its closest neighbouring channels. Meanwhile, compared with FWM of continuous waves, FWM between optical pulses generally has larger conversion efficiency under the same average power when they overlap in time [4.7]. Therefore, NRZ pulses will suffer more from this impairment as the overlap happens for a whole bit period. This fact shows that by using the RZ-DPSK format, FWM-induced crosstalk can also be successfully reduced [4.8]. However, overall, the FWM interactions will still be higher than in the case of RZ, as the FWM interactions occur in every bit period (constant average power per bit period). Here we should also note that when data are transmitted over long distances at high bit-rates, RZ modulation formats will suffer from dispersion more than NRZ, due to the fact that RZ has a wider optical bandwidth.

As it was previously shown in [4.9], crosstalk suppression in a single pump FOPA can be achieved by using the RZ-DPSK modulation format. In this section we confirmed these results. This is basically achieved by greatly reducing XGM (as described in section 4.2.1), by using a constant power per bit period, modulation scheme. In addition, because the improvement when using RZ-DPSK is so significant for all input power levels and bit rates, it is apparent that the dominant impairment experienced by RZ and NRZ is XGM, while FWM and other impairments are less significant.

Moreover, in accordance with [4.10], our observations suggest that there is a performance gain for RZ formats (for carefully selected d.c.) over NRZ formats in terms of the FWM-induced crosstalk level. This is due to the lower duty cycle of RZ signal pulses for the reasons explained before.

Even with a 100 GHz channel spacing at 40 Gb/s and with eight WDM channels, the RZ-DPSK signal easily outperformed its OOK counterpart by 4 dB reduction of the power penalty. These observations suggest that the XGM was the dominant source of crosstalk even with high channel count and dense channel spacing. Based on these results we can assert that FOPAs can be used in conjunction with RZ-DPSK channel modulation in WDM communication systems.

**References**

[4.1] M. Murakami, T. Matsuda and T. Imai, "FWM generation in higher order fiber dispersion managed transmission line", Photonics Technology Letters, vol.14, no.4, pp. 474-476, (2002).

[4.2] L. Christen, I. Fazal and M. Giltrelli, "PMD and CD sensitivity enhancement in directly modulated transmission systems through RZ DM-DPSK", European Conference on Optical Communication , paper Th224, Glasgow, Scotland, September 25 - 30 (2005).

[4.3] T. Mizuochi, K. Ishida, T. Kobayashi, J. Abe, K. Kinjo, K. Motoshima and K. Kasahara, "A Comparative Study of DPSK and OOK WDM Transmission Over Transoceanic Distances and Their Performance Degradations Due to Nonlinear Phase Noise", Journal of Lightwave Technology, vol. 21, pp. 1933, (2003).

[4.4] L. Xiang and Y.-H. Kao, "Chirped RZ-DPSK based on single Mach-Zehnder modulator and its nonlinear transmission performance", Photonics Technology Letters, vol.17, no.7, pp. 1531-1533, (2005).

[4.5] W. A. Atia and R. S. Bondurant, "Demonstration of return-to-zero signaling in both OOK and DPSK formats to improve receiver sensitivity in an optically preamplified receiver", IEEE Laser and Electro-Optics Society Annual Meeting, paper TuM3, San Francisco, USA, November 8 - 11 (1999).

[4.6] A. H. Gnauck, G. Raybon, S. Chandrasekhar, J. Leuthold, C. Doerr, L. Stulz and E. Burrows, "25×40-Gb/s copolarized DPSK transmission over 12×100-km NZDF with 50-GHz channel spacing", Photonics Technology Letters, vol.15, no.3, pp. 467-469, (2003).

[4.7] M. Shtaif, R. Nagar and G. Eisenstein, "Four-wave mixing among short optical pulses in semiconductor optical amplifiers", Photonics Technology Letters, vol. 7, no. 9, pp. 1001–1003, (1995).

[4.8] S. Kumar, "Analysis of degenerate four-wave-mixing noise in return-to zero optical transmission systems including walk-off," Journal of Lightwave Technology, vol. 23, no. 1, pp. 310-320, (2005).

[4.9] B. P. -P. Kuo, P. C. Chui, K. K. -Y. Wong, "Suppression of WDM signal crosstalk in fiber optical parametric aAmplifier by using RZ-DPSK modulation format", Optical Fiber Communication Conference, paper OWB3, Anaheim, USA, March 25 - 29 (2007).

[4.10] B. P. -P. Kuo, P. C. Chui, K. K. -Y. Wong, "A comprehensive study on crosstalk suppression techniques in fiber optical parametric amplifier by modulation format", IEEE Journal of Selected Topics in Quantum Electronics, vol.14, no.3, pp. 659-665, (2008).

# Chapter 5 Gain-clamping FOPAs using a ring configuration

## *5.1 Introduction*

As discussed in Chapter 1, FOPAs have not been extensively studied in the context of AAPNs or generally, in multi-channel dynamic environments. Only recent advancements such as HNLFs and high power pumps sources at the 1500 nm region have allowed FOPAs to be considered as an alternative amplifier technology for optical telecommunications.

Multi-channel configurations have been demonstrated [5.1],[5.2], while some of the most important weaknesses of FOPAs have also been investigated [5.3],[5.4]. Specifically, as is the case for all optical amplifiers, when operating well below the saturated regime, the gain provided to each signal is independent of its input power as long as there is enough pump power to provide enough gain. However, when the amplifier operates close to its saturated regime, the gain provided depends not only on the total input signal power $P_{S,tot}$, but in the case of FOPAs, on the position of the channels present in the amplifier. This property is due to complex FWM interactions taking place amongst all signals present in the fibre. In an environment where frequent channel add/drops take place, such a situation makes the gain provided to the individual channels very unstable. In addition, generally speaking, the rule "the higher the $P_{S,tot}$, the lower the gain the amplifier can provide" does not always hold true in FOPAs as shown in Chapter 3. Particularly, the gain spectrum strongly depends on the number of input signals. Again, any change as a result of variations in PCIP is irregular and not predictable due to the complex nature of the nonlinear FWM interactions. It has also been shown that large gain-excursions can be observed in the case of channel add/drop. These gain excursions strongly depend on the position of the surviving channel.

In the cases of other amplifier technologies such as EDFAs or FRAs, such hindrances have been tackled by employing several methods of gain control. One popular approach is AOGC using either a ring configuration or a linear cavity. Other techniques include signal control and pump control. In this chapter, we investigate for the first time the use of AOGC in FOPAs.

## *5.2 Motivation and Gain-Control Techniques*

For most amplifiers, when they operate well below the saturated regime, the gain the amplifier provides to each signal is independent of its input power as long as there is adequate pump power to provide sufficient gain. On the other hand, when the amplifier operates close to its saturated regime, the gain it provides depends on the total input signal power $P_{S,tot}$. Generally speaking, the higher the $P_{S,tot}$, the lower the gain the amplifier can provide.

The reason for this phenomenon is apparent. As the signal input power grows, the pump power required to achieve the same gain increases. Obviously, for small input signals the pump power is sufficient to provide a lot of gain; for large input powers the pump power is only sufficient to provide a few dB of gain. More specifically, when the amplifier is far from being saturated (i.e., when there is plenty of pump power), the total gain depends on the gain coefficient of the fibre and its total length. In other words there is enough pump power to be transferred to the signal and the only limiting factors are the physical characteristics of the amplifier. However, as $P_{S,tot}$ increases, the amplifier approaches its saturated regime and the available pump power becomes more and more depleted while the amplifier is not able to provide the same gain as before. At this point the decisive factor is the available pump power and not the gain coefficient or the amplifier length.

Ostensibly, gain saturation is unacceptable in dynamic optical network where channel add/drop and redistribution occur frequently. In this way, fluctuations of input signal power, and thus gain, can become severe. The problem becomes more evident after several cascaded amplifiers. The variations in the gain can become so considerable so as to result in significant system performance degradation. Therefore, effective gain control is important for FOPAs as is for other amplifiers operating in such an environment.

Fig. 5.1 illustrates the gain as a function of total input signal power for an amplifier with and without gain-control.

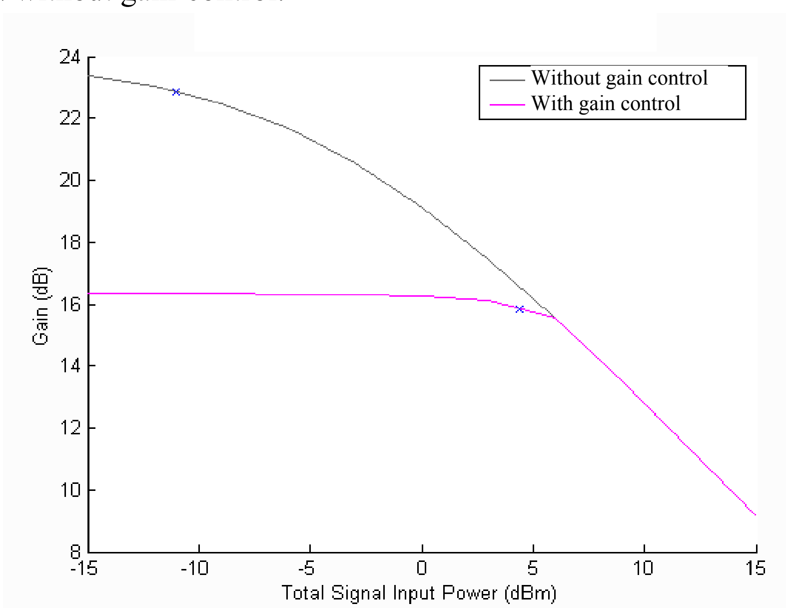


**Fig. 5.1** Gain as a function of total signal input power for an optical amplifier with and without gain control.

Without gain control, the gain varies significantly with the input power. On the other hand, with gain control, the gain is effectively locked or clamped to a specific value over a range of input signal powers. In the following section, we will discuss some of the most popular technologies for gain control.

### 5.2.1 Gain Changes and Gain-Control Techniques

In a typical optical amplifier without gain control, as the TIP is increased, the steady-state gain provided by the amplifier decreases. Due to this effect, certain signals in the system may not receive sufficient gain, in which case their power would be too low for detection at the receiver. On the other hand, as the TIP is decreased, the gain that the amplifier provides increases so that a certain signal may receive too much gain and be at too high a power level to be properly detected at the receiver, or its high power may result in the appearance of undesirable nonlinear effects.

Several of the phenomena that act as impediments in FOPAs that we described in this thesis so far can be summarized as a variation of gain the amplifier provides, when the operating conditions of the system change. Alternatively, we can say that the FOPA fails to supply a constant gain that is independent of the operating conditions, such as the PCIP, the number and the position of the channels that enter the amplifier or even the actual information encoded in the channels themselves. These phenomena have been recognised and controlled in both EDFAs [5.5], [5.6], and in DFRAs [5.11], [5.7]. In the following section we will present several of the techniques that have been used as means of mitigating the above described phenomena.

These gain-control techniques we present are applied to both EDFAs and DFRAs. We first look at the active gain control technique, i.e., pump control, and we then consider the passive AOGC technique.

### 5.2.2 Pump Control

One of the fist approaches of implementing gain-control has been pump control [5.8]. In the pump control, a small portion of the output power from the amplifier is tapped. The monitor channel that has been fed into the amplifier is then filtered out, detected, and used to define an electrical signal to the pump driver. When the input signal power varies, changes in the power of the probe signal can be detected at the feedback loop first and then the pump driver circuit will continuously adjust the pump power injected to the amplifier until the preset gain value of the probe signal is obtained. The purpose of the pump control method is to suppress gain saturation by increasing or decreasing the pump power as the input signal power changes.

Fig. 5.2 graphically depicts the configuration of a pump-controlled gain-locking feedback loop in an FRA (a similar technique is used for EDFAs as well). To lock the gain of the amplifier for variable channel loading, the input pump power must be varied. Negative-feedback control derived from a monitoring channel output power has been introduced in the amplifier. In this case, results showed that the power excursion for the surviving channel in an FRA providing 10 dB of gain, due to the removal/addition of six channels in an eight-channel multi-wavelength system can be reduced to less than 0.1 dB when the pump-power-feedback parameters are properly selected [5.8].

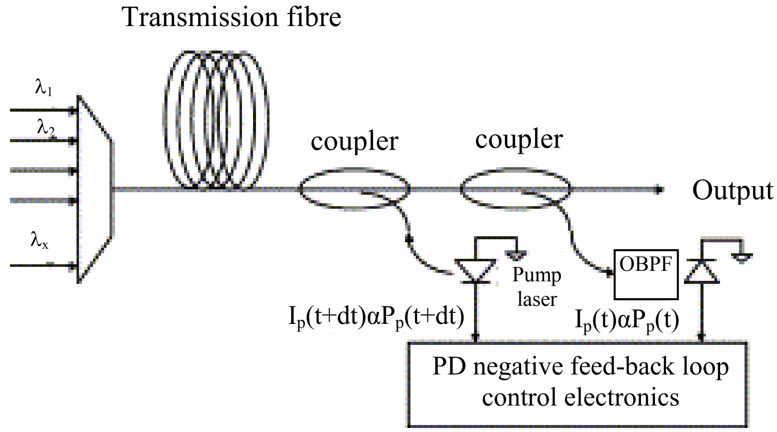


**Fig. 5.2** Schematic diagram of RFA with pump-power-controlled gain-locking system.

Although pump control shows promise, the complexity of the required additional electronic circuitry poses serious difficulties for practical implementation. The speed requirements are very stringent; pump control circuitry must be able to process fall/rise times of less than 30 μs [5.8].

### 5.2.3 Signal Control

Signal control can be implemented with active and passive approaches. One active method is to use a similar feedback loop structure as in Fig. 5.3 to monitor the variations of the signal power at the output. Instead of changing the pump power, an additional laser signal (auxiliary signal) is added at the input and the power level injected to the amplifier can be adjusted based on its output power. The function of this additional signal is to compensate the variations of input signal power by keeping the total input power to the amplifier constant. Therefore, gain saturation of this amplifier is fixed to a level which leads to a constant gain for all the input signals.

An example of a passive signal control method in FRAs was proposed by Seo *et al.* [5.9]. A new type of all-optical variable attenuator based on the SRS process was theoretically proposed to equalize the power imbalance induced by Raman crosstalk without degradation of the signal-to-noise ratio. More specifically, when a germanium-doped Raman fibre medium is pumped with 270 mW at 1.46 μm, WDM channels tilted with initially 5 dB of power difference in the spectral range of 1.571–1.591 μm were equalized to within 0.93 dB. The configuration and its resulting output are shown in Fig. 5.3.

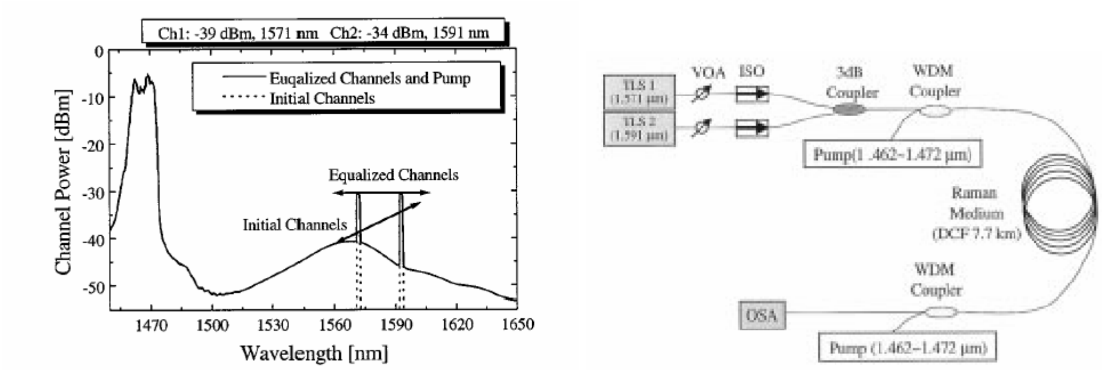


**Fig. 5.3** a) Power equalization of two initially tilted channels, 1571 nm at -39 dBm and 1591 nm at -43 dBm, for a pump power of 250 mW b) Experimental setup for channel equalization using a Raman fibre amplifier [5.9].

Although the above methods are very effective in clamping the signal gain, they exhibit a few important drawbacks. First, they require additional optical and optoelectronic devices such as a tap, filter and detector to pick up the optical probe signal, then process and generate an electronic control signal in the feedback loop in order to do gain control, thereby greatly increasing the cost. Second, gain-locking is not self-regulated by the amplifier; i.e., it is controlled by processing electronics in addition to a pump driver circuit or LD driver circuit in the feedback loop. Therefore, the pump power or LD output power needs to be varied over a large range to compensate the gain variations. This requires a very complicated pump/LD driver circuit in order to achieve a better clamping performance. Moreover, concerning FOPAs, based on our investigation in the previous chapters, these methods would be impractical and extremely complex to implement as the FWM interactions occur amongst all signals and the output of the amplifier is difficult to predict.

### 5.2.4 All-Optical Gain-Clamping

The second gain control technique used to mitigate gain transients in optical amplifiers is the passive AOGC. The AOGC consists in introducing a lasing signal generated inside the amplifier at a wavelength outside the channel bandwidth. This lasing signal then acts as a feedback control signal. When the power of the signals to be amplified varies at the amplifier input, the power of the lasing signal adjusts so that the gain of the signals remains unchanged. AOGC presents the advantage of not requiring expensive optoelectronic devices and its response time is not limited by the electronic circuits. However, the response time of the AOGC depends on the length of the lasing signal cavity as this response time is directly related to the time it takes for the lasing signal to re-establish its steady-state. Thus, reducing the length of the amplifier enables the reduction of the response time. The AOGC can be realized in two different configurations: the travelling-wave and the standing-wave configurations.

**Standing-Wave AOGC With the Use of Fibre Bragg Gratings**

The lasing signal that keeps the saturation level of the amplifier at constant levels can be formed using two FBGs. This method has been successfully used in EDFAs and DFRAs in order to suppress gain transients generated by channel add/drop [5.10], [5.11].

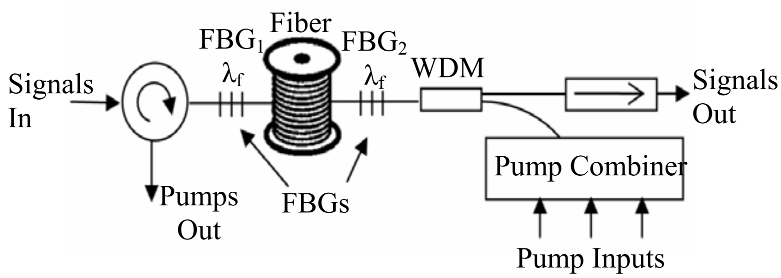


**Fig. 5.4** Configuration of forward pumped, gain-clamped FRA with FBG fibre laser structure

A typical configuration is shown in Fig. 5.4 for an FRA. A pair of FBGs is placed at the two ends of the amplifier creating a standing wave. FBG is a band-pass reflector in which an optical signal centred at the Bragg wavelength will be reflected; other wavelengths, however, will be transmitted. Hence, signals other than the feedback wavelength ($\lambda_f$) are not affected by the FBG. Spontaneous optical noise is amplified throughout the gain medium until the gain is clamped to the losses. When the optical power at this wavelength arrives into the right end of the amplifier it is reflected back while allowing a small amount of power to leak through the FBG. The process is repeated as the lasing signal is travelling backwards towards the first FBG. The reflectivities of the FBG set the losses of the cavity and thus the gain experienced by the lasing signal. The gain equals the total losses in the cavity:

$$g = \alpha - \frac{1}{l}\ln\left(R_1 R_2\right) \qquad \text{Eq. (5.1)}$$

where $g$ is the gain, $\alpha$ the losses of the gain medium and $R_1$, $R_2$ are the reflectivities $FBG_1$ and $FBG_2$, respectively. The feedback level, and hence gain, is determined largely by the FBG reflectivities $R_1$ and $R_2$ at $\lambda_f$. It is also possible to adjust the wavelength of the lasing signal and the losses of the cavity by straining or compressing the FBGs. This configuration presents the advantage of neither affecting the WDM signals, nor increasing the noise.

**Traveling-Wave AOGC**

The traveling-wave configuration consists in building the lasing signal with a ring cavity. In this configuration, a small amount of power is tapped out of the amplifier (usually 1%), propagates through the feedback loop and re-enters the amplifier from its other side. This way a high power lasing signal is formed inside the amplifier. The gain of that the lasing signal experiences equals the losses of the cavity. This lasing signal makes the amplifier gain-clamped. Adding an optical attenuator in the ring allows for the variation of the losses of the ring cavity, thereby adjusting the degree of gain-clamping for the amplifier. In such a configuration, the losses are equal to the tapped amount of power plus all passive component losses.

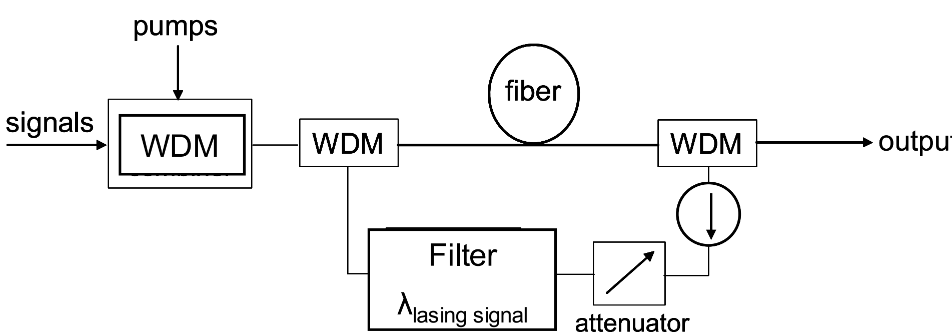


**Fig. 5.5** Diagram of a FRA with AOGC using a ring laser configuration

This gain-control technique has two major advantages: it is possible to vary the wavelength of the lasing signal by using an adjustable bandpass filter and to vary the losses of the ring cavity using a VOA. However, this technique exhibits one important drawback. Part of the WDM signals is also tapped out together with the lasing signal, resulting in a power loss.

The ring configuration AOGC was first used in order to study the steady-state characteristics of a gain-clamped DFRA [5.12], [5.13] and its efficiency in maintaining the signal gain constant over a certain range of input power was clearly demonstrated.

## *5.3 Gain Clamping a FOPA with a Ring configuration*

For the FOPA, we decided to use a ring configuration in order to clamp our amplifier. The ring configuration was chosen over the standing wave configuration because of the superior performance it has demonstrated when used in other amplifier technologies (smaller overshoots, less time to reach steady state) which is mainly because of the shorter length the lasing signal travels in order to complete one full trip inside the cavity. Moreover, signals in FOPAs are only amplified when co-propagating with the pump. Therefore, in the case of the standing-wave configuration, during half of its trip, the feedback wavelength would not be affected by the changes occurring inside the amplifier.

### 5.3.1 System Layout and Parameters

The layout of a FOPA using a laser feedback in a ring configuration can be seen in Fig. 5.6. The feedback loop only consists of a few passive, all-optical devices. In this method, gain control is done purely in the optical domain.

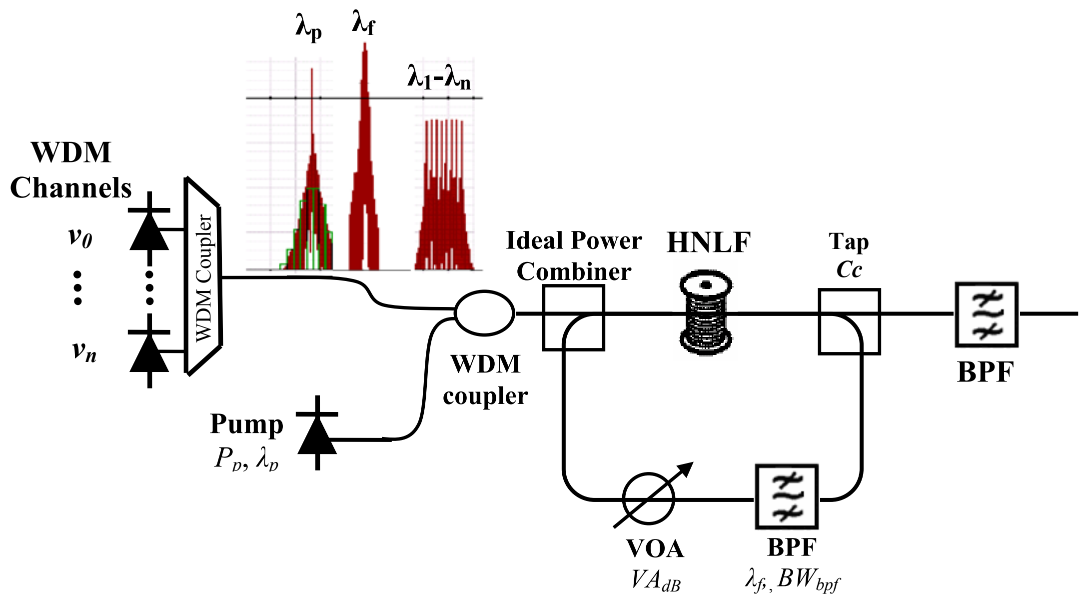


**Fig. 5.6** Gain-clamped FOPA using a ring configuration.

An amount of the optical power at the output of the amplifier is tapped. The coupling coefficient (*Cc*) determines how much of the total power will enter the ring. The residual noise that is found at the wavelength selected by the BPF ($\lambda_f$) starts travelling inside the ring and is constantly amplified in every round trip. This way the lasing signal is created inside the ring and enters the amplifier together with the data (DWDM) signals. The bandwidth of the BPF ($BW_{bpf}$) defines the width of the lasing signal. Due to the lasing condition (i.e., in steady state, the gain should be equal to the total cavity loss which can be set by adjusting the variable attenuation ($VA_{dB}$), the gain of this lasing signal inside the amplifier is clamped to a level which in turn clamps the gain provided by the amplifier to a specific level. When the signal power increases further than a certain point, the amplifier is not able to provide the same gain levels and clamping fails along with the lasing of the feedback. In other words, the $\lambda_f$ stops lasing as the amplifier cannot provide enough gain to sustain it. The fibre parameters of the HNLF used in all configurations are the ones given in Table 3.1, except for the dispersion slope $S$ which is 0.09 ps/(nm$^2$·km).

### 5.3.2 Gain vs. PCIP

Fig. 5.7 illustrates the gain as a function of input signal power for a single channel configuration for a FOPA with and without gain control. The parameters for the specific example used to demonstrate the use of gain-clamping are the following: $P_p$ = 30 dBm, $\lambda_p$ = 1535 nm, $\lambda_f$ = 1545 nm, coupling coefficient ($Cc$) = 1%, $L$ = 0.5 km, $BW_{bpf}$ = 50 GHz, $\lambda_0$ = 1530.5 nm, $v_0$ = 194.55 THz, $VA_{dB}$ = 0 dB. The channels are numbered from $v_0$ to $v_n$ in ascending order (increasing frequencies).

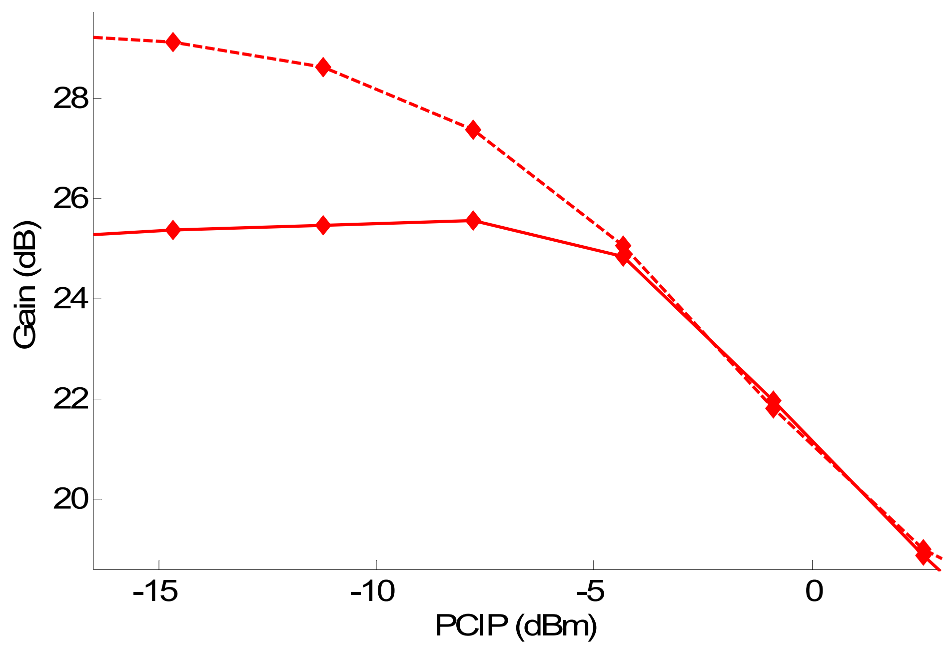


**Fig. 5.7** Gain vs. PCIP for single channel configuration without laser feedback (diamonds with red dashed line) and with laser feedback (diamonds with red solid line).

Without gain control, the gain varies significantly with the input power. On the other hand, with gain control, the gain is effectively locked or clamped to a specific value over a range of input signal powers. In the above example, $P_{cr}$ for the unclamped amplifier is -12 dBm while when clamped this value reaches -5 dBm. We have to note here that the definition of critical power does vary in the literature, from being the input signal power at which the lasing signal breaks down [5.14] to the PCIP at which the amplifier provides less than 0.5 dB of gain than it did in the small-signal regime [5.15]. However, in FOPAs as the gain can grow along with the PCIP these arbitrary definitions can be reformed. In this case we define $P_{cr}$ as the PCIP at which the gain the amplifier provides has changed by more than 0.5 dB; in other words $P_{cr}$ has been reached when

$$\left|G_{SSR} - G_{PCIPx}\right| \geq 0.5dB \qquad \text{Eq. (5.2)}$$

where $G_{SSR}$ is the small-signal regime gain and $G_{PCIPx}$ is the gain provided for a specific PCIP$_x$.

Similarly, when more than one channel enters the amplifier, AOGC has a similar effect as shown in Fig. 5.8. In the example below, two channels are introduced into the amplifier. As has been studied before [5.16], the strong FWM interaction between adjacent channels can lead to the increase of gain received by specific channels for an increase in PCIP. With the introduction of the high-power lasing signal the pump is depleted even when operating in the small-signal regime. However, there is a strong FWM interaction between the lasing signal and the WDM channels.

The parameters for this FOPA are the following: $P_p$ = 30 dBm, $\lambda_p$ = 1532 nm, $\lambda_f$ = 1543 nm, $Cc$ = 6%, $L$ = 0.4 km, $BW_{bpf}$ = 50 GHz, $\lambda_0$ = 1530.5 nm, $v_0$ = 193.8 THz and $v_1$ = 193.85 THz, $VA_{dB}$ = 2 dB.

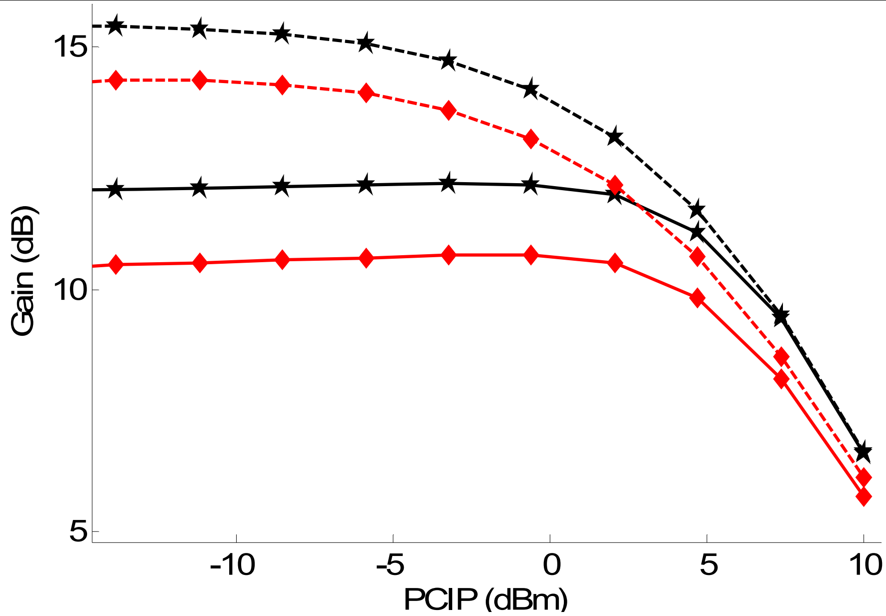


**Fig. 5.8** Gain vs. PCIP for two channel configuration, 193.8 THz (red diamonds) and 193.85 THz (black stars) without laser feedback (blue dashed line) and with laser feedback (red solid line).

The situation repeats itself even when 4 channels are introduced into the amplifier. In Fig. 5.9 one can see the Gain vs. PCIP plots for the exact system described before; only this time two more channels have been added into the amplifier, increasing in frequency in increments of 50 GHz; that is $v_3$ = 193.9 THz and $v_4$ = 193.95 THz.

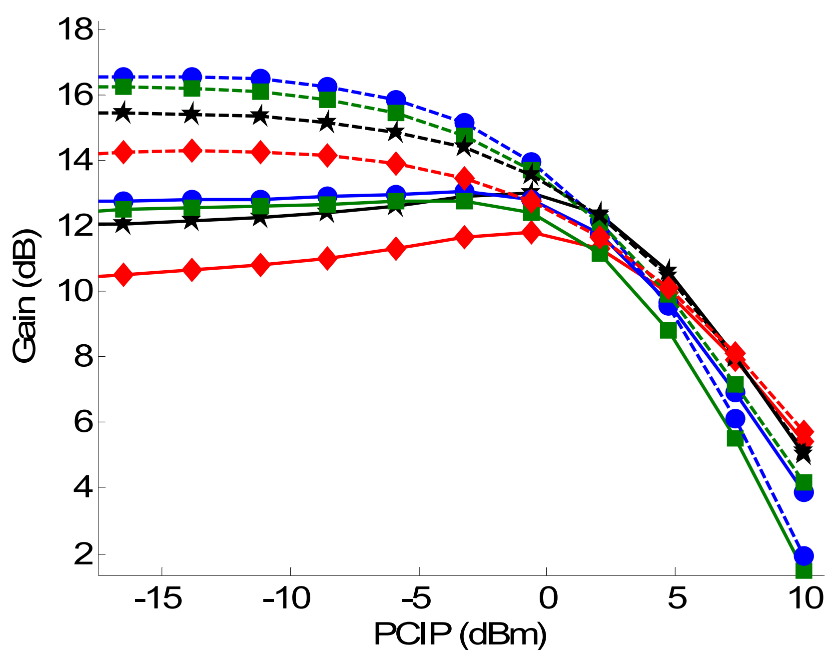


**Fig. 5.9** Gain vs. PCIP for four channel configuration without laser feedback (dashed) and with laser feedback (solid). The frequencies of the WDM channels are: 193.85 THz

(red diamonds), 193.85 THz (black stars), 193.9 THz (green squares), and 193.5 THz (blue circles).

A number of useful information can be extracted comparing Fig. 5.8 and Fig. 5.9. First, the two channels at $v_0$ and $v_1$ (193.8 THz and 193.85 THz) receive the same small signal regime gain in both cases (9.9 dB and 11.8 dB accordingly). This is expected as at these PCIPs the amplifier is unsaturated and thus the introduction of two more WDM channels does not alter the interactions between the signals present into the amplifier. As the PCIP is uniformly increased for all 4 WDM channels, we observe a distinct change from Fig. 5.8. The gain of $v_0$ is increasing further than in the 2 channel case, before reaching $P_{cr}$ where the gain clamping condition breaks down. Channel $v_1$ behaves in a similar way as well. Furthermore, $P_{cr}$ is 0 dBm for both channels, as opposed to 5 dBm in the 2 channel case.

### 5.3.3 Optimizing the AOGC

For a fixed pump and lasing wavelength, as well as zero dispersion wavelength, there are 3 variables with which we can control the feedback conditions of the GC amplifier and affect the GC conditions: the pump power, the bandwidth of the feedback signal and the value of the VOA. Following from the previously presented results, in the section below we will demonstrate how each of these variables can be used in order to improve the GC conditions of the system.

**Effect of $VA_{dB}$, $Cc$ and $BW_{bpf}$ parameters**

In this section we investigate the impact of varying the $Cc$ and the $VA_{dB}$. First, we increase $Cc$ to 10% while in the same time we reduce the $VA_{dB}$ to 1 dB. As before, $v_0$ is located at 193.8 THz, while the channel spacing is 50 GHz. The result is presented in Fig. 5.10.

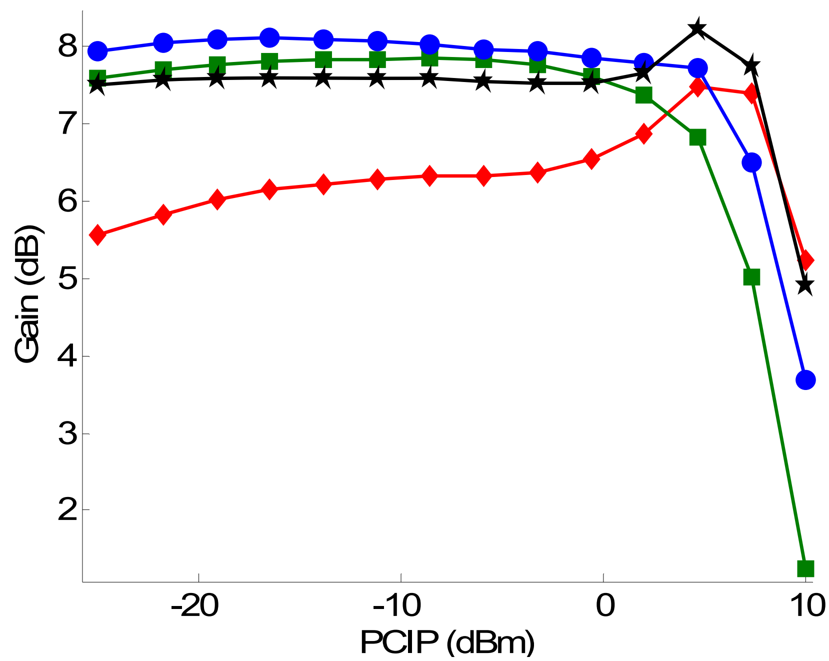


**Fig. 5.10** Gain vs. PCIP for four channel configuration (193.8 - 193.95 THz) when $Cc$ = 10% and $VA_{dB}$ = 1 dB. The frequencies of the WDM channels are: 193.8 THz (red diamonds), 193.85 THz (black stars), 193.9 THz (green squares), and 19.95 THz (blue circles).

Clearly, the amplifier is gain clamped for a large range of input powers. However, the following effects have taken place:

1. The small-signal gain for all channels has been reduced compared to Fig. 5.9 as a result of higher feedback for the lasing signal (thus less pump power available for the channels) and because of the increase in $Cc$, which now taps more power from the WDM channels into the ring.
2. Channel $v_0$ received substantially less gain than the other channels. This is probably a result of the shrinking and falling of the gain spectrum of the FOPA as a result of the increased power drawn by $\lambda_f$.
3. The gain provided to $v_0$ increases by 2.2 dB when the PCIP reaches 5 dBm. This behaviour indicates that as the PCIP increases, FWM interactions become stronger and as a result the channels that are located closer to the

pump and the lasing signal, transfer more energy to $v_0$, which is the located at the greatest distance from the pump.

When a channel is placed at 193.8 THz, it is positioned at the falling edge of the classic gain lobe of the FOPA gain spectrum; hence the reduced small-signal regime gain. As PCIPs are growing, energy is increasingly being transferred by the channels positioned closer to the pump and the lasing signal, towards the ones that are positioned further from them. The analogous trend is occurring between the lasing signal and all the channels as we will see in the following results.

In order to correct this phenomenon, we increase the frequency of all of our channels by 50 GHz. Therefore, the $v_0$ = 193.85 THz, $v_1$ = 193.9 THz, $v_2$ = 193.95 THz and $v_3$ = 194 THz. In addition, we reduce $VA_{dB}$ to 0 dB. This way, the channels are positioned closer to the pump and $v_0$ is no longer located on the falling edge of the amplification spectrum anymore.

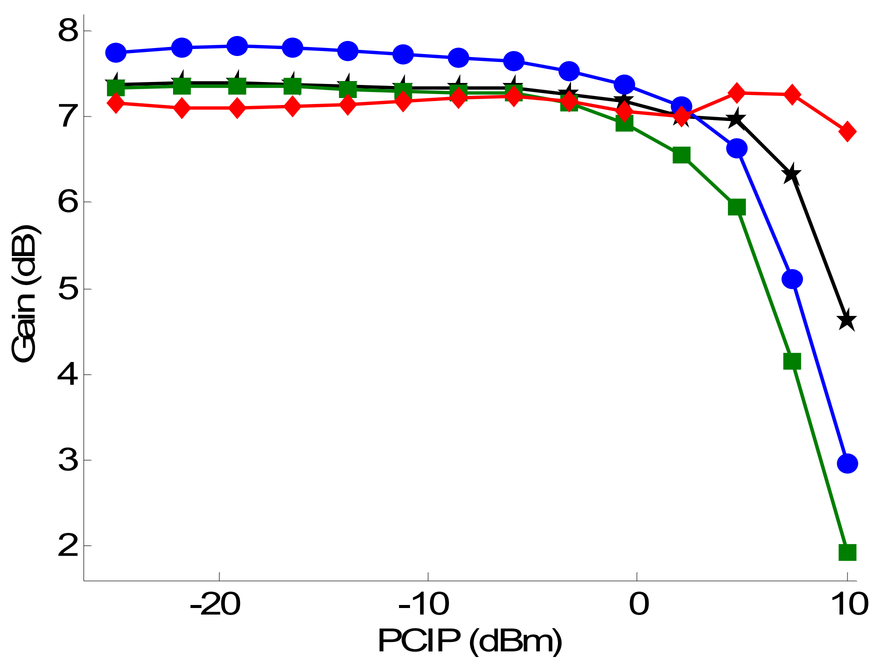


**Fig. 5.11** Gain vs. PCIP for four channel configuration (193.85 - 194 THz) when $Cc$ = 10% and $VA_{dB}$ = 0 dB. The frequencies of the WDM channels are: 193.85 THz (red diamonds), 193.9 THz (black stars), 193.95 THz (green squares), and 194 THz (blue circles)

The effects of the aforementioned changes become obvious looking at Fig. 5.11. First, $v_1$ now receives a similar gain as the other 3 channels. The spread of the small-signal regime gain for all 4 channels is less than 0.6 dB. Secondly, $P_{cr}$ is at least 4 dBm for each of the channels (extending further for 2 of them), and finally the initial increase of received gain for increasing PCIPs for $v_0$ and $v_1$ has all but disappeared. In other words, $\frac{\partial G}{\partial PCIP} \to 0$. Therefore, we can suggest that by increasing the value of $VA_{dB}$, $\frac{\partial G}{\partial PCIP}$ becomes more positive. In order to verify this claim we present a second example.

We now increase $Cc$ to 12% (see Fig. 5.12). As expected, the small-signal regime gain of all channels has dropped as the lasing signal depletes the pump further. The spread of the gains of the channels has almost doubled, reaching 1.1 dB.

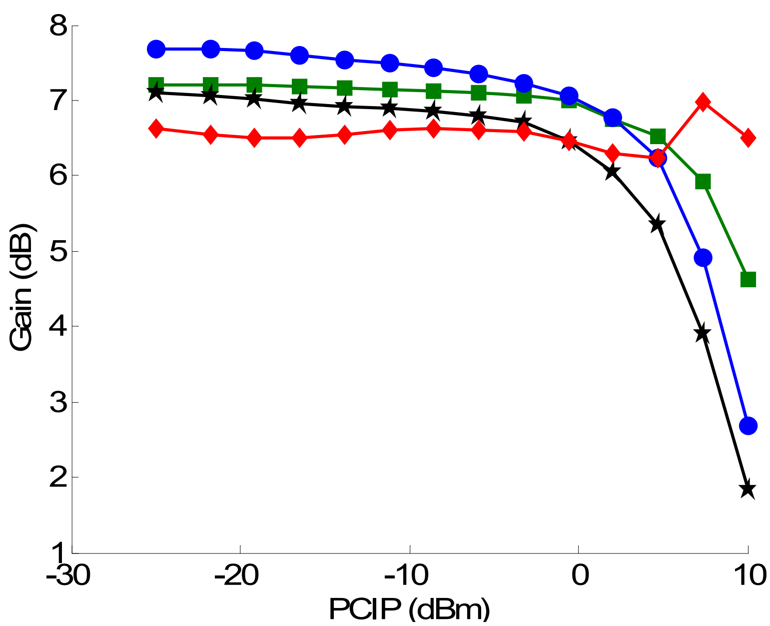


**Fig. 5.12** Gain vs. PCIP for four channel configuration (193.85 - 194 THz) when $Cc$ = 12% and $VA_{dB}$ = 0 dB. The frequencies of the WDM channels are: 193.85 THz (red diamonds), 193.9 THz (black stars), 193.95 THz (green squares), and 194 THz (blue circles)

If we now increase $VA_{dB}$ say to 4 dB, we expect $\frac{\partial G}{\partial PCIP}$ to increase as well as was the case in Fig. 5.9.

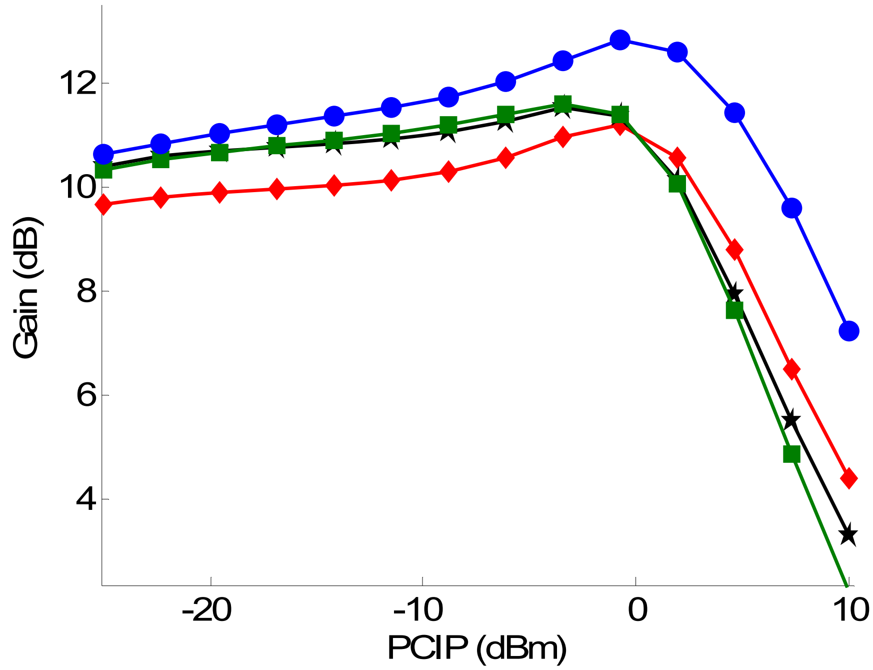


**Fig. 5.13** Gain vs. PCIP for four channel configuration when $Cc$ = 12% and $VA_{dB}$ = 4 dB. The frequencies of the WDM channels are: 193.85 THz (red diamonds), 193.9 THz (black stars), 193.95 THz (green squares), and 194 THz (blue circles).

Fig. 5.13 demonstrates how our hypothesis indeed holds. Following from the syllogism when describing Fig. 5.11, when $VA_{dB}$ is zero, the lasing signal depletes the pump more, itself becoming a pump that transfers energy to the WDM channels as well. Through this high depletion, less energy is transferred directly from the pump to the channels. When $VA_{dB}$ is increased the pump depletion drops and with it the indirect transfer of energy from the lasing signal to the channels. As the PCIPs grow, the channels are increasingly competing with the lasing signal for energy drawn directly from the pump, and thus their gain increases as the indirect transfer of energy from the lasing to the channels is decreasing. This indicates that the power of the lasing signal is falling in parallel, until PCIP reaches $P_{cr}$ whereas the lasing signal breaks down.

More insight can be attained by increasing $BW_{bpf}$. In the following plot we increase $BW_{bpf}$ from 50 GHz to 200 GHz.

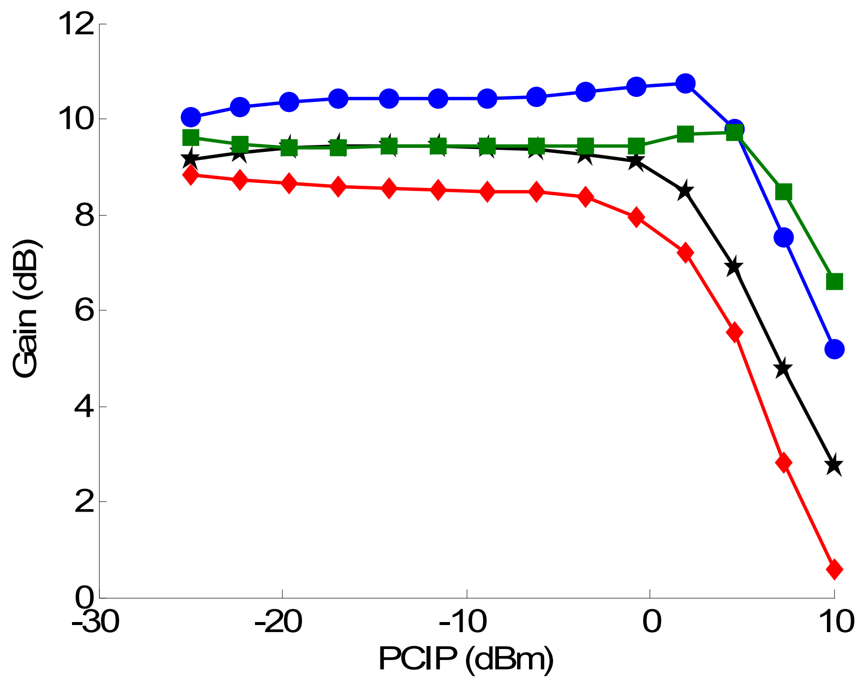


**Fig. 5.14** Gain vs. PCIP for four channel configuration when $Cc$ = 12%, $VA_{dB}$ = 4 dB and $BW_{bpf}$ = 200 GHz. The frequencies of the WDM channels are: 193.85 THz (red diamonds), 193.9 THz (black stars), 193.95 THz (green squares), and 194 THz (blue circles)

An indefinite increase of $BW_{bpf}$ would make the feedback signal stop lasing. However, as lasing is still sustained, the increased $BW_{bpf}$ allows for the laser to draw more power. That is why the gain of all channels drops by up to 1 dB. In the same time, as the lasing signal has become so much broader, its own gain spectrum reaches further. Following from the above rationalisation, the flatter G vs. PCIP function is easily understood.

Other parameters that so far we have kept constant, but can play an important role in the imrovement of the gain vs. PCIP response, are the pump power and the amplifier length. In Fig. 5.15, we show how the response for both an unclamped and an AOGC FOPA with an increased pump power and amplifier length. The characteristics of this configuration are the following: $L$ = 450 m, $\lambda_p$ = 1532 nm, $P_p$ = 31 dBm, $\lambda_f$ = 1543 nm, $VA_{dB}$ = 0 dB, $BW_{bpf}$ = 25 GHz and $Cc$ = 5% tap.

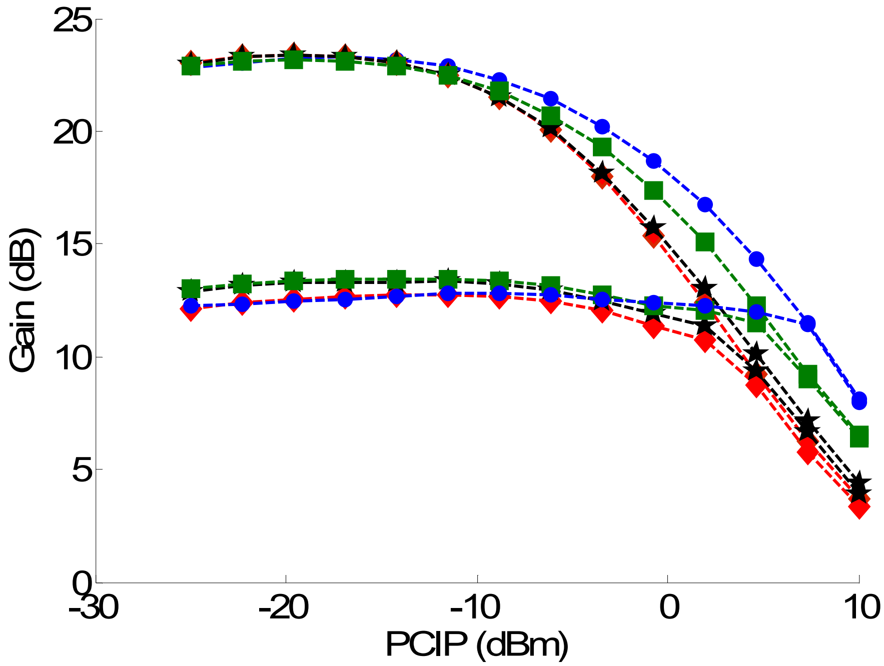


**Fig. 5.15** Gain as a function of PCIP for the 4 WDM channels with and without AOGC. The frequencies of the WDM channels are: 193.85 THz (blue circles), 193.9 THz (red diamonds), 193.95 THz (green squares), and 194 THz (black stars).

Fig. 5.15 shows the FOPA gain as a function of PCIP for all four WDM channels with and without AOGC. As before, without AOGC, the gain varies significantly with the input power. On the other hand, with AOGC, the gain is effectively clamped to around 12.4 dB over a broad range of input signal powers. In particular, for the unclamped amplifier, -14 dBm ≤ $P_{cr}$ ≤ -11 dBm only, whereas with AOGC, -4 dBm ≤ $P_{cr}$ ≤ 1 dBm. Thus, by introducing AOGC, we achieve a nearly constant gain over a larger range (10 dB) of input powers. The longer fibre length in this configuration, allows the feedback signal to more efficiently be amplified, thus draw power from the pump and clamp the amplifier.

### 5.3.4 Summary

To summarize, we have shown that by introducing a feedback lasing signal using a ring configuration, it is possible to gain clamp a FOPA with satisfactory results. For a

$P_p$ of 30 dBm we could achieve a $P_{cr}$ of around 5 dBm for all 4 WDM channels. Moreover, we demonstrated how we are able tailor the response of the system by adjusting parameters such as $BW_{bpf}$, $VA_{dB}$ and $Cc$. The level of clamping, as well as the function of $\frac{\partial G}{\partial PCIP}$ can be modified, allowing us to achieve the desirable level of flat response and/or $P_{cr}$.

It is apparent that all the above hold for a configuration where the pump, the lasing signal and the channels are positioned in sequence with this specific order. If on the other hand, the lasing signal was located on the left of the pump and the signals on the right, the interactions and thus the relations between the varying quantities, would change considerably. The interactions between the lasing signal and the WDM channels would be lessened, as it would be positioned further from the pump, while the lasing signal would not be extending the gain spectrum of the existing pump further to the right.

In any case, the results presented here can motivate further studies on the effects of the signal location (pump, feedback and channels) with respect to each other but also with respect to $\lambda_0$. Moreover, varying other parameters can give even better results than the ones we have so far obtained. Certainly, designing an AOGC-FOPA will be even more challenging when we have to face 32 or 64 channel systems.

## *5.4 Gain Transients Mitigation*

In this section, we recap the hindrances demonstrated in section 3.3.3 and then demonstrate how the gain clamping technique described in section 5.3, can be used to mitigate these problems. Once more, whereas WDM networks have become the standard for optical networks offering increased capacity and flexibility reconfigurable dynamic networks face multiple challenges. The number of channels passing through a FOPA can significantly vary as a result of network reconfiguration or failures which can induce channels to be dropped. As the amplifiers in such conditions operate near saturation, the gain of each channel is depended on the total input power (TIP) entering the amplifier as well as the position of the surviving channels as it was discussed in [5.16]. Such changes in TIP can induce gain transients in the surviving channels via cross-saturation as it is shown in section 3.3.3. In the same section it was also shown that these gain excursions strongly depend on the position of the surviving channel and can vary from insignificant, for the channels positioned in the outer edges of the channel band, to several dBs for the midband cannels. The rise and fall times of these excursions are very short and independent of the PCIP. Moreover, during channel add/drop, no overshoots or undershoots were observed. Such gain transients constitute a major issue for AAPN where channels are dropped or added frequently, especially after the channels have passed through a number of cascaded amplifiers. This is the reason why mitigating such transients is important if FOPAs are to be considered as an alternative technology used in AAPNs.

So far, in our investigation of AOGC-FOPAs, we have assumed CW operation for all channels. In order to investigate the effects of gain clamping in the dynamic properties of the amplifier we have to use modulated WDM channels. We now consider a system with 4 NRZ modulated WDM channels. We demonstrate how gain excursions that occur after channel adding or dropping, can be effectively mitigated by gain-clamping the amplifier with the technique described in the preceding section.

### 5.4.1 System Setup and Results

Fig. 5.16 shows the setup of the AOGC-FOPA and the system under investigation. In this investigation the following parameters are used: $L =$ 450 m and

$\lambda_0$ = 1530 nm and $S$ = 0.09 ps/nm$^2$/km. The rest of the HNLF parameters are the same as the ones given in Table 3.1. We use a pump at 1532 nm with 30 dBm power. A feedback path comprising a 6% tap at the output of the FOPA and an ideal power combiner at the input are used to create a lasing signal for AOGC. As before, the wavelength of the lasing signal, $\lambda_f$, is defined by a bandpass filter (BPF) with a 3 dB bandwidth of 90 GHz placed in the feedback path (here we set $\lambda_f$ = 1541 nm).

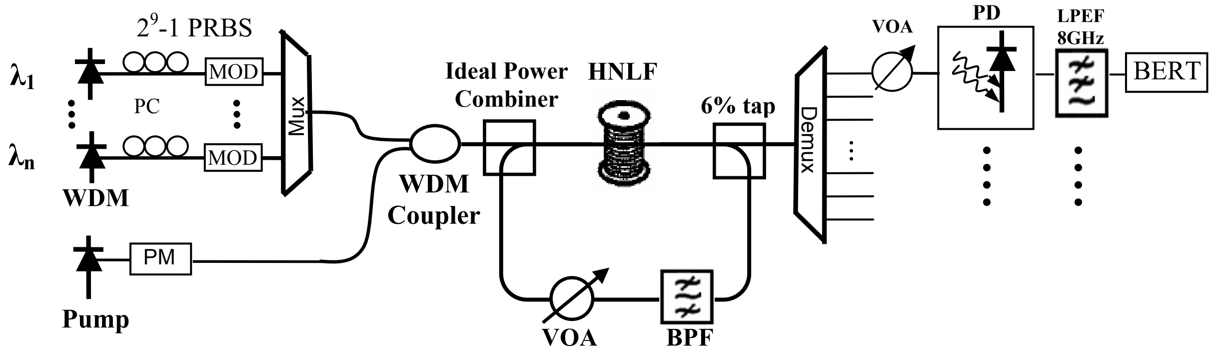


**Fig. 5.16** Gain-clamped FOPA using a ring configuration. MOD: electro-optic modulator, PM: phase modulator, PD: photodiode, LPEF: low-pass electrical filter, and BERT: bit-error-rate tester.

Of the 4 WDM channels, the first is centred at 193.9 THz and the remaining channels increase in frequency with a separation of 100 GHz. The channels all have random phases and their central frequencies can deviate randomly from the ideal value by up to 3% of the channel spacing. Each channel is NRZ modulated at 10 Gb/s by independent $2^9 - 1$ PRBS and the average launch power per channel is -12 dBm (all passive components are assumed ideal with no insertion loss). Three of the four channels are dropped and then added twice during the simulation time window of 512 bits. The channels are separated using a WDM demultiplexer with 100 GHz channel spacing and 3 dB bandwidth of 12 GHz. The detected signals are then filtered using a low-pass electrical filter with a bandwidth of 8 GHz before the bit-error-rate is calculated. We monitor the performance of the surviving channel $v_0$ at 193.9 THz.

The FOPA provides 32 dB gain at the surviving channel wavelength without AOGC; with AOGC, the gain reduces to 23 dB. In the inset of Fig. 5.17 (a), we show the eye diagrams obtained at the receiver for the ROP indicated. By observing the eye diagrams, we can clearly see that without AOGC there is a rail in the middle of the eye diagram which corresponds to the new steady-state output power level following channel add. In other words when the three WDM channels are added, the TIP is now 4 times higher. The FOPA cannot continue to provide the same gain as previously to all 4 channels and thus the gain is reduced. As a result, for the receiver, the “1s” now have a lower value than before. Without re-adjusting the threshold value of the receiver, this will lead to errors.

On the other hand, with AOGC, even though the lasing signal introduces additional FWM noise as expected, the rail in the middle of the eye diagram that was present before due to the gain transients, is clearly suppressed. In other words, the power level of the surviving channel is kept relatively constant through add/drop operations, see Fig. 5.17 (b), thus avoiding the BER floor in the case without AOGC.

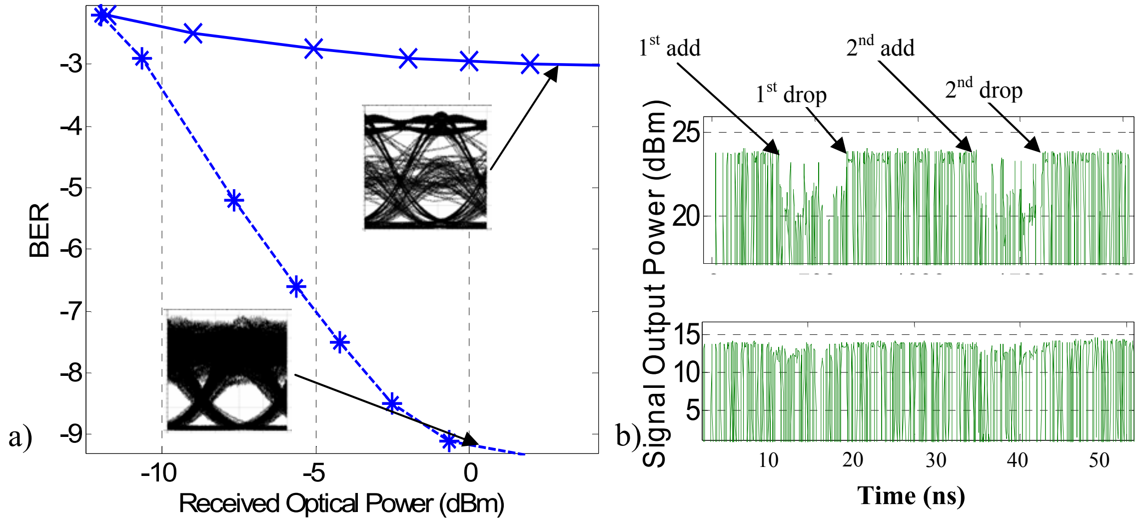


**Fig. 5.17** (a) The BER curves for the FOPA with (dashed and stars) and without (solid line and ×) AOGC. The insets show the eye diagrams of the surviving channel. (b) Time waveforms of the surviving channel at the output of the FOPA without (top) and with (bottom) AOGC.

In particular, for a fixed receiver threshold, with AOGC, we can obtain error-free transmission whereas without AOGC, we obtain an error floor at a BER = $10^{-3}$. The low receiver sensitivity seen in Fig. 5.17 (a) is due to the lack of pre-amplification at the receiver end. When operating in the small-signal regime, the gain excursions would be of minor importance; on the other hand, when operating close to saturation, the gain transients can reach several dB. In our example, the gain transients without AOGC case reach almost 4 dB whereas they are suppressed below 0.6 dB when using AOGC.

In this study we demonstrated how to GC can dramatically improve the performance in a dynamic network that is using FOPAs and NRZ modulation. The problem that we described above arises from the fact that different levels of power symbolize “1s” and “0s”. In other words, all amplitude modulated shift keying formats, such as RZ and NRZ, suffer a lot from gain excursions. In DPSK schemes, were the phase is used in order to encode the data, such a problem would not be as severe.

However, a large change in the amplitude of the phase modulated RZ pulses could also result in a fall of the contrast ratio between consecutive pulses. However, this should be the objective of further investigation.

## *5.5 Impact of GC on the BER*

As it has been shown in other technologies, gain-clamping an amplifier with the use of a lasing feedback can lead to a small noise increase and BER degradation [5.17]. This is one of the tradeoffs in exchange for decreased gain variations in response to TIP, PCIP or power distribution changes (in frequency) in the amplifier. Introducing a high power signal in the amplifier heightens the FWM interactions and thus the noise experienced by the WDM channels. This part of the investigation is not to be confused with section 5.4. In the present section, we will investigate the effect on the BER performance of a static system, in which the number of channels and their PCIP are constant.

### 5.5.1 Impact of *Cc* on the BER

In order to verify if indeed GC degrades the BER performance of the system due to the additional noise generated by the lasing signal, we examined a single channel, NRZ modulated at 10 Gb/s system, both when the FOPA is clamped and unclamped. In the clamped case we also investigated the effect of increase in the feedback level to the BER performance.

For our example we consider the following system: A FOPA consisting of 300 m of HNLF with the characteristics given in Table 3.1, except that the zero-dispersion wavelength is at 1530.5 nm, and the dispersion slope is 0.09 ps/(nm$^2$·km). The pump is positioned at 1535 nm with 30 dBm power. The signal frequency $\nu_0$ is 194.2 THz and its average power is -8 dBm. The wavelength of the lasing signal, $\lambda_f$, is defined by a bandpass filter (BPF) with a 3 dB bandwidth of 50 GHz placed in the feedback path. Here we set $\lambda_f = 1541$ nm.

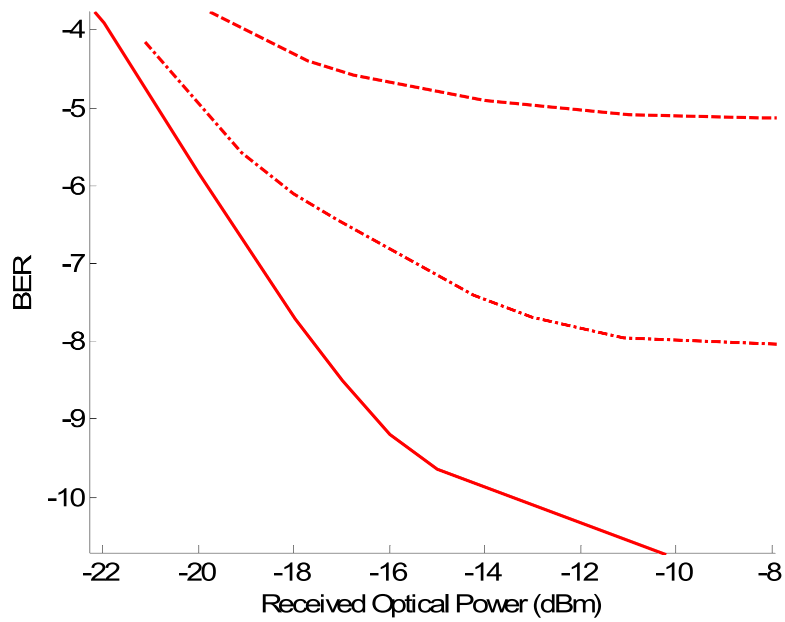


**Fig. 5.18** BER measurements vs. Received Optical Power when feedback tap is 7% (dashed line), 5% (dashed-dotted line) and without feedback (solid line)

In Fig. 5.18, it becomes apparent that the introduction of a feedback lasing signal has induced strong FWM interactions that significantly degrade the system's performance. Whereas when no feedback exists ($Cc = 0$) we obtain error-free operation at -17 dBm of ROP, when $Cc$ is set to 5% we obtain an error floor at BER = $10^{-8}$. When $Cc$ is further increased to 7% the FWM noise is augmented to the point of barely achieving an error floor at BER = $10^{-5}$.

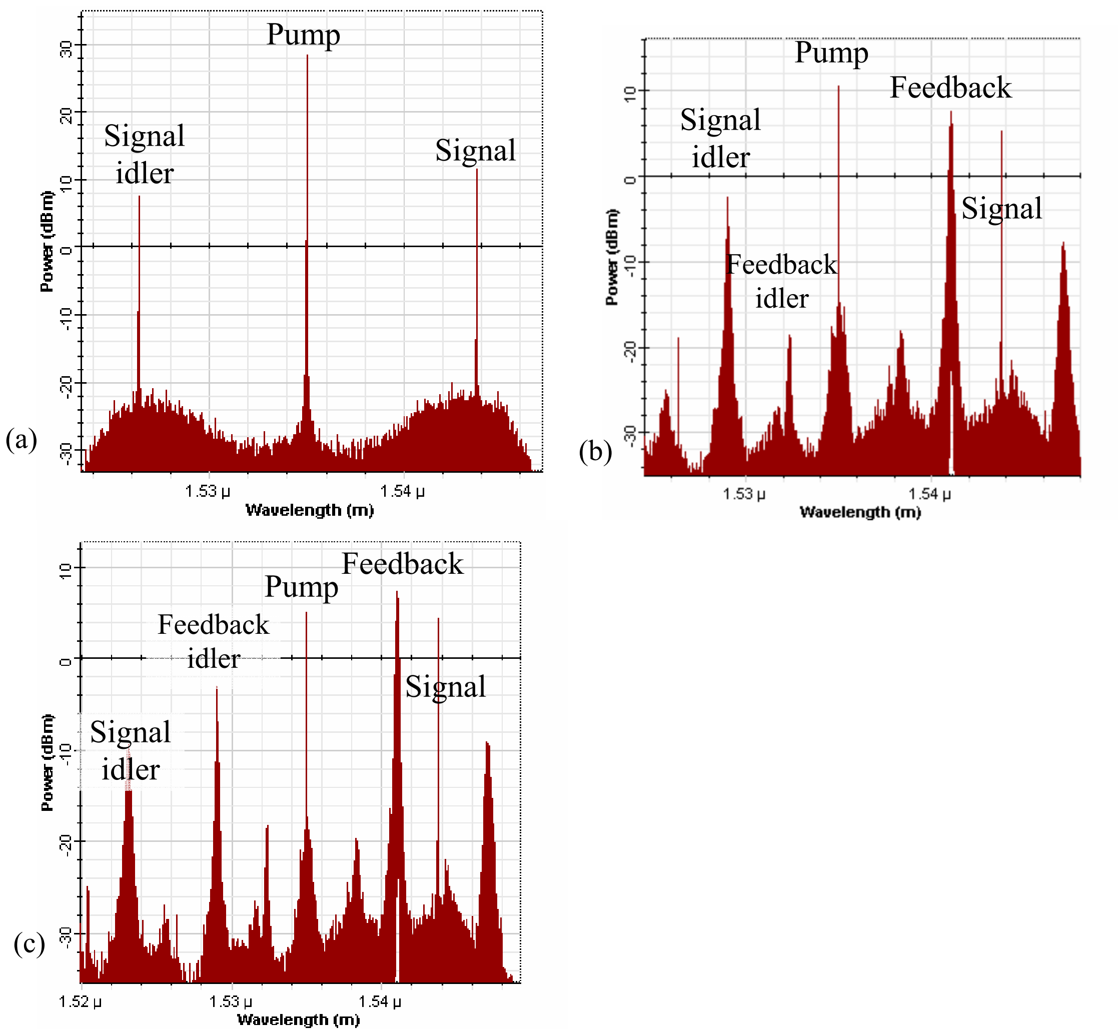


**Fig. 5.19** Optical spectrum as seen at the output of the amplifier for a) no feedback, b) *Cc* = 5% and c) *Cc* = 7%.

In Fig. 5.19 one can clearly see the aforementioned effect as illustrated in the optical spectrum at the output of the FOPA. In Fig. 5.19 (a) the part of the graph on the left, when no feedback has been introduced (i.e. the amplifier is unclamped), the optical spectrum forms two classic lobes on both sides of the pump. No high power FWM products are observed within the bandwidth of interest. When feedback is introduced, see Fig. 5.19 (b), several FWM products are generated, some of which are really high power, which in turn induce noise in the channels, degrading the BER performance of the system. Further increasing the *Cc* [Fig. 5.19 (c)] evidently increases the pump depletion through the lasing signal amplification and the further generation of FWM products, consequently creating more FWM noise. Again, in the present section we investigated the effect of GC on the BER performance within the context off a static system, in which the number of channels and their PCIP remain constant. Therefore, even if AOGC seems to be degrading the performance in a static system it solves the gain excursions problem as described in section 5.4. In other words, as mentioned repeatedly, AOGC is a valuable technique in dynamic networks even if in a static network it can degrade the performance of the system.

Following directly from our analysis in Chapter 4, we now examine the effect AOGC has on the system when a different modulation format is used. Hence, we investigate the BER performance in a system employing NRZ and RZ-DPSK modulation both in the clamped and the unclamped cases.

Evidently, the choice of $\lambda_f$ and $v_0$ play an important role as well. By placing the channel close to the first order FWM product of the laser- pump interaction we introduce large amounts of noise to our modulated data. As we previously saw, the AOGC condition can be satisfied using lower *Cc* values just by choosing a more appropriate $\lambda_f$. In this case *Cc* is set to 3%. In this investigation the parameters used are the same as in the system described above. We however, change the signal frequency $v_0$ to 194.3 THz and the $\lambda_f$, to 1546 nm. The average power for all cases is -11 dBm.

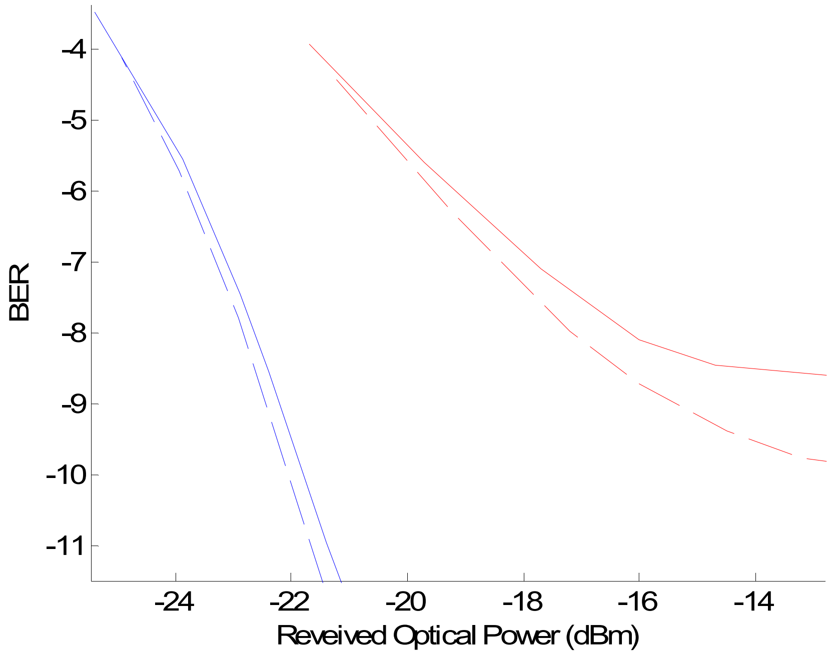


**Fig. 5.20** BER measurements vs. Received Optical Power when the channel is RZ-DPSK (blue lines) and NRZ (red lines) modulated for an unclamped (dashed lines) and a GC (solid lines) FOPA.

Fig. 5.20 shows the BER vs. ROP, when the channels are modulated using RZ-DPSK (blue lines) and NRZ (red lines) in the cases where an unclamped (dashed lines) and an AOGC-FOPA (solid lines) is used. Clearly, the RZ-DPSK shows its increased immunity from XGM and FWM noise as demonstrated previously in section 4.2.6. The power penalty for clamping the amplifier reaches 2 dB when NRZ modulation is used. This drops to less than 0.2 dB in the case of RZ-DPSK. However, the power penalty reduction for RZ-DPSK compared to NRZ, is more than 6 dB both for the clamped and unclamped cases.

As we analyzed in length in Chapter 4, the employment of RZ-DPSK greatly improves the receiver sensitivity and the AOGC-FOPA is no exemption. By using RZ-DPSK modulation format, XGM induced crosstalk in FOPAs is drastically suppressed.

Therefore, even after the introduction of a high power feedback signal, these interactions are kept to a minimum.

In summary, if a GC-FOPA is used in conjunction with a RZ-DPSK modulated WDM channels in a dynamic operating conditions, a high performance system can be designed mitigating most hindrances often met in such an environment such as XGM induced crosstalk, add/drop induced gain excursions and channel input power induced gain changes.

## *5.6 Conclusion*

In the current chapter of this thesis, we presented how some of the drawbacks of FOPAs that we described in Chapter 3 and Chapter 4 can be mitigated or resolved. In particular, with the use of a feedback signal we managed to control one of the inherent properties of optical amplifiers; that of gain change as a function of PCIP.

The ring configuration was preferred over the FBG cavity configuration for two main reasons. First, investigations in other amplifier technologies [5.18] have shown that this method of gain clamping is more efficient. Secondly, the implementation of a ring configuration laser is considerably easier and cheaper, eliminating the need for FBGs substituting them with a simple tap and a band pass filter.

In other amplifier technologies, $\frac{\partial G}{\partial PCIP}$ is always negative. In the case of the FOPAs it can be either positive or negative, posing additional challenges. By modifying $BW_{bpf}$, $VA_{dB}$ and $Cc$, we managed to obtain a flat gain response to PCIP variation for a large range of PCIPs. For a system with a $P_p$ of 30 dBm and 4 WDM channels, we achieved a $P_{cr}$ of 5 dBm.

Furthermore, by the use of AOGC, we successfully mitigated the gain excursions observed when channel add/drops occur. Correcting this problem improves system performance two-fold. First, we benefit by making gain independent of the number of channels present in the system. This way, after a large number of cascaded amplifiers operating at different network conditions (distribution and number of channels, PCIPs etc.) the gain provided to the channels remains the same, thus minimizing power variations as the channels reach their destination. Secondly, as we demonstrated in section 5.4, in an unclamped amplifier during add/drop operations the BER is dramatically affected as the receiver has to readjust its threshold; for now, the power level indicating a "1" has changed. In an AOGC-FOPA this problem is significantly mitigated and the BER performance is drastically improved.

Finally, we investigated the impact of gain clamping on the BER performance of an amplifier operating in static conditions. As expected, due to the additional FWM products that a high power lasing signal introduces, we experience a significant power penalty. Nevertheless, by using RZ-DPSK modulation, instead of common OOK, we solve this hindrance and dramatically improve system performance both in the unclamped and clamped cases. The power penalty is reduced to a mere 0.2 dB, while overall the use of RZ-DPSK helps relax receiver sensitivity constrains by more than 6 dB even in the clamped case.

## References

[5.1] T. Torounidis, H. Sunnerud, P. Hedekvist and P. Andrekson, "Fiber optical parametric amplifier in WDM applications", Optical Fiber Communication Conference, paper ThK2, Atlanta, USA, March 23 - 28 (2003).

[5.2] K. K. -Y. Wong, Guo-Wei Lu and Lian-Kuan Chen, "Polarization-interleaved WDM signals in a fiber optical parametric amplifier with orthogonal pumps", Optics Express, vol. 15, pp. 56-61, (2007).

[5.3] P. O. Hedekvist, M. Karlsson and P. A. Andrekson, "Fiber four-wave mixing demultiplexing with inherent parametric amplification", Journal of Lightwave Technology, vol. 15, pp. 2051-2058, (1997).

[5.4] K. K. -Y Wong, M. E Marhic, K. Uesaka and L. G. Kazovsky, "Polarization-independent one-pump fiber-optical parametric amplifier", Photonics Technology Letters, vol.14, no.11, pp. 1506-1508, (2002).

[5.5] M. Zirngibl, "Gain control in erbium-doped fibre amplifiers by an all optical feed back loop", Electronic Letters, vol. 27, no. 7, pp. 560, (1991).

[5.6] H. Okamura, "Automatic optical loss compensation with Erbium-doped fiber amplifier", Journal of Lightwave Technology, vol. 10, pp. 1110, (1992).

[5.7] H. S. Seo, J. T. Ahn, B. J. Park and W. J. Chung, "Effective gain clamping technique in a Raman amplifier with a resonant cavity", Conference of Lasers and Electro-Optics Europe, pp.1-1, (2007).

[5.8] M. Karasek and M. Menif, "Protection of surviving channels in pump-controlled gain-locked Raman fibre amplifier", Optics Communications, vol. 210, pp. 57, (2002).

[5.9] H. S. Seo, K. Oh and U. C. Paek, "Gain optimization of germanosilicate fibre Raman amplifier and its applications in the compensation of Raman-induced crosstalk among wavelength division multiplexing channels", Journal of Quantum Electronics, vol. 37, pp. 1110, (2001).

[5.10] E. Delevaque, T. Georges, J. F. Bayon, M. Monerie, P. Niay and P. Bernage, "Gain control in erbium-doped fiber amplifiers by lasing at 1480nm with photoinduced Bragg gratings written on fiber ends", Electronic Letters, vol. 29, no.12, pp. 1112-1114, (1993).

[5.11] J. Gest and L. R. Chen, "Comparison of Two All-Optical Gain-Clamping Techniques for Discrete Fiber Raman Amplifiers", 22nd Biennial Symposium on Communications, paper 33, Kingston, Ontario, (2004).

[5.12] A. Ahmad, M. I. M. Ali, A. K. Zamzuri and M. A. Mahdi, "Gain-control Raman fiber amplifier incorporating ring cavity", International Conference on Communication, paper Th03-223, Malaysia, November 16 - 18 (2005).

[5.13] X. Zhou, H. H. M. Shalaby, C. H. Lu, P. Shum and T. Cheng, "Theoretical investigation of fiber Raman amplifier with dynamic gain control", Optical Fiber Communication Conference, paper WDD17-1, Anaheim, USA, March 17 - 22 (2001).

[5.14] J.C. Simon, P. Doussiere P. Lamouler, I. Valiente and F. Riou, "Travelling wave semiconductor optical amplifier with reduced nonlinear distortions", Electronics Letters, vol. 30, no. 1, pp. 49-50, (1994).

[5.15] S. W. Harun, N. M. Samsuri and H. Ahmad, "All-Optical Gain Clamped Double-Pass L-Band EDFA Based on Partial Reflection of ASE", Electronics Express, vol. 1, no. 7, pp.171-175, (2004).

[5.16] N. Gryspolakis and L. R. Chen, "Response of fibre optic parametric amplifiers to channel add/drop in agile all-photonic networks", Optics Communications, vol. 278, no. 1, pp. 168-174, (2007).

[5.17] T. Zambelis, N. Gryspolakis and L. R. Chen, "Design of all-optical gain-clamped discrete fiber Raman amplifiers", IEEE Laser and Electro-Optics Society Annual Meeting, paper ThFF1, Tucson, Arizona, October 27 - 28 (2003).

[5.18] J. Gest and L. R. Chen, "Performance analysis of all-optical gain-clamped discrete fiber Raman amplifiers" IEEE Laser and Electro-Optics Society Annual Meeting, paper ThV3, Rio Grande, Puerto Rico, November 7 - 11 (2004).

# Chapter 6 Conclusion

In this thesis we studied the suitability of FOPAs for AAPNs. In particular, we investigated and identified the hindrances that these amplifiers can face in such an environment. We demonstrated how AOGC can be used to mitigate several of the drawbacks of FOPAs and in conjunction with the use of RZ-DPSK to improve their performance in a dynamic, multi-channel environment.

We first explored the quasi-static characteristics of FOPAs by assuming realistic conditions for WDM systems under which channel power sways and add/drops are a frequent phenomenon. We took into account the change in PCIP, number of channels and their locations inside the spectrum, in order to asses how these parameters affect the gain tilt as well as its the dynamic characteristics, namely the generation of under or over-shoots at the transition point. We found that the gain spectrum depends strongly on the number of input signals and any changes as a result of variations in PCIP are irregular and not predictable due to the complex nature of the nonlinear FWM interactions. The gain tilt depends on various parameters such as the position of the surviving channels and the TIP. Furthermore, we have shown that the gain spectrum is a strong function of channel spacing and found that more sparsely spaced configurations are more robust to channel add/drop. We also showed that the gain excursions observed in the case of channel add/drop strongly depend on the position of the surviving channel. The rise and fall times are very short and independent of the PCIP and there are no overshoots nor undershoots during channel add/drop.

Moreover, we examined the behaviour of FOPAs in a multi-wavelength bursty packet traffic environment. We found that, when FOPAs operate in a dynamic network close to saturation or when the power fluctuations on packet-to-packet basis are substantial, the WDM channels suffer from significant gain excursions that can degrade overall amplifier performance. We concluded that these deleterious phenomena have to be controlled if FOPAs are to be considered suitable for use in AAPNs.

In Chapter 4 we introduced modulated channels to the amplifier in order to compare their effect on the BER performance. We considered the impact on the amplifier's performance when different modulation formats (namely RZ, NRZ and RZ-DPSK) are used. We have shown that crosstalk suppression in a single pump FOPA can be achieved by using the RZ-DPSK modulation format. This is basically achieved by greatly reducing XGM with a constant power per bit period, modulation scheme. In addition, because the improvement when using RZ-DPSK is so significant for all input power levels and bit-rates, it became apparent that the dominant impairment experienced by RZ and NRZ is XGM, while FWM and other impairments are less significant. Moreover, we showed that there is a performance gain for RZ formats (for carefully selected d.c.) over NRZ formats in terms of the FWM-induced crosstalk level

Finally, in Chapter 5 using AOGC for the first time in FOPAs, we achieved all-optical gain clamping alleviating gain excursions and attaining gain, independent of channel input power for a large range of PCIP. In particular, we presented how some of the drawbacks of FOPAs that we described in Chapter 3 and Chapter 4 can be mitigated or resolved with the use of a ring configuration optical feedback signal. Furthermore, by the use of GC, we successfully mitigated the gain excursions observed when channel add/drops occur. Alleviating this problem improves system performance first by making gain independent of the number or the power of channels present in the system, but also, by eliminating the need to readjusting the receiver's threshold in order to be able to detect the "1s", the power level of which is changing during the add/drop operations. Finally, we showed that when using AOGC, we experience a significant power penalty due to the additional FWM products that a high power lasing signal introduces to the system. Nonetheless, by using RZ-DPSK modulation, instead of common OOK, we solved this hindrance and dramatically improved system performance.

Our work demonstrates that the behaviour of FOPAs within the context of AAPNs, in many cases is atypical of fibre optical amplifiers, such as EDFAs and DFRAs. Especially in dynamic multi-channel networks, the complex nature of FWM interactions makes it an arduous and complicated task to design an amplifier that can tackle these challenges if no gain control is used. By the use of RZ-DPSK we can significantly reduce channel cross talk, while by a properly designed AOGC-FOPA, many of the drawbacks of this amplifier technology, can be solved. Having demonstrated that AOGC does work in FOPAs, a lot of research can be conducted in order to show how other disadvantages that have been demonstrated in the literature, can now be eliminated. Thus, we believe that if properly designed, with the use of constant power modulation formats and with the correct design of AOGC, FOPAs can be considered as a candidate for AAPNs.

However, their complex nature and the great variety of precautions that have to be taken into account in order for them to satisfactory operate (orthogonally polarized pumps, polarization controlled signals, etc.) make them unattractive for the time being. Even if FOPAs will not replace the well established EDFAs and DFRAs in optical communications anytime soon, the future of FOPAs can be brighter once the need for more bandwidth, outside the two low-loss SMF windows, arises. That can serve as a motivation for the development of necessary components, such as fibres with low dispersion in other bands, as well as pumps in more extreme wavelengths.

# Appendix

## *Appendix I*

**Statistical Moments (and the Shape of Distributions)**

The mean and the variance provide information on the location and variability (spread, dispersion) of a set of numbers, and by doing so, provide some information on the appearance of the distribution (for example, as shown by the histogram) of the numbers. The mean and variance are the first two statistical moments, and the third and fourth moments also provide information on the shape of the distribution.

First sample central moment = $\sum_{i=1}^{n}\left(x_i - \overline{X}\right)^1$ and is by definition equal to zero. In other words, mean is the value of $x$ that makes the above statement true, and consequently indicates where the individual numbers generally lie.

The second central moment is recognized as the numerator of the variance:

$$\text{Second sample central moment} = \sum_{i=1}^{n}\left(x_i - \overline{X}\right)^2$$

which gives information on the spread or scale of the distribution of numbers.

The sample third central moment, $\sum_{i=1}^{n}\left(x_i - \overline{X}\right)^3$ is used to define the *skewness* of a distribution. For a sample of $n$ values the sample skewness is:

$$\text{Skewness} = \frac{m_3}{m_2^{\frac{3}{2}}} = \frac{\frac{1}{n}\sum_{i=1}^{n}\left(x_i - \overline{X}\right)^3}{\left(\frac{1}{n}\sum_{i=1}^{n}\left(x_i - \overline{X}\right)^2\right)^{\frac{3}{2}}}$$

where $x_i$ is the $i^{th}$ value, $\overline{x}$ is the sample mean, $m_3$ is the sample third central moment, and $m_2$ is the sample variance.

## Appendix

Skewness is a measure of the symmetry of the shape of a distribution. If a distribution is symmetric, the skewness will be zero. If there is a long tail in the positive direction, skewness will be positive, while if there is a long tail in the negative direction, skewness will be negative.

The sample fourth central moment, $\sum_{i=1}^{n}\left(x_i-\overline{X}\right)^4$ is used to define the kurtosis of a distribution. For a sample of $n$ values the sample kurtosis is:

$$\text{Kurtosis} = \frac{m_4}{m_2^2} = \frac{\frac{1}{n}\sum_{i=1}^{n}\left(x_i-\overline{X}\right)^4}{\left(\frac{1}{n}\sum_{i=1}^{n}\left(x_i-\overline{X}\right)^2\right)^2}$$

Kurtosis is a measure of the flatness or peakedness of a distribution. A distribution with positive excess kurtosis is called leptokurtic, or leptokurtotic. In terms of shape, a leptokurtic distribution has a more acute peak around the mean (that is, a higher probability than a normally distributed variable of values near the mean) and thicker tails (that is, a higher probability than a normally distributed variable of extreme values). Examples of leptokurtic distributions include the Laplace distribution and the logistic distribution.

A distribution with negative excess kurtosis is called platykurtic, or platykurtotic. In terms of shape, a platykurtic distribution has a lower, wider peak around the mean (that is, a lower probability than a normally distributed variable of values near the mean) and thinner tails (if viewed as the height of the probability density—that is, a lower probability than a normally distributed variable of extreme values). Examples of platykurtic distributions include the continuous or discrete uniform distributions, and the raised cosine distribution.